Dissertations and Thesis

Fall 12-16-2017

Development of a Parsimonious Urban Landscape Nutrient Model using Representations of Terrestrial Denitrification Controls

Emily Stephan
SUNY College of Environmental Science and Forestry, eastepha@syr.edu

Follow this and additional works at: http://digitalcommons.esf.edu/etds

Recommended Citation

Stephan, Emily, "Development of a Parsimonious Urban Landscape Nutrient Model using Representations of Terrestrial Denitrification Controls" (2017). *Dissertations and Thesis*. 5.
http://digitalcommons.esf.edu/etds/5

This Open Access Dissertation is brought to you for free and open access by Digital Commons @ ESF. It has been accepted for inclusion in Dissertations and Thesis by an authorized administrator of Digital Commons @ ESF. For more information, please contact digitalcommons@esf.edu, cjkoons@esf.edu.

DEVELOPMENT OF A PARSIMONIOUS URBAN LANDSCAPE NUTRIENT MODEL

USING REPRESENTATIONS OF TERRESTRIAL DENITRIFICATION CONTROLS

by

Emily A. Stephan

A dissertation
submitted in partial fulfillment
of the requirements for the
Doctor of Philosophy Degree
State University of New York
College of Environmental Science and Forestry
Syracuse, New York
November 2017

Department of Environmental Resources Engineering

Approved by:
Theodore Endreny, Major Professor
David Newman, Chair, Examining Committee
Theodore Endreny, Department Chair
S. Scott Shannon, Dean, The Graduate School

Acknowledgments

TABLE OF CONTENTS

LIST OF FIGURES

LIST OF APPENDICES

Abstract

E. A. Stephan. Development of a Parsimonious Urban Landscape Nutrient Model Using Representations of Terrestrial Denitrification Controls, 148 pages, 8 tables, 15 figures, 2017.

Nonpoint source pollution of nitrogen (N) and phosphorus (P) creates pervasive water quality and eutrophication problems around the world, adversely affecting rivers, lakes, and estuaries. Urban land use generates excess N and P pollutants and land use conversion removes natural N and P filtration services provided by undeveloped ecosystems. Management of these problems might first be approached using scoping level nonpoint source runoff models that are defined as balancing process complexity and algorithm simplicity, as well as balancing data availability and predictive accuracy. The contributing area / dispersal area (CADA) concept brings land cover and elevation data along with runoff and filtering likelihood algorithms into the Export Coefficient (EC) model to map likely variations in nutrient loading across the landscape. In this research, we enhance scoping level models by 1) adding spatial variation through the mapping of runoff and buffering likelihoods, 2) introducing the temporal driver of rainfall intensity to enhance nutrient export, and 3) determining the environmental variables most highly correlated with denitrification.

In this study, we enhance the EC model to account for spatial and temporal variations, allowing for better estimates of nutrient loading across space and time. This research also determines key predictors of denitrification potential in mixed-use watersheds, through which denitrification hotspots can be identified. The creation of spatially- and temporally-distributed scoping models for nutrient loading through the landscape will assist managers in identifying areas of high loading potential, which generate high concentrations of nutrients and have little opportunity for downslope filtration. The identification of high denitrification potential zones also allows for facilitation of nitrate removal by routing nitrate-rich water to these zones. The low-level data needs and process-based features of the scoping model allow for its implementation into the i-Tree Hydro toolkit, a peer-reviewed software suite that is used to assess the effects of management and land use change on water quality and quantity.

Keywords: nonpoint source pollution, watershed management, nutrients, runoff, land use/land cover change, urbanization, rainfall intensity, denitrification

E.A. Stephan
Candidate for the degree of Doctor of Philosophy, November 2017
Theodore Endreny, Ph.D.
Department of Environmental Resources Engineering
State University of New York College of Environmental Science and Forestry, Syracuse, New York

CHAPTER 1: INTRODUCTION

Overview

Nonpoint source pollution is a pervasive water quality problem around the world, adversely affecting rivers, lakes, and estuaries (e.g., Carpenter et al., 1998; Kaushal et al., 2011). Eutrophication, the enrichment of waters by excess nutrients, causes excessive plant and algae growth. Cultural eutrophication, acceleration of natural eutrophication in response to human nitrogen (N) and phosphorus (P) enrichment, is the primary impairment facing most surface waters today (Smith & Schindler, 2009). Watershed management seeks to reduce nitrogen (N) and phosphorus (P) loading from human activities to protect aquatic ecosystem health (Conley et al., 2009; Lewis, Wurtsbaugh, & Paerl, 2011). Urban land use generates excess N and P pollutants (Kaye, Groffman, Grimm, Baker, & Pouyat, 2006) and diminishes the extent of aquatic ecosystems and environmental services of N and P filtration provided by natural processes in undeveloped ecosystems (Bettez & Groffman, 2012).

Urban biogeochemical cycles and their influence on N and P loading are more complex than widely studied rural N and P loading mechanisms due to interactions between society and the built environment (Kaye et al., 2006). Nutrient limitations within ecosystems are influenced by the N:P ratio of external inputs, which tends to be lower in urban systems, favoring N limitation (Howarth & Marino, 2006). Inland waters which drain urban systems also transport high N loads to receiving coastal waters, creating problems of eutrophication downstream. Predictive models of N and P cycling were initially developed in agricultural ecosystems to focus on nonpoint source loading (e.g.,

Young, Onstad, Bosch, & Anderson, 1989); consequently, complex urban biogeochemistry has not been incorporated into N and P loading models.

In this research we consider, and seek to improve, scoping level models for N and P pollutant loading that are relatively simple and attempt to balance complexity with data availability and accuracy. The Export Coefficient (EC) model (Reckhow & Simpson, 1980) is a scoping model initially designed for rural areas that uses empirically derived export coefficients to represent the annual N or P load for each land cover type. The Event Mean Concentration (EMC) model (U.S. Environmental Protection Agency, 1983) is another scoping model developed for urban watersheds that uses a statistical distribution of empirically-derived storm event pollutant concentrations representing a lumped land cover class, together with runoff volume to predict the pollutant load. The EC or EMC models do not consider how spatial arrangement of land cover and landscape features alter nutrient processing in the pollutant loading to surface waters.

Export Coefficient Modeling

The export coefficient (EC) model framework provides a relatively simple, manageable way to predict loading of N and P to an outlet based on the land use of the catchment. Traditionally, models developed to predict changes in N and P loading based on land use changes have been complex, physically based, and developed specifically for the study area of interest (Johnes, 1996). EC models can be easily calibrated based on observed water quality data from catchments composed of varying land uses, or export coefficient values can be derived from literature sources (Johnes, 1996). These EC values represent annual nutrient loads from each land class, expressed in units of mass per area per time.

The total export of nutrient *N* can be expressed using the following equation:

$$L_N = \sum_{i=1}^{M}[E_i * A_i] + P \qquad (1)$$

Where L_N is the basin nutrient load (kg/yr), E_i is the export coefficient (kg/ha/yr) for land class *i*, A_i is the area of the watershed in land class *i*, and *P* represents point sources (Endreny & Wood, 2003; Reckhow & Simpson, 1980).

Due to the lack of spatial consideration of buffering potential, the EC model was modified to include weighting by buffering likelihoods along flowpaths through the landscape. Endreny and Wood [2003] introduced the CADA framework into the EC model to represent the likelihood for runoff and likelihood for buffering downslope for each cell in a gridded watershed of interest. Endreny and Wood [2003] expressed relative potential for runoff using the topographic index, developed by Beven and Kirkby [1979], which represents saturation and runoff likelihood in landscapes. The topographic index, as originally devised by Beven and Kirkby, appears in the following form:

$$TI = \ln\left(\frac{a}{\tan \beta}\right) \qquad (2)$$

where *a* is the upslope contributing area per unit contour length (m) and (tan*β*) is the local surface topographic slope.

Buffering likelihood in the CADA weighted EC model is calculated based on the presence of vegetated buffer strips in the dispersal area from each cell. Dispersal area is calculated by applying the flow accumulation routine in ArcMap to a negated DEM (Endreny & Wood, 2003). This application focuses specifically on particulate phosphorus for simplicity, which proves to be the dominant form in agricultural and

forested runoff, and thus is the focus of mitigation and management efforts (Endreny & Wood, 2003).

The representation of runoff and filtering likelihoods across landscapes has been developed to identify critical pollutant areas in landscapes. In areas without artificial inflows or drainage, runoff likelihood at any watershed location can be represented as a function of the contributing area and local slope (Beven & Kirkby, 1979), and downslope pollutant filtering potential can be represented as a function of exposure to vegetative buffers in the runoff dispersal area (Haycock, 1997). Endreny and Wood [2003] utilized the contributing area and dispersal area (CADA) framework to represent runoff and filtering likelihoods for P in the EC model, based on assumptions of P having primarily shallow subsurface or surface runoff pathways. N loading simulations, however, must consider more transformation processes, pathways, and sinks than P loading simulations (Endreny & Wood, 2003). The complexity of nitrogen sources, sinks, pathways, and transformations introduces challenges in application of this CADA weighted EC model; in particular, the important of landscape denitrification highlights the need to model denitrification areas.

Denitrification

Denitrification, the conversion of nitrate, NO_3^-, to N_2 gas, provides a N sink which removes reactive N permanently from the environment (Robertson & Groffman, 2007). Landscape N mass balance studies demonstrate substantial terrestrial N losses via denitrification, accounting for 51% of N loss in some northeastern U.S. watersheds (Breemen et al., 2002). This provides an opportunity to actively manage landscapes for denitrification, which is dependent on NO_3^- availability, organic carbon availability as

4

energy for heterotrophic denitrifiers, anoxic conditions for the anaerobic denitrifiers, and the presence of denitrifiers (Boyer et al., 2006). Laboratory tests of denitrification potential allow for the identification of landscape locations which have the capacity for substantial NO_3^- removal.

Since soil moisture and soil organic matter have been shown to correlate well with denitrification processes (P.M. Groffman & Crawford, 2003), landscape mapping of high soil moisture and soil organic matter likelihoods may help identify areas of high denitrification potential. Efforts to model landscape denitrification potential have explored the use of topographic controls as a proxy for soil moisture, to simulate suitable anaerobic denitrifying conditions (e.g., Anderson, 2013; Florinsky, McMahon, & Burton, 2004). These studies, however, fail to consider the impact of urban infrastructure on soil moisture likelihoods, including pipe leakage, sewer drainage, and altered physical soil properties (i.e. compaction, urban fill). In addition, contributions of organic matter in urban environments are expected to increase, due to the presence of leaves and eroded soils trapped in gutters, curbs, and swales (Kaushal & Belt, 2012). Strong correlations between denitrification potential and both soil moisture and soil organic matter (Groffman & Crawford, 2003) highlight the need for understanding these variables in urban landscapes.

This research seeks to improve scoping level models to account for variation in biogeochemical cycles in urban environments. The CADA weighting framework has represented spatial variation in P loading, and will be modified and enhanced to represent N loading via runoff and filtration likelihoods, including vegetative buffering and denitrification potential. The simplicity of this model will allow for first-order

estimates of high N and P loading areas on the landscape using widely available datasets, and will help identify critical areas for management and pollutant reduction.

The regulatory drivers of the N and P cycles, altered urban hydrology, and the emergence of a new "urban biogeochemistry" (Kaye et al., 2006), provide context for challenges to modelling N and P loading to surface waters in urban landscapes. In the following section, prior research is used to contextualize questions of N and P transport, as well as denitrification drivers and potential modeling opportunities. Existing landscape-scale denitrification models are discussed to highlight the conditions and processes that drive these models, as well as the framework in which they are used. Urban denitrification studies are evaluated to evaluate correlations between denitrification potential and soil moisture and organic matter. Landscape soil moisture and organic matter trends are reviewed, emphasizing the differences between these two variables in urban and undisturbed landscapes.

Landscape denitrification processes and models

Human activity has accelerated fixation of atmospheric N to plant-available N forms (Vitousek et al., 1997), and increased availability of reactive N has encouraged studies of regional N fate and transport. Breemen et al. [2002] performed such analysis in sixteen large watersheds in the northeastern United States. Landscape denitrification was estimated as the remaining N loss once known input, output and storage terms were considered. Although these landscape denitrification estimates incorporate accumulated uncertainties from other terms, soil denitrification reflects the dominant sink for N inputs to the watersheds, accounting for 34% of total storage and loss on average (Breemen et al., 2002). Regional mass balances are helpful in quantifying the

large magnitude of landscape denitrification occurring, but provide no predictive power or spatial variation in denitrification potentials.

Regional-scale denitrification models vary in complexity and driving factors, as well as in their approach (Boyer et al., 2006). Rather than attempting to model microbial processes and dynamics, these regional models explore environmental conditions in which denitrification is expected to occur. The DAYCENT model (Parton et al., 1996) assumes denitrification is controlled by soil NO_3^- concentration, organic carbon availability, and oxygen availability. The DNDC model (Li, 1996) is a soil biogeochemistry model which utilizes sub-models of soil climate, plant growth, and decomposition to predict soil environmental factors, which drive kinetics of relevant biochemical or geochemical reactions. Agricultural management models often simulate denitrification in soils; one such model is EPIC (J. R. Williams, C. A. Jones, & P. T. Dyke, 1984), which simulates all major N cycling processes in agricultural soils (i.e., mineralization, nitrification, immobilization) on a daily time step. EPIC requires specific field validation to obtain necessary parameters. Like other models, EPIC denitrification processing is governed by the NO_3^- availability, carbon availability, soil temperature, and soil moisture content (Boyer et al., 2006). SWAT (Soil Water Assessment Tool), developed by the United States Department of Agriculture Agricultural Research Service, uses climate, soil, topography, vegetation, and land management data to predict water movement, sediment transport, crop growth, and nutrient cycling. Inputs required for SWAT are extensive, in order to simulate processes in watersheds of varying characteristics. RHESSys (Tague & Band, 2004) couples hydrology with C and N cycling, simulating denitrification through computation of a maximum denitrification

rate (based on available soil nitrate), which is then scaled by soil moisture, temperature, and carbon availability (Tague & Band, 2004). While these models cover a wide range of perspectives and conceptual frameworks (i.e., agricultural, hydrological, ecological), none are explicitly designed for use in urban landscapes, where hydrology and biogeochemistry depend on human inputs and alterations of the system. The models all require extensive knowledge of the specific landscape system being studied, which limits use to highly specialized purposes.

Urban denitrification studies

Field studies are necessary to validate the above models, as well as to understand trends of denitrification as they relate to spatial land use and management patterns. Denitrification is difficult to model at a landscape scale because of the presence of hotspots and hot moments (Groffman et al., 2009; Groffman, 2012), and better predictive capacity requires more field measurements to assess the spatial variation of these disproportionately high nitrate sinks (Groffman et al., 2009). Although there are numerous means of calculating denitrification processes, denitrification potential measurements measure the denitrification enzyme activity (DEA), revealing the biological capacity of soils for denitrification to occur (Groffman et al., 2006). This has proven a useful metric for comparing soil properties in undisturbed forested areas, as well as agricultural or urban landscapes (e.g., Bettez & Groffman, 2012; Bruland, Richardson, & Whalen, 2006; Groffman & Crawford, 2003). These studies focus on the surficial soils (0-10cm), since overland flow is likely to dominate in these urban landscapes.

Studies of DEA in urban riparian zones have demonstrated that urban conditions do not necessarily lead to low denitrification potentials. Much of this work has been focused on the Baltimore Ecosystem Study Long Term Ecological Research Station (BES LTER). A study conducted in watersheds with various levels of disturbance in the Baltimore area demonstrated no significant differences in DEA between urban versus rural, or between forested versus herbaceous sites (Groffman & Crawford, 2003). As long as these soils were wet and with high levels of organic matter, they had high denitrification potentials (Groffman & Crawford, 2003). These correlations are useful in determining methods for identifying key denitrification zones in the landscape of the area of interest.

In another Baltimore LTER study, denitrification potentials were compared between natural riparian areas and stormwater control measures (SCMs), structures designed to mitigate the increased volume and intensity of runoff from urban landscapes (Bettez & Groffman, 2012). Because SCMs are becoming used increasingly in urban areas (i.e. Save the Rain in Syracuse, NY; Green City, Clean Waters in Philadelphia, PA; Green LA in Los Angeles, CA), there is increasing interest in determining their effectiveness in mitigating nutrient loading into receiving waters. Bettez and Groffman found that the SCM denitrification potential was significantly higher than that of the natural riparian areas. Even though the drivers of denitrification potential, soil moisture and organic matter, were similar between the riparian and SCM areas, the SCM DEA values were higher, indicating that SCMs may function as hotspots of denitrification (McClain et al., 2003). The overall effect of these SCMs on water quality at a watershed scale remains uncertain, and variability between different

SCMs in N removal effectiveness is large (Bettez & Groffman, 2012). The unique

conditions in these built SCMs, then, must differ from the natural riparian areas, and the

differences between these structures is important in assessing relative magnitudes of

denitrification within an urban area.

Topographic controls on denitrification

The topographic index is used to predict areas of likely runoff generation, and

therefore maps areas of likely soil wetness across landscapes. A slight variation on the

topographic index presented in Equation 2 is the soil topographic index (STI) (e.g.,

(Agnew et al., 2006; Lyon, Walter, Gérard-Marchant, & Steenhuis, 2004):

$$STI = \ln\left(\frac{T_{avg}a}{\tan(\beta)*T}\right) = TI - \ln(T) + \ln(T_{avg}) \tag{3}$$

where T_{avg} is the mean transmissivity (m^2/day) of the watershed and T is the

transmissivity of the specific cell (Sivapalan, Beven, & Wood, 1987). Transmissivity is

generated through soil databases by multiplying the depth to water table (m) by the

saturated hydraulic conductivity (m/day). As soil datasets become more widely available

(e.g., SSURGO, STATSGO), the hydraulic conductivity and soil depth are incorporated

to assess likelihood of saturation in shallow soils (Agnew et al., 2006; Lyon et al., 2004;

Walter et al., 2002).

The soil topographic index (Eq. 2), which combines many primary denitrification

controls such as 1) upland drainage-area size, 2) depth and permeability of saturated

sediments, and 3) topographic slope, has shown to correlate well with field rates of

denitrification in an agricultural watershed (T. Anderson, 2013). This correlation has not

been proven for urban areas, but proves promising for application in urban areas due to

its applicability in a disturbed, albeit rural, setting. It is important to note that Anderson measured *in situ* denitrification rates, not denitrification potentials.

Nitrate transport to streams

Because urban environments represent a new frontier in ecological and hydrological modeling, nutrient sources and sinks must be identified and further characterized in urban environments (Carey et al., 2013). In the same sixteen northeastern United States watersheds used to produce large-scale N budgets (Breemen et al., 2002), inputs of anthropogenic N were characterized and assessed in their contribution to riverine nitrate (Boyer, Goodale, Jaworski, & Howarth, 2002). This study explored watersheds of varying characteristics and helps quantify N inputs for various distributions of land uses, as human influence becomes more pervasive with regards to nutrient inputs.

Nitrate yield in suburban and urban watersheds has also been shown to be more than 10 times higher than that of completely forested watersheds, and yet retention of N in these disturbed watersheds was surprisingly high, approaching that of forested catchments (Groffman, Law, Belt, Band, & Fisher, 2004). The sources of N in disturbed watersheds, as well as the flowpaths and removal mechanisms in these watersheds, must be linked in order to get a full picture of how we can manage N water quality concerns. The mechanism of transport of nitrate between soil water and surface streamflow in disturbed and undisturbed streams was examined in a review paper by (Sudduth, Perakis, & Bernhardt, 2013), and no pattern or relationship was found for the disturbed stream nitrate concentrations. While we will not be explicitly exploring nitrate pathways in this study, we will attempt to map nitrate throughout the surface landscape

in urban environments, informing where we expect nitrate to concentrate. Further work is necessary to quantify nitrate loading mechanisms in urban watersheds.

This research will enhance understanding of nitrate removal processes in urban environments, and guide management decisions to protect the areas of high removal capacities. It will also help managers by informing placement of green infrastructure, where the confluence of soil moisture and soil organic matter would assist in removal of high nitrate water. This hotspot mapping model will also be incorporated into i-Tree Hydro, giving land managers a parsimonious model which can guide management decisions and help explore alternative scenarios and the impact on nutrient loading.

Research Questions

1)   Land cover specific export coefficients (EC) and event mean concentration (EMC) values for nitrogen do not account for spatial variation in hydrological transport processes in the runoff contributing area and dispersal area (CADA). Can the topographic index theory for runoff likelihood and the buffer index theory for nitrogen filtration likelihood (e.g., uptake, immobilization, transformation) in surface and subsurface flow through natural and constructed buffers (combined soil and vegetation systems) be used to weight land cover specific EC and EMCs to represent the likely spatial variation in nitrogen loading to waterbodies across the landscape?

2)   Models using export coefficients (EC) and event mean concentration (EMC) values fail to represent temporally changing conditions which may explain differences in seasonal and annual nutrient loading. Although temporal variation in nutrient loading has been represented in select catchments of interest through modification of the EC model, a widespread methodology for these analyses has not been developed. The

application of temporal variation has thus far depended on the availability of site-specific data. Can national datasets which represent temporal variation in potential discharge rates be incorporated into a modified EC model to represent changing weather and discharge conditions to better predict annual nutrient loading variation?

3) Soil moisture and soil organic matter have been shown to correlate well with denitrification potential (Groffman & Crawford, 2003). Topographic indices have been used as predictors for denitrification hotspots in agricultural landscapes (T. R. Anderson, Groffman, & Walter, 2015), but have not been developed for mixed-use and urban watersheds. Maps of denitrification potential, approximated by relevant soil variables (e.g., soil moisture, organic matter) are needed to identify key nitrogen-processing areas. Which key soil variables have the largest influence on denitrification potential in urban and mixed-use landscapes, and how can these variables be combined to develop a predictive denitrification model?

Overall, this study seeks to improve the capability of scoping level models to represent variation in nutrient loading both spatially and temporally. Chapter 2 focuses on the inclusion of runoff likelihood and buffering likelihood indices to distribute nutrient loading contributions to pixels based on their landscape orientation. Chapter 3 enhances the Export Coefficient model with daily rainfall data, to represent likely runoff magnitudes and therefore, introduce temporal variation to an otherwise static model. Chapter 4 explores the most influential soil variables in predicting denitrification potential in the mixed-use sampling locations of the Baltimore Long-Term Ecological Research site. These improvements on scoping models enhance nutrient loading predictions without requiring more extensive data collection. The implications of this

research extend to community organizations, planners, and managers seeking a better understanding of the effects of different decisions on water quality. This research will also enhance understanding of nitrate removal processes in urban environments, and guide management decisions to protect the areas of high removal capacities.

References

Agnew, L. J., Lyon, S., Gérard-Marchant, P., Collins, V. B., Lembo, A. J., Steenhuis, T. S., & Walter, M. T. (2006). Identifying hydrologically sensitive areas: Bridging the gap between science and application. *Journal of Environmental Management*, *78*(1), 63–76. https://doi.org/10.1016/j.jenvman.2005.04.021

Anderson, T. (2013). Denitrification In Riparian Zones And Other Saturated Soils Of A Northeastern Agricultural Landscape. Retrieved from http://ecommons.library.cornell.edu/handle/1813/34368

Anderson, T. R., Groffman, P. M., & Walter, M. T. (2015). Using a soil topographic index to distribute denitrification fluxes across a northeastern headwater catchment. *Journal of Hydrology*, *522*, 123–134. https://doi.org/10.1016/j.jhydrol.2014.12.043

Bettez, N. D., & Groffman, P. M. (2012). Denitrification Potential in Stormwater Control Structures and Natural Riparian Zones in an Urban Landscape. *Environmental Science & Technology*, *46*(20), 10909–10917. https://doi.org/10.1021/es301409z

Beven, K. J., & Kirkby, M. J. (1979). A physically based, variable contributing area model of basin hydrology / Un modèle à base physique de zone d'appel variable de l'hydrologie du bassin versant. *Hydrological Sciences Bulletin*, *24*(1), 43–69. https://doi.org/10.1080/02626667909491834

Boyer, E. W., Alexander, R. B., PARTON, W. J., Li, C., Butterbach-Bahl, K., Donner, S. D., … Grosso, S. J. D. (2006). MODELING DENITRIFICATION IN TERRESTRIAL AND AQUATIC ECOSYSTEMS AT REGIONAL SCALES. *Ecological Applications*, *16*(6), 2123–2142. https://doi.org/10.1890/1051-0761(2006)016[2123:MDITAA]2.0.CO;2

Boyer, E. W., Goodale, C. L., Jaworski, N. A., & Howarth, R. W. (2002). Anthropogenic

nitrogen sources and relationships to riverine nitrogen export in the northeastern

U.S.A. *Biogeochemistry*, *57–58*(1), 137–169.

https://doi.org/10.1023/A:1015709302073

Breemen, N. van, Boyer, E. W., Goodale, C. L., Jaworski, N. A., Paustian, K.,

Seitzinger, S. P., … Billen, G. (2002). Where did all the nitrogen go? Fate of

nitrogen inputs to large watersheds in the northeastern U.S.A. *Biogeochemistry*,

57–58(1), 267–293. https://doi.org/10.1023/A:1015775225913

Bruland, G. L., Richardson, C. J., & Whalen, S. C. (2006). Spatial variability of

denitrification potential and related soil properties in created, restored, and paired

natural. *Wetlands*, *26*(4), 1042–1056. https://doi.org/10.1672/0277-

5212(2006)26[1042:SVODPA]2.0.CO;2

Carey, R. O., Hochmuth, G. J., Martinez, C. J., Boyer, T. H., Dukes, M. D., Toor, G. S.,

& Cisar, J. L. (2013). Evaluating nutrient impacts in urban watersheds:

Challenges and research opportunities. *Environmental Pollution*, *173*, 138–149.

https://doi.org/10.1016/j.envpol.2012.10.004

Carpenter, S. R., Caraco, N. F., Correll, D. L., Howarth, R. W., Sharpley, A. N., & Smith,

V. H. (1998). NONPOINT POLLUTION OF SURFACE WATERS WITH

PHOSPHORUS AND NITROGEN. *Ecological Applications*, *8*(3), 559–568.

https://doi.org/10.1890/1051-0761(1998)008[0559:NPOSWW]2.0.CO;2

Conley, D. J., Paerl, H. W., Howarth, R. W., Boesch, D. F., Seitzinger, S. P., Havens, K.

E., … Likens, G. E. (2009). Controlling Eutrophication: Nitrogen and Phosphorus.

Science, *323*(5917), 1014–1015. https://doi.org/10.1126/science.1167755

Endreny, T. A., & Wood, E. F. (2003). Watershed Weighting of Export Coefficients to

    Map Critical Phosphorous Loading Areas1. *JAWRA Journal of the American*

    Water Resources Association, *39*(1), 165–181. https://doi.org/10.1111/j.1752-

    1688.2003.tb01569.x

Florinsky, I. V., McMahon, S., & Burton, D. L. (2004). Topographic control of soil

    microbial activity: a case study of denitrifiers. *Geoderma*, *119*(1–2), 33–53.

    https://doi.org/10.1016/S0016-7061(03)00224-6

Groffman, P. M. (2012). Terrestrial denitrification: challenges and opportunities.

    Ecological Processes, *1*(1), 11. https://doi.org/10.1186/2192-1709-1-11

Groffman, P. M., Altabet, M. A., Böhlke, J. K., Butterbach-Bahl, K., David, M. B.,

    Firestone, M. K., … Voytek, M. A. (2006). METHODS FOR MEASURING

    DENITRIFICATION: DIVERSE APPROACHES TO A DIFFICULT PROBLEM.

    Ecological Applications, *16*(6), 2091–2122. https://doi.org/10.1890/1051-

    0761(2006)016[2091:MFMDDA]2.0.CO;2

Groffman, P. M., Butterbach-Bahl, K., Fulweiler, R. W., Gold, A. J., Morse, J. L.,

    Stander, E. K., … Vidon, P. (2009). Challenges to incorporating spatially and

    temporally explicit phenomena (hotspots and hot moments) in denitrification

    models. *Biogeochemistry*, *93*(1–2), 49–77. https://doi.org/10.1007/s10533-008-

    9277-5

Groffman, P. M., & Crawford, M. K. (2003). Denitrification potential in urban riparian

    zones. *Journal of Environmental Quality*, *32*(3), 1144–1149.

Groffman, P. M., & Crawford, M. K. (2003). Denitrification Potential in Urban Riparian

    Zones. *Journal of Environment Quality*, *32*(3), 1144.

    https://doi.org/10.2134/jeq2003.1144

Groffman, P. M., Law, N. L., Belt, K. T., Band, L. E., & Fisher, G. T. (2004). Nitrogen

    Fluxes and Retention in Urban Watershed. *Ecosystems*, *7*(4), 393–403.

    https://doi.org/10.1007/s10021-003-0039-x

Haycock, N. (1997). *Buffer Zones: Their Processes and Potential in Water Protection :*

    the Proceedings of the International Conference on Buffer Zones, September

    1996. Quest Environmental.

Howarth, R. W., & Marino, R. (2006). Nitrogen as the limiting nutrient for eutrophication

    in coastal marine ecosystems: Evolving views over three decades. *Limnology*

    and Oceanography, *51*(1_part_2), 364–376.

    https://doi.org/10.4319/lo.2006.51.1_part_2.0364

J. R. Williams, C. A. Jones, & P. T. Dyke. (1984). A Modeling Approach to Determining

    the Relationship Between Erosion and Soil Productivity. *Transactions of the*

    ASAE, *27*(1), 0129–0144. https://doi.org/10.13031/2013.32748

Johnes, P. J. (1996). Evaluation and management of the impact of land use change on

    the nitrogen and phosphorus load delivered to surface waters: the export

    coefficient modelling approach. *Journal of Hydrology*, *183*(3–4), 323–349.

    https://doi.org/10.1016/0022-1694(95)02951-6

Kaushal, S. S., & Belt, K. T. (2012). The urban watershed continuum: evolving spatial

    and temporal dimensions. *Urban Ecosystems*, *15*(2), 409–435.

    https://doi.org/10.1007/s11252-012-0226-7

Kaushal, S. S., Groffman, P. M., Band, L. E., Elliott, E. M., Shields, C. A., & Kendall, C. (2011). Tracking Nonpoint Source Nitrogen Pollution in Human-Impacted Watersheds. *Environmental Science & Technology*, *45*(19), 8225–8232. https://doi.org/10.1021/es200779e

Kaye, J. P., Groffman, P. M., Grimm, N. B., Baker, L. A., & Pouyat, R. V. (2006). A distinct urban biogeochemistry? *Trends in Ecology & Evolution*, *21*(4), 192–199. https://doi.org/10.1016/j.tree.2005.12.006

Lewis, W. M., Wurtsbaugh, W. A., & Paerl, H. W. (2011). Rationale for Control of Anthropogenic Nitrogen and Phosphorus to Reduce Eutrophication of Inland Waters. *Environmental Science & Technology*, *45*(24), 10300–10305. https://doi.org/10.1021/es202401p

Li, C. (1996). The DNDC Model. In D. S. Powlson, P. Smith, & J. U. Smith (Eds.), *Evaluation of Soil Organic Matter Models* (pp. 263–267). Springer Berlin Heidelberg. Retrieved from http://link.springer.com/chapter/10.1007/978-3-642-61094-3_20

Lyon, S. W., Walter, M. T., Gérard-Marchant, P., & Steenhuis, T. S. (2004). Using a topographic index to distribute variable source area runoff predicted with the SCS curve-number equation. *Hydrological Processes*, *18*(15), 2757–2771. https://doi.org/10.1002/hyp.1494

McClain, M. E., Boyer, E. W., Dent, C. L., Gergel, S. E., Grimm, N. B., Groffman, P. M., … Pinay, G. (2003). Biogeochemical Hot Spots and Hot Moments at the Interface of Terrestrial and Aquatic Ecosystems. *Ecosystems*, *6*(4), 301–312. https://doi.org/10.1007/s10021-003-0161-9

Parton, W. J., Mosier, A. R., Ojima, D. S., Valentine, D. W., Schimel, D. S., Weier, K., &

  Kulmala, A. E. (1996). Generalized model for N2 and N2O production from

  nitrification and denitrification. *Global Biogeochemical Cycles*, *10*(3), 401–412.

  https://doi.org/10.1029/96GB01455

Reckhow, K. H., & Simpson, J. T. (1980). A Procedure Using Modeling and Error

  Analysis for the Prediction of Lake Phosphorus Concentration from Land Use

  Information. *Canadian Journal of Fisheries and Aquatic Sciences*, *37*(9), 1439–

  1448. https://doi.org/10.1139/f80-184

Robertson, G. P., & Groffman, P. M. (2007). 13 - NITROGEN TRANSFORMATIONS. In

  E. A. Paul (Ed.), *Soil Microbiology, Ecology and Biochemistry (Third Edition)* (pp.

  341–364). San Diego: Academic Press. Retrieved from

  http://www.sciencedirect.com/science/article/pii/B9780080475141500172

Sivapalan, M., Beven, K., & Wood, E. F. (1987). On hydrologic similarity: 2. A scaled

  model of storm runoff production. *Water Resources Research*, *23*(12), 2266–

  2278. https://doi.org/10.1029/WR023i012p02266

Smith, V. H., & Schindler, D. W. (2009). Eutrophication science: where do we go from

  here? *Trends in Ecology & Evolution*, *24*(4), 201–207.

  https://doi.org/10.1016/j.tree.2008.11.009

Sudduth, E. B., Perakis, S. S., & Bernhardt, E. S. (2013). Nitrate in watersheds: Straight

  from soils to streams? *Journal of Geophysical Research: Biogeosciences*,

  118(1), 291–302. https://doi.org/10.1002/jgrg.20030

Tague, C. L., & Band, L. E. (2004). RHESSys: Regional Hydro-Ecologic Simulation

System--An Object-Oriented Approach to Spatially Distributed Modeling of

Carbon, Water, and Nutrient Cycling. *Earth Interactions*, *8*(1), 1–42.

U.S. Environmental Protection Agency, W., DC. (1983). Results of the Nationwide

Urban Runoff Program: Volume 1 - Final Report. Water Planning Division.

Vitousek, P. M., Aber, J. D., Howarth, R. W., Likens, G. E., Matson, P. A., Schindler, D.

W., … Tilman, D. G. (1997). HUMAN ALTERATION OF THE GLOBAL

NITROGEN CYCLE: SOURCES AND CONSEQUENCES. *Ecological*

Applications, *7*(3), 737–750. https://doi.org/10.1890/1051-

0761(1997)007[0737:HAOTGN]2.0.CO;2

Walter, M. T., Steenhuis, T. S., Mehta, V. K., Thongs, D., Zion, M., & Schneiderman, E.

(2002). Refined conceptualization of TOPMODEL for shallow subsurface flows.

Hydrological Processes, *16*(10), 2041–2046. https://doi.org/10.1002/hyp.5030

Young, R. A., Onstad, C. A., Bosch, D. D., & Anderson, W. P. (1989). AGNPS: A

nonpoint-source pollution model for evaluating agricultural watersheds. *Journal of*

Soil and Water Conservation, *44*(2), 168–173.

CHAPTER 2: WEIGHTING NITROGEN AND PHOSPHORUS PIXEL POLLUTANT LOADS TO REPRESENT RUNOFF AND BUFFERING LIKELIHOODS

ABSTRACT: Watershed models often estimate annual nitrogen (N) or phosphorus (P) pollutant loads in rural areas with export coefficients (EC) (kg/ha/yr) values based on land cover, and in urban areas as the product of spatially uniform event mean concentration (EMC) (mg/L) values and runoff volume. Actual N and P nonpoint source (NPS) pollutant loading has more spatial complexity due to watershed variation in runoff likelihood and buffering likelihood along surface and subsurface pathways, which can be represented in a contributing area dispersal area (CADA) NPS model. This research develops a CADA NPS model to simulate how watershed properties of elevation, land cover, and soils upslope and downslope of each watershed pixel influence nutrient loading. The model uses both surface and subsurface runoff indices (RI), and surface and subsurface buffer indices (BI), to quantify the runoff and buffering likelihood for each watershed pixel, and generate maps of weighted EC and EMC values that identify NPS pollutant loading hotspots. The research illustrates how CADA NPS model maps and pixel loading values are sensitive to the spatial resolution and accuracy of elevation and land cover data, and model predictions can represent the lower and upper bounds of NPS loading. The model provides managers with a tool to rapidly visualize, rank, and investigate likely areas of high nutrient export.

KEY TERMS: nonpoint source pollution, watershed management, nutrients, runoff, land use/land cover change, urbanization

INTRODUCTION

Nonpoint source (NPS) pollution is a pervasive water quality problem around the world, delivering excess nitrogen (N) and phosphorus (P) nutrients to rivers, lakes, and estuaries and causing cultural, or accelerated, eutrophication with excessive plant and algae growth (Carpenter et al., 1998; Kaushal et al., 2011). Cultural eutrophication due to N and P runoff from human activities is the primary impairment facing most surface waters today (Smith & Schindler, 2009). To address this impairment and improve aquatic ecosystem health, watershed management programs often seek to identify and then reduce human generated N and P loading (Conley et al., 2009; Lewis, Wurtsbaugh, & Paerl, 2011). Management for NPS runoff must consider that some loading of N and P is required to support aquatic plant and algae growth, and the relative abundance of these limiting nutrients in rivers, lakes, and estuaries is what triggers cultural eutrophication (Conley et al., 2009). Concentrated human activities within urban areas represents a unique problem, both generating complex sources and elevated magnitudes of N and P pollutant runoff (Kaye, Groffman, Grimm, Baker, & Pouyat, 2006) and diminishing interaction between runoff and vegetated land cover that provide nutrient sinks through filtration and transformation (Bettez & Groffman, 2012). Watershed water quality models can assist with NPS identification nutrient loading hotspots, but must balance model accuracy and complexity with data availability and feasibility (e.g., Borah & Bera, 2004; Zhang et al., 2012).

Urban managers seeking spatially distributed, rainfall-runoff watershed models to identify NPS hotspots and predict receiving water loading of N and P often model mixed-use watersheds, comprised of urban, agricultural, and forested land covers. A

variety of tools are available for urban runoff simulation, including the EPA SWMM

(stormwater management model) (Huber, 1995), RHESSys (Regional Hydro-Ecologic

Simulation System) (Tague & Band, 2004) and USDA i-Tree Hydro (Wang, Endreny, &

Nowak, 2008). SWMM simulates the routing of pervious and impervious runoff from

user-defined sub-watersheds into storm sewers, with the option for the user to insert a

best management practices upstream of the storm sewer. The SWMM tool does not use

elevation and land cover data to predict runoff pathways and the intersection of runoff,

pollutants, and filtration, but instead has the user define connections between runoff

sources, treatments, and sinks. RHESSys is a continuous simulation, spatially-

distributed tool using advanced governing equations to represent the hydrologic budget

within a spatially distributed geographic information system (GIS) representation of

watershed elevation and land cover data, operating at a daily time step to predict runoff

generation, flow paths, and N nutrient processes (Tague & Band, 2004). This tool is

typically applied to highly instrumented watersheds, requiring extensive

parameterization, and might be considered a higher order model. By contrast, the i-Tree

Hydro (v5) model is a continuous simulation, statistically-distributed first order, or

parsimonious, model of the hydrologic budget, using the basic governing equations to

predict the distribution of soil saturation and runoff response to rainfall and snowfall for

each hydrologically similar area, defined by the topographic index (Beven & Kirkby,

1979). The i-Tree Hydro model uses nationally available datasets with a database of

location data, including leaf on and off dates, to represent the influence of elevation,

soils, and vegetation on saturation excess and infiltration excess runoff (Wang,

Endreny, & Nowak, 2008). The i-Tree Hydro model, like SWMM, combines the total

surface runoff with Event Mean Concentration (EMC) values (mg/L) to simulate the NPS pollutant load entering receiving waters.

Simulation of rural watershed areas should account for agricultural and forest land cover, and popular continuous simulation, spatially-distributed models include the USDA's SWAT (Soil Water Assessment Tool) (Douglas-Mankin, Srinivasan, & Arnold, 2010), EPA's HSPF (Hydrologic Simulation Program - Fortran) (Donigian, Bicknell, & Imhoff, 1995), and AgNPS (Agricultural NonPoint Source) (Young, Onstad, Bosch, & Anderson, 1989), each developed more than thirty years ago. While these models can represent the spatial heterogeneity of land cover, only AgNPS simulates the effect of runoff flow paths on changes in water quality, with user defined flow paths establishing connectivity between land use types (Fisher, Abrahart, & Herbinger, 1997). An alternative to the higher order, extensively parameterized models (e.g. SWAT, HSPF, AgNPS) is the first order, empirical Export Coefficient model which estimates the watershed annual nonpoint source (NPS) load of N or P, and can use GIS to map and sum the product of land cover type area and the Export Coefficient (EC) value (kg/ha/yr) specified for each land cover type (EPA, 1980; Reckhow & Simpson, 1980).The Export Coefficient model was combined with theory of variable source area hydrology and vegetative filtering of nutrients in the contributing area and dispersal area (CADA) model (Endreny & Wood, 2003). The CADA model used biophysical algorithms to auto-calculate flow paths surrounding each pixel EC value; runoff from the pixel was given a likelihood based on the topographic index, which is the quotient of the contributing area and pixel slope while filtering below the pixel was given a likelihood based on a

buffering index, which is the quotient of dispersal area and flow path slope through land cover types known to buffer NPS pollution.

The CADA EC model predicted which watershed pixels were P loading hotspots using existing terrain and land cover maps and a regional EC dataset. For each land cover pixel, the product of runoff likelihood, buffer likelihood, and EC value provided a weighted EC value, which was mapped across the watershed and summed to provide the total watershed P load (Endreny & Wood, 2003). While the CADA EC model could rapidly identify potential hotspots of P loading, it was not extended to simulate N loading, EMC loads from urban areas, the difference between impervious and pervious runoff likelihood, or the difference in buffer likelihood along subsurface vs surface flow paths, which are important characteristics of mixed-use watersheds.

This paper presents an enhanced CADA NPS model that includes: a) flexibility to use EC, EMC or other NPS loading data for N or P loads; b) representation impervious and pervious runoff paths in the contributing area; and c) representation of surface and subsurface buffer paths in the dispersal. In the methods section the model algorithms and data sources are introduced, and in the results section a sensitivity test is examined that explains model response to differences in the horizontal resolution of the terrain and land cover inputs that are critical in contributing and dispersal area calculations.

MATERIALS & METHODS

Site Description

The watershed used for this study is delineated from Onondaga Creek at Spencer Street (USGS gage 02420010, located at 43°03'27", -76°09'45") and it drains south to north, with headwaters in the Appalachian Plateau reaching an elevation of 587

m, its outlet in the City of Syracuse at an elevation of 110 m (Figure 1). The watershed

has an area of 298 km^2, of which 53 km^2 is classified as developed, and an area of 24.1

km^2 held as sovereign land by the people of the Onondaga Nation. Based on the 2006

NLCD impervious surface maps, only 6% of the study area is designated as impervious

cover, and this is concentrated near the northern watershed outlet (see NLCD classes

21, 22, 23, and 24 in Figure 1). The annual average precipitation for Syracuse, NY is

96.5 cm depth, with an average annual liquid equivalent snowfall of 32 cm, and average

monthly total precipitation ranging between 8.1 and 10.4 cm. The average annual air

temperature is 9.1°C with a February average low of -8.3°C and July average high of

27.8°C. Flow in Onondaga Creek is regulated by an earthen dam near the northern

edge of Onondaga Nation land, designed to allow non-flood flows to pass at grade with

the channel bed through a 2 m diameter concrete culvert; when floods fill the reservoir

behind the dam the culvert constrains maximum discharge to 36 m^3/s.

Model Structure

The enhanced CADA NPS model is built upon the framework of Endreny and

Wood (2003) to create a map of watershed runoff likelihood and buffer likelihood values

using publicly available GIS inputs, which include digital elevation model (DEM) data,

National Land Cover Data (NLCD), Soil Survey Geographic (SSURGO) data, as well as

annual rainfall data and look-up tables of EC and EMC NPS values. The enhanced

CADA model: 1) calculates separate urban and rural NPS pollutant loads for each pixel,

using ECs on rural pixels and EMCs on urban pixels; 2) calculates a separate surface

and subsurface runoff index (RI) for each pixel based on the fraction of imperviousness

and perviousness in each upslope pixel, which is related to an estimate of surface and

subsurface wetness; and 3) calculates a separate surface and subsurface buffer index

(BI) for each pixel based on flow resistance and potential energy, which is related to

runoff velocity and an estimate of NPS buffering. The entire set of pixel specific RI and

BI values are normalized to the watershed mean RI and BI values (or median values,

depending on user preference), and multiplied by the land cover NPS load to quantify

pollutant loading likelihood, which will range from relatively high to low across the

watershed. The updated CADA NPS equations calculate weighted surface and

subsurface NPS loads for each pixel i, $NPS_{surf,i,weighted}$ and $NPS_{sub,i,weighted}$ as:

$$NPS_{surf,i,weighted} = NPS_{surf,i} \times \frac{RI_{surf,i}}{RI_{surf,avg}} \times \frac{BI_{surf,avg}}{BI_{surf,i}} \qquad\qquad 1$$

$$NPS_{sub,i,weighted} = NPS_{sub,i} \times \frac{RI_{sub,i}}{RI_{sub,avg}} \times \frac{BI_{sub,avg}}{BI_{sub,i}} \qquad\qquad 2$$

where NPS_i represents the unweighted NPS load (kg/ha/yr) for land cover type i, RI_i is

the pixel's surface or subsurface runoff index value, the RI_{avg} is the corresponding

average surface or subsurface runoff index in the watershed, the BI_i is the pixel's

surface or subsurface buffer index value, and BI_{avg} is the corresponding average

surface or subsurface buffer index in the watershed. The RI and BI terms in Equation 1

use algorithms specific to subsurface and surface runoff and buffer processes.

Urban and rural, surface and subsurface pollutant loads

Land cover EC values (kg/ha/yr) were obtained from a local Onondaga Creek

study (Coon & Reddy, 2008) as well as from a range of nationally reported values (see

Table 1), while EMC values (mg/L) were obtained from the i-Tree Hydro model, which

compiled data from the USEPA and others (USEPA, 1983; Reckhow, Beaulac, &

Simpson, 1980) (Table 1). The NPS pollutant of P was simulated as total phosphorus

entrained in surface runoff processes, denoted as NPS$_{surf,i}$ in equation 1. The NPS

pollutant of N was simulated as dissolved nitrate in subsurface runoff processes,

denoted as NPS$_{sub,i}$ in equation 2.

EMC values (mg/L) were converted to mass per hectare per year loads NPS$_i$

(kg/ha/yr) by taking the product of the EMC value and estimated annual runoff depth

(m), and accounting for unit conversions. The annual runoff depth was determined using

a modified version of the EPA Simple Method:

$$NPS_i = 10{,}000{\times}P{\times}P_j{\times}R_v{\times}EMC_i \qquad\qquad 3$$

where NPS_i represents the pixel i pollutant load (kg/ha/yr), 10,000 is a unit conversion

factor, P is annual rainfall (m), P_j is fraction of annual rainfall events that cause runoff

(default is 0.9), R_v is the runoff coefficient, and EMC_i is the pixel i pollutant concentration

(mg/L). Uniform EMC values of 0.266 mg/L for TP and 0.666 mg/L for nitrate were used

on each developed NLCD class 21-24, which range from low to high intensity developed

and are concentrated in the city limits (Figure 1); the choice of uniform values is in

keeping with EPA Nationwide Urban Runoff Program (NURP) findings (U.S.

Environmental Protection Agency, 1983). EMC values for a range of land uses can be

found in Table 2; we have chosen to use uniform EMC values reported above due to the

lack of statistical difference between land use types. The CADA model predicts variation

in EMC derived loads (e.g., NPS$_i$) due to variation in the R_v, which were set based on

the fraction of pixel imperviousness (I_a), where $R_v = 0.05 + 0.9(I_a)$ (Schueler, 1987).

The EMC values reported by NURP are lognormally distributed, so we can

determine the 10th (Equation 4) and 90th (Equation 5) percentile values to get a range of

low to high EMC estimates:

$$10_x = \exp\left(\ln(50_x + z_{10} * \sigma)\right) \qquad\qquad 4$$

$$90_x = \exp\left(\ln(50_x + z_{90} * \sigma)\right) \qquad\qquad 5$$

where 50_x is the median EMC value, z is the z-score corresponding to the desired percentile, and σ is the standard deviation for the distribution (in this case, both nitrate and phosphorus had σ ranging from 0.5 to 1, so 0.75 was used).

Runoff indices – surface and subsurface

Surface runoff index

The surface runoff index, $RI_{surf,i}$, is based on the topographic index equation for saturation likelihood (Beven and Kirby, 1979), which was modified to only accumulate for each pixel i its upslope area in impervious cover:

$$RI_{surf,i} = \ln\left(\frac{FA_{imp,i}}{S_{surf,i}}\right) \qquad\qquad 6$$

where $FA_{imp,i}$ is the flow accumulation of impervious area per pixel width, $S_{surf,i}$ is the local pixel surface terrain slope (tan ß, where ß is in degrees). $FA_{imp,i}$ was computed with the ArcGIS flow accumulation function, which uses a flow direction grid, derived from the DEM, to determine the upslope pixels that drain to the local pixel i, and a weighting grid of a scalar values that will be accumulated, or summed, within the upslope area. For $FA_{imp,i}$ the weighting grid was set to total impervious area per pixel width; e.g., an upslope pixel with 10 m x 10 m sides has a contour width of 10 m, and if it had 85% impervious cover, it would contribute 8.5 m = [10 m x 10 m x 0.85]/10 m.

Subsurface runoff index

The subsurface runoff index, $RI_{sub,i}$ is based on the soil topographic index equation for saturation likelihood (Sivapalan, Beven, & Wood, 1987), which was modified to only accumulate for each pixel i its upslope area in pervious cover:

$$RI_{sub,i} = \ln\left(\frac{T_{avg}FA_{imp,i}}{T_i S_{sur,i}}\right) \qquad 7$$

where T_{avg} is the mean transmissivity (m²/day) of the watershed and T_i is the

transmissivity of the specific cell, where transmissivity is defined as the product of

watertable depth and hydraulic conductivity, $FA_{per,i}$ is the flow accumulation of pervious

area per pixel width, and $S_{sub,i}$ is the local subsurface watertable slope (tan ß, where ß

is in degrees). The pixel impervious cover fraction, and its compliment of pervious cover

fraction, was provided by NLCD 2006 data. The pixel transmissivity was provided by

SSURGO data; pixels without SSURGO data, such as the Onondaga Nation in our

study area, set $T_i = T_{avg}$.

Buffering indices – surface and subsurface

Surface buffering index

The surface buffering index is derived as the inverse of travel time from the

source pixel to the receiving water, along a lateral surface flow path that follows the

terrain slopes. Travel time is derived as the quotient of travel length and velocity:

$$\tau_{surf,i} = \frac{l_i}{V_{surf,i}} \qquad 8$$

where *l* (m) is travel path distance across pixel *i*, and V_{surf} (m/s) is the surface runoff

velocity for pixel *i,* computed with the Manning equation:

$$V_{surf} = \frac{C_m}{n} R^{2/3} S^{1/2} \qquad 9$$

where C_m is the Manning coefficient of 1 for SI units (1.486 for BG units), *R* is the

hydraulic radius (m) of flow depth, which varies by land cover (Wurbs & James, 2002,

Table 8.1), *S* is the slope (tan ß, where ß is slope angle) of the surface pixel, and n is

the Manning roughness coefficient (unitless; Table 1, Engman, 1986; Wurbs & James,

2002). The $\tau_{surf,i}$ is set to 0 for all surface water pixels, which are considered receiving waters that have no buffering. The surface buffering index is then calculated as the flow accumulation of travel times for all pixels in the dispersal area:

$$BI_{surf} = FA_{\tau_{surf,i}} \qquad\qquad 10$$

where $FA_{\tau_{surf,i}}$ uses a flow direction grid derived from a negated DEM (i.e., relatively large positive elevations along ridges become large negative elevations, lower than those of relatively small negative elevations within valleys), and a weighting grid of $\tau_{surf,i}$. The BI_{surf} calculation is based on longer travel times equating to greater chances for pollutant removal through a range of biophysical processes, such as particle settling, filtration, decay, uptake and other mechanisms.

Subsurface buffering index

The subsurface buffering index is derived as a function of travel time from the source pixel to the receiving water, along a lateral groundwater flow path that follows the watertable slopes. Travel time is derived as the quotient of travel length and velocity:

$$\tau_{sub,i} = \frac{l_i}{V_{sub,i}} \qquad\qquad 11$$

where l (m) is travel path distance for pixel i, and V_{sub} (m/s) is the subsurface runoff velocity for pixel i, computed with the Darcy equation:

$$V_{sub,i} = -K_i \, {}^{dz_i}\!/_{dl} * 1/p_i \qquad\qquad 12$$

where K_i represents the pixel hydraulic conductivity (m/s), ${}^{dz_i}\!/_{dl}$ represents the watertable gradient across the pixel, where z_i is pixel depth to watertable (m), and p is

the pixel soil porosity. The $\tau_{sub,i}$ is set to 0 for all surface water pixels, which are considered receiving waters that have no buffering. The z_i term was determined as a function of runoff index, similar to the approach used by Endreny & Wood (1999):

$$z_i = \bar{z} - \frac{1}{f}(RI_{sub,i} - RI_{sub,avg}) \qquad\qquad 13$$

where f parameterizes the decay of soil transmissivity with depth, and $\bar{z}$ represents the watershed average depth to watertable, which can be set using expert knowledge, calibration, or using the SSURGO dataset to determine the depth to the restrictive layer, as was done in this study. For the Onondaga Creek watershed, SSURGO reported watertable depths ranged from 36 to 201 cm, and saturated hydraulic conductivity ranged from 1 to 25 cm/hr. The subsurface buffering index is then calculated as the flow accumulation of travel times for all pixels in the subsurface dispersal area:

$$BI_{sub} = FA_{\tau_{sub,i}} \qquad\qquad 14$$

where the $FA_{\tau_{sub,i}}$ algorithm uses flow directions derived from a negated watertable elevation map and a weighting grid of $\tau_{sub,i}$. The BI_{sub} calculation is based on longer travel times equating to greater chances for pollutant removal through a range of biophysical processes, such as particle filtration, decay, uptake and other mechanisms.

CADA model sensitivity tests

The CADA model predictions of N and P loading were tested for sensitivity to the spatial resolution of elevation and land cover inputs and the selection of EC and EMC values. Elevation and land cover are the data principal inputs for computation of the RI and BI terms in Equations 6, 7, 10 and 14. The spatial resolution of elevation and land cover was varied within a 4.2 ha sewershed in the City of Syracuse that had been

surveyed using high resolution airborne remote sensing to acquire elevation maps with 0.3 m horizontal resolution and 0.01 m vertical accuracy, and land cover maps at 0.3 m horizontal resolution classified into tree cover, pervious grass cover, and impervious cover. The 0.3 m resolution elevation and land cover inputs were resampled into coarser 1 and 10 m resolution products, representing resolutions that contain sub-grid heterogeneity within an urban landscape of crowned roads, curbs, herbaceous lawns, trees, sidewalks, and buildings. While the CADA runs required that SSURGO data be resampled into corresponding grids of 0.3, 1, and 10 m resolution, the initial SSURGO polygon areas were all larger than 100 m^2, and there was no loss of soil information moving between 0.3 and 10 m grid sizes. Using a fixed 10 m resolution for all inputs, the CADA model was also run with 3 different combinations of pixel NPS inputs, using EC values for all urban and rural pixels, EMC values for all urban and rural pixels, and EC values for rural pixels and EMC values for urban pixels.

RESULTS & DISCUSSION

Urban and rural, surface and subsurface pollutant loads

The spatial distribution and total watershed load of CADA predicted P and N values are highly sensitive to the selection of pixel NPS inputs. The spatial distribution of weighted P and N loads for each pixel have heterogeneity in rural areas and more uniformity in urban areas when CADA was run with a combination of EC and EMC values (Figure 2 A and D), while P and N loads were more uniform throughout the watershed when CADA was run with EC values (Figure 2 B and E), and P and N loads were more heterogeneous when CADA was run with EMC values (Figure 2 C and F). The CADA predicted watershed P load was 14.9 tonne/yr when estimated by the

34

combination of EC and EMC values, slightly climbed to 15.6 tonne/yr when estimated with only EC values, and significantly dropped to 6.7 tonne/yr when estimated by only EMC values; the high and low P load range spanned 60% of the P load estimated by the load estimated by the combination of EC and EMC values. The CADA predicted watershed N load was 152.4 tonnes/yr when estimated by the combination of EC and EMC values, dropped to 138.9 tonnes/yr when estimated by only EC values, and climbed to 178.2 tonnes/yr when estimated by only EMC values; the high and low N load range spanned 25% of the N load estimated by the combination of EC and EMC values. For the CADA simulation using EC and EMC data, the 17.6% of the watershed area classified as developed land received EMC inputs, and EC inputs were applied to the remaining watershed area, and account for the majority of the P and N watershed loads. The 60% variation in CADA estimated P loads vs a 25% variation in N loads is explained by the large variation in P EMC and EC inputs vs N EMC and EC inputs (Table 1).

Use of EC input values for CADA estimates of NPS loads is recommended for rural land cover pixels, while EMC input values are recommended for NPS loads in urban land cover pixels. When EC inputs where used to estimate NPS loads on urban pixels (NLCD 21-24, Figure 1), the CADA model predicted fewer P loading hotspots in those urban areas than when hotspots were predicted using EMC inputs, where hotspots are defined as red colored pixels with a NPS P load >3.3 kg/ha/yr; this contrast in hotspots is illustrated in Figure 2 B and C within the City of Syracuse polygon at the north end of the watershed. By contrast, the EC input values led to higher P estimates for rural agricultural pixels (NLCD 81 and 82, Figure 1) than estimated with EMC input

values, which is noted by more yellow and orange colored pixels with a NPS P load

>1.3 kg/ha/yr (see Figure 2 B and C, to the south of the City of Syracuse, along

Onondaga Creek tributaries). For CADA estimates of NPS N loads, the EC input values

led to lower N loads on urban pixels than N loads estimated by the EMC input values,

which is noted by fewer yellow colored pixels (>5.4 kg/ha/yr) in the City of Syracuse

(Figure 2 E and F). The EC input values led to higher estimates of NPS N loads for rural

agricultural pixels than N loads estimated with EMC input values, noted by more orange

and red pixels (>9.1 kg/ha/yr) along the headwater tributaries. Due to the small variation

in impervious cover and the associated runoff coefficient, R_v, there was little spatial

variation in CADA estimated P and N loads for rural areas when EMC input values were

used (see large area in blue color with 0-0.5 kg/ha/yr of P in Figure 2E, and large area

in yellow color with 5.4-9.1 kg/ha/yr of N in Figure 2F). By contrast, when EC input

values were used, loading was not sensitive to the R_v, but instead correlated strongly

with land cover classes; note the greater heterogeneity with EC-based loads than EMC-

based loads in the southern watershed (Figure 2 E vs F). The CADA model estimates of

NPS N and P loads in this case were more sensitive to EMC and EC inputs than to

buffering processes in the runoff distribution area.

The accuracy of CADA predicted NPS loads was constrained by the first-order

and parsimonious nature of the model equations and by our choice to not calibrate the

model inputs of EC or EMC or vary inputs across years. In a test of accuracy, the CADA

predicted P load using a combination of EC and EMC inputs was 25% above the

observed 11.16 tonne/yr load, while the CADA predicted N load was 6.6% below the

observed 162.5 tonne/yr load. These observed loads represent a 6 year average,

obtained using water quality and discharge data collected by the USGS at the Onondaga Creek Spencer Street USGS gage between October 1, 1997 and September 30, 2003 as part of the Onondaga County Ambient Monitoring Program (Coon & Reddy, 2008). The USGS used these observed loads to derive EC input values, which were within the range provided by the national datasets (Table 1). While most watersheds will not have observed loads to calibrate the EC and EMC datasets, the CADA model remains a useful tool for estimating a range of possible NPS loads. Ranges of loads were also calculated, using the lowest and highest EC values from Table 1 combined with the 10th and 90th percentiles of EMC values (Equations 4 and 5), respectively. The results showed that for the lowest values scenario, we observed 59.9 tonne/year and 3.3 tonne/year loads for N and P, respectively. The highest value scenario resulted in 313.3 tonne/year and 108.1 tonne/year loads for N and P, respectively. These ranges provide bounds for minimum and maximum loading expected over different years. Based on the Onondaga Lake Ambient Monitoring Program, managed through the Onondaga County Department of Water Environment Protection, the range of loading values from Onondaga Creek to Onondaga Lake is 140-220 tonnes/year for nitrate and 11-25 tonnes/year for phosphorus. We recommend using the model with a range of feasible input values for each pixel, varying EC and EMC (see Table 1 ranges), as well as varying R_v, R, n, T, and other terms in order to capture input uncertainty and provide an upper and lower bound for estimated NPS loads.

Runoff indices – surface and subsurface

The spatial distribution of the surface runoff index and subsurface runoff index reflect the impact of contributing areas to the CADA estimated NPS loads. Both runoff

indices use contributing area and as a result they generally reflect an increasing

likelihood for runoff with proximity to the stream network; however, there are regions

where RI_{surf} varies significantly from RI_{sub}. In the urban areas, such as those in the

northern end of the Onondaga Creek watershed, the RI_{surf} tended toward higher values

(blue colored pixels, Figure 3A), while the RI_{sub} had lower values (green and yellow

colored pixels, Figure 3B), which captures the effect of imperviousness partitioning

precipitation into overland flow. By contrast, rural land cover will have greater

perviousness and partition precipitation into subsurface flow, generating relatively low

RI_{surf} values (see yellow to orange color pixels in the rural southern watershed region,

Figure 3A) and relatively high RI_{sub} values (see green colored higher pixels in the rural

southern watershed region, Figure 3B). The spatial differences between RI_{sub} and RI_{surf}

are also due to the RI_{sub} calculation using soil transmissivity and watertable elevation

data, while the RI_{surf} used surface elevation data. The mean RI_{sub} value was 8.4, 50%

higher, in natural log space, than the mean RI_{surf} value of 5.6. The significantly larger

RI_{sub} value is attributed to the much larger watershed area in pervious cover, estimated

at 94%, and as a result the Onondaga Creek watershed RI_{sub} values correspond with

reported ranges for neighboring, predominantly rural, Finger Lakes region catchments

(e.g., Anderson, Groffman, & Walter, 2015).

Buffer indices – surface and subsurface

The spatial distribution of surface runoff velocities (Figure 4A) and subsurface

runoff velocities (Figure 4B) largely regulate the corresponding BI_{surf} and BI_{sub}. Road

networks have the lowest Manning n roughness values, which create a signature

pattern of high surface velocities where roads contrast with non-road pixels (see linear

bands of red colored pixels in the mid to southern sections of the watershed, and swaths in the City of Syracuse in Figure 4A). The predicted surface velocities ranged from 0.0002 m/s to 1.7 m/s, with the upper limits agreeing with values expected for runoff over roads. The predicted subsurface velocities were two orders of magnitude lower than surface velocities, and correspond to residence times of days to years for flow through the watershed. Slope had a large influence on velocity, and in a west to east transect across the urban area in the north of the watershed, the surface velocities are at their lowest in the center of the transect corresponding to the urban floodplain despite a dense network of roads (see blue colored pixels bounded by red colored pixels in Figure 4A). By contrast, the subsurface velocities are not influenced by roads and are relatively low values in the northern urban area; they are highest in the mid to southern sections of the watershed along the steep valley walls bounding Onondaga Creek (Figure 4B); the valley is glacially carved and has classic U-shaped valley walls.

The BI_{surf} and BI_{sub} values were often highest at the two geographic extremes of watershed ridges and valleys or floodplains (see Figures 5A and B). The ridges corresponded with the greatest flow path distances to the receiving waters, and hence relatively long travel times, while the valleys and floodplains corresponded with relatively flat slopes and long travel times. In addition to flow path length and slope, the BI_{surf} is also affected by the vegetative cover in the dispersal area flow path. When urban stormwater management involves efforts to slow down surface runoff, the dispersal area can be planted in higher roughness land cover types to reduce increase the likelihood for pollutant buffering and reduce NPS loading. In efforts to reduce subsurface loading, management options may include creation of higher transmissivity

preferential flow paths to guide runoff into treatment cells, perhaps with aeration or biological treatment, as envisioned by Vaux (1968) for improving aquatic conditions.

Impacts of elevation and land cover spatial resolution

The CADA NPS model predictions of P and N loading hotspots were highly sensitive to the spatial resolution of elevation and land cover. The outputs of P and N hotspots predicted with 0.3 m and 1 m horizontal resolution inputs captured the pattern of roads and houses in the 14 ha sewershed (Figure 6A and B), while the 10 m resolution did not capture road patterns and only weakly captured houses (Figure 6C). The even coarser 30 m spatial resolution inputs from NLCD are likely the most common resolution for land cover data, and clearly would not capture spatial patterns of the urban landscape missed by the 10 m data. Maps of predicted NPS loading can guide managers toward watershed areas in need of runoff control measures, and to capture the influence of urban landscape features such as roads and houses, the 1 m or finer resolution data are recommended for CADA simulations. The confidence in the CADA model predicted hotspots, defined as disproportionately high P or N loads, and their opposite, coldspots, can be quantified with the Getis-Ord statistic at values of 95% (Table 3). The Getis-Ord statistic, for both hotspots and coldspots, differentiates statistically significant clusters of high or low valued pixels from pixel clusters that may are randomly organized (Getis-Ord < 95%). The patterns of Getis-Ord hotspots and coldspots corresponded with the road network within the 14 ha watershed, noted in the simulation using 0.3 m resolution input data (Figure 6D), but less so for the 1 m and 10 m resolution simulations (Figure 6E and F). At a 0.3 m resolution, a total of 49.7% of the sewershed fell within hotspots or coldspots with >95% confidence; the percentage drops

down to 28% and 3.8% for resolutions of 1 m and 10 m, respectively. This trend is explained by the coarser inputs causing a blending of otherwise distinct boundaries between land cover, thereby generating fewer differences in pixel P and N loading values. With finer input resolution, there is more opportunity for the CADA NPS model to confidently predict the spatial variation of P and N hotspot and coldspot clusters.

The pixel NPS loads also changed significantly with the resolution of the CADA input data of elevation and land cover. The CADA predicted a maximum pixel N load of 11.7 kg/ha/yr for the 0.3 m resolution simulation, and this maximum pixel N load decreased by 35% to 7.6 kg/ha/yr for the 10 m resolution simulation (Figure 7A and C). As elevation and land cover input resolution coarsened beyond 1 m, there was a reduction in maximum pixel NPS load values and a lowering of the Getis-Ord confidence in the hotspots, and coldspots, pixel clusters. The CADA model predictions of watershed NPS load, defined as the sum of all pixel NPS loads, had less sensitivity to the spatial resolution of elevation and land cover in the sewershed simulations. Despite pixel load sensitivity for CADA simulations of P, the watershed P load only varied by 0.7% between the simulations using 0.3 and 10 m inputs. The 0.3m resolution inputs of elevation and land cover generated watershed P loads of 1.51 kg/yr, while the 10m resolution inputs generated 0.7% larger watershed P loads. Despite the sensitivity of maximum pixel NPS loads to input resolution, the watershed N load from the sewershed did not vary significantly with input resolution. The 0.3 m simulation generated a CADA predicted watershed N load of 16.93 kg/yr, while the 1 m and 10 m simulations generated watershed N loads within 1%, at 16.72 kg/yr and 16.53 kg, respectively.

The CADA predicted pixel P and N loads (Figure 2A and D) were based on the RI_{surf} , RI_{sub} , BI_{surf}, and BI_{sub} values, which are regulated by Manning and Darcy velocity equations 9 and 12 and very sensitive to slope values calculated by the ArcGIS method. For each pixel, the CADA model calculated the slopes to each of the 8 neighboring pixels, and selected the steepest slope for the velocity calculations, but this may not necessarily be the actual flow path for runoff in urban areas where sub-grid elevation heterogeneity such as curbs and gutters and riffles may regulate flow slopes. In land cover classes designated as urban, the CADA slope calculations were constrained to a maximum slope of 6%, in order to ensure road slopes are within the recommended maximum (American Association of State Highway and Transportation, 2011), and runoff velocities along roads were not excessively rapid. In cases where higher slopes do exist, flow would likely become unsteady and depart from Manning assumptions, which would require alternative, perhaps hydraulic-based, estimates for velocity.

SUMMARY & CONCLUSIONS

This research enhanced the CADA NPS model to achieve three goals in watershed simulation of nutrient hotspot mapping: a) flexibility to use EC, EMC or other NPS loading data for N or P loads; b) representation impervious and pervious runoff paths in the contributing area; and c) representation of surface and subsurface buffer paths in the dispersal area. These updates are critical for the co-management of P and N, which often occur in the surface and subsurface runoff flowpaths at different proportions. Historically, freshwater systems have been assumed P limited, due to the abundance of N in freshwater via N fixing cyanobacteria (Conley et al., 2009). Therefore, many freshwater management efforts have focused more on P than N.

However, the urban biogeochemistry of complex social-infrastructure-environmental interactions result in elevated nutrient concentrations along accelerated flow paths with a high level of apparently random individual decisions affecting receiving water quality (Kaye et al., 2006). Nutrient loads to urban receiving waters have been shown to have lower N:P ratios, which results in N as the limiting nutrient to eutrophication (Howarth & Marino, 2006). Coastal receiving waters are N limited (Nixon, 1995), and urban and rural drainage with elevated N loads, from sanitary waste, agricultural runoff, and other sources, also accelerates eutrophication in coastal systems. The enhanced CADA NPS model allows for simulation of urban and rural pollutant sources from mixed land use watersheds, and the surface and subsurface runoff pathways connecting this pollution with contributing area and dispersal area processes, providing an important management tool for inland and coastal communities.

The enhanced CADA NPS model provides spatial maps of the weighted EC and EMC hotspots and coldspots contributing to watershed nutrient loads, and allows managers to differentiate between interventions that reduce surface transported pollutants, such as particulate phosphorus, from interventions targeting subsurface transported pollutants, such as dissolved nitrate. While the spatial maps and provide a first order estimate of loading hotspots, they do not represent the uncertainty in the predictions and users should run CADA NPS with low and high values of EC and EMC inputs to simulate a range of possible NPS loads, which are more likely to capture the observed loading value for the pixel and the watershed (Theodore A. Endreny & Wood, 2003). One proposed update for the CADA NPS model includes simulation of denitrification as a nutrient removal process, to better represent the spatial dependency

between organic matter, moisture, and losses of nitrate in the landscape (Sudduth, Perakis, & Bernhardt, 2013). Another proposed update for the CADA NPS model is to provide storm-based temporal variation in load estimates, allowing for managers to examine loading sensitivity to storm intensity, which is sensitive to climate change, and where rain drop splash intensity and pollutant displacement might be managed by vegetative cover. Each of these proposed updates would strive to keep CADA NPS a parsimonious first order model that uses available datasets, and facilitates its use in many watershed projects evaluating how changes in land cover might affect the distribution of nutrients in the landscape and loads to receiving waters.

ACKNOWLEDGMENTS

LITERATURE CITED

American Association of State Highway and Transportation. (2011). *A Policy on Geometric Design of Highways and Streets, 2011*. AASHTO.

Anderson, T. R., Groffman, P. M., & Walter, M. T. (2015). Using a soil topographic index to distribute denitrification fluxes across a northeastern headwater catchment. *Journal of Hydrology*, *522*, 123–134. http://doi.org/10.1016/j.jhydrol.2014.12.043

Bettez, N. D., & Groffman, P. M. (2012). Denitrification Potential in Stormwater Control
Structures and Natural Riparian Zones in an Urban Landscape. *Environmental
Science & Technology*, *46*(20), 10909–10917. http://doi.org/10.1021/es301409z

Beven, K. J., & M. J. Kirkby. (1979). A physically based, variable contributing area
model of basin hydrology. *Hydrological Sciences Bulletin*, *24*(1), 43–69.
http://doi.org/10.1080/02626667909491834

Borah, D. K., & Bera, M. (2004). Watershed-scale hydrologic and nonpoint-source
pollution models: review of applications. *Trans. ASAE*, *47*, 789–803.

Carpenter, S. R., Caraco, N. F., Correll, D. L., Howarth, R. W., Sharpley, A. N., & Smith,
V. H. (1998). NONPOINT POLLUTION OF SURFACE WATERS WITH
PHOSPHORUS AND NITROGEN. *Ecological Applications*, *8*(3), 559–568.
http://doi.org/10.1890/1051-0761(1998)008[0559:NPOSWW]2.0.CO;2

Conley, D. J., Paerl, H. W., Howarth, R. W., Boesch, D. F., Seitzinger, S. P., Havens, K.
E., … Likens, G. E. (2009). Controlling Eutrophication: Nitrogen and Phosphorus.
Science, *323*(5917), 1014–1015. http://doi.org/10.1126/science.1167755

Coon, W. F., & Reddy, J. E. (2008). *Hydrologic and water-quality characterization and
modeling of the Onondaga Lake Basin, Onondaga County, New York*. US
Geological Survey.

Donigian, A. S., Jr., Bicknell, B. R., & Imhoff, J. C. (1995). Hydrological Simulation
Program - Fortran (HSPF)., 395–442.

Douglas-Mankin, K. R., Srinivasan, R., & Arnold, J. G. (2010). SOIL AND WATER
ASSESSMENT TOOL (SWAT) MODEL: CURRENT DEVELOPMENTS AND
APPLICATIONS. *Transactions of the ASABE*, *53*(5), 1423–1431.

Endreny, T. A., & Wood, E. F. (1999). Distributed Watershed Modeling of Design

      Storms to Identify Nonpoint Source Loading Areas. *Journal of Environment*

      Quality, *28*(2), 388. http://doi.org/10.2134/jeq1999.00472425002800020004x

Endreny, T. A., & Wood, E. F. (2003). Watershed Weighting of Export Coefficients to

      Map Critical Phosphorous Loading Areas1. *JAWRA Journal of the American*

      Water Resources Association, *39*(1), 165–181. http://doi.org/10.1111/j.1752-

      1688.2003.tb01569.x

Engman, E. (1986). Roughness Coefficients for Routing Surface Runoff. *Journal of*

      Irrigation and Drainage Engineering, *112*(1), 39–53.

      http://doi.org/10.1061/(ASCE)0733-9437(1986)112:1(39)

Fisher, P., Abrahart, R. J., & Herbinger, W. (1997). The Sensitivity of Two Distributed

      Non-Point Source Pollution Models to the Spatial Arrangement of the Landscape.

      Hydrological Processes, *11*(3), 241–252. http://doi.org/10.1002/(SICI)1099-

      1085(19970315)11:3<241::AID-HYP438>3.0.CO;2-T

Howarth, R. W., & Marino, R. (2006). Nitrogen as the limiting nutrient for eutrophication

      in coastal marine ecosystems: Evolving views over three decades. *Limnology*

      and Oceanography, *51*(1_part_2), 364–376.

      http://doi.org/10.4319/lo.2006.51.1_part_2.0364

Huber, W. C. (1995). EPA Storm Water Management Model - SWMM., 783–808.

Kaushal, S. S., Groffman, P. M., Band, L. E., Elliott, E. M., Shields, C. A., & Kendall, C.

      (2011). Tracking Nonpoint Source Nitrogen Pollution in Human-Impacted

      Watersheds. *Environmental Science & Technology*, *45*(19), 8225–8232.

      http://doi.org/10.1021/es200779e

Kaye, J. P., Groffman, P. M., Grimm, N. B., Baker, L. A., & Pouyat, R. V. (2006). A

distinct urban biogeochemistry? *Trends in Ecology & Evolution*, *21*(4), 192–199.

http://doi.org/10.1016/j.tree.2005.12.006

Lewis, W. M., Wurtsbaugh, W. A., & Paerl, H. W. (2011). Rationale for Control of

Anthropogenic Nitrogen and Phosphorus to Reduce Eutrophication of Inland

Waters. *Environmental Science & Technology*, *45*(24), 10300–10305.

http://doi.org/10.1021/es202401p

Modeling Phosphorus Loading and Lake Response Under Uncertainty: A Manual and

Compilation of Export Coefficients | US EPA. (1980).

Nixon, S. W. (1995). Coastal marine eutrophication: A definition, social causes, and

future concerns. *Ophelia*, *41*(1), 199–219.

http://doi.org/10.1080/00785236.1995.10422044

Reckhow, K. H., & Simpson, J. T. (1980). A Procedure Using Modeling and Error

Analysis for the Prediction of Lake Phosphorus Concentration from Land Use

Information. *Canadian Journal of Fisheries and Aquatic Sciences*, *37*(9), 1439–

1448. http://doi.org/10.1139/f80-184

Schueler, T. R. (1987). Controlling Urban Runoff: A Practical Manual for Planning and

Designing Urban BMPs. *Metropolitan Washington Council of Governments*.

Sivapalan, M., Beven, K., & Wood, E. F. (1987). On hydrologic similarity: 2. A scaled

model of storm runoff production. *Water Resources Research*, *23*(12), 2266–

2278. http://doi.org/10.1029/WR023i012p02266

Smith, V. H., & Schindler, D. W. (2009). Eutrophication science: where do we go from

      here? *Trends in Ecology & Evolution*, *24*(4), 201–207.

      http://doi.org/10.1016/j.tree.2008.11.009

Sudduth, E. B., Perakis, S. S., & Bernhardt, E. S. (2013). Nitrate in watersheds: Straight

      from soils to streams? *Journal of Geophysical Research: Biogeosciences*,

      118(1), 291–302. http://doi.org/10.1002/jgrg.20030

Tague, C. L., & Band, L. E. (2004). RHESSys: Regional Hydro-Ecologic Simulation

      System--An Object-Oriented Approach to Spatially Distributed Modeling of

      Carbon, Water, and Nutrient Cycling. *Earth Interactions*, *8*(1), 1–42.

U.S. Environmental Protection Agency, W., DC. (1983). Results of the Nationwide

      Urban Runoff Program: Volume 1 - Final Report. Water Planning Division.

Vaux, W. G. (1968). Intergravel Flow and Interchange of Water in a Streambed. *Fishery*

      Bulletin, *66*(3), 479–489.

Wang, J., Endreny, T. A., & Nowak, D. J. (2008). Mechanistic Simulation of Tree Effects

      in an Urban Water Balance Model1. *JAWRA Journal of the American Water*

      Resources Association, *44*(1), 75–85. http://doi.org/10.1111/j.1752-

      1688.2007.00139.x

Wurbs, R. A., & James, W. P. (2002). *Water Resources Engineering* (1st ed.). Prentice

      Hall.

Young, R. A., Onstad, C. A., Bosch, D. D., & Anderson, W. P. (1989). AGNPS: A

      nonpoint-source pollution model for evaluating agricultural watersheds. *Journal of*

      Soil and Water Conservation, *44*(2), 168–173.

Zhang, T., Soranno, P. A., Cheruvelil, K. S., Kramer, D. B., Bremigan, M. T., &

    Ligmann-Zielinska, A. (2012). Evaluating the effects of upstream lakes and

    wetlands on lake phosphorus concentrations using a spatially-explicit model.

    Landscape Ecology, *27*(7), 1015–1030. http://doi.org/10.1007/s10980-012-9762-

    z

TABLES

Table 1: Export coefficients for land uses

NLCD Class	Land Use Description	Area (ha)	Locally derived EC value – TP (kg/ha/yr)	Locally derived EC value – Nitrate (kg/ha/yr)	EC TP range (kg/ha/yr)	EC Nitrate range (kg/ha/yr)
11	Open Water	86	0.00	0.00	----	----
21	Developed, Open Space	1876	0.86	1.79	----	----
22	Developed, Low Intensity	1626	0.54	2.35	----	----
23	Developed, Medium Intensity	1251	0.54	2.35	----	----
24	Developed, High Intensity	513	1.15	4.93	----	----
31	Barren Land(Rock/Sand/Clay)	66	0.86	1.79	.19 – 6.23	.49 – 3.0
41	Deciduous Forest	9132	0.10	3.70	.019 - .830	.59 – 4.6
42	Evergreen Forest	312	0.10	3.70	.019 - .830	.59 – 4.6
43	Mixed Forest	728	0.10	3.70	.019 - .830	.59 – 4.6
52	Shrub/Scrub	2798	0.10	3.70	.019 - .830	.59 – 4.6
71	Grassland/Herbaceous	183	0.10	3.70	.019 - .830	.59 – 4.6
81	Pasture/Hay	6163	0.28	6.50	.14 - 4.90	4.6 – 20.4
82	Cultivated Crops	3185	2.37	12.44	.10 - 18.6	4.6 – 20.4
90	Woody Wetlands	1835	0.05	0.34	.05 - .21	----
95	Emergent Herbaceous Wetlands	83	0.05	0.34	.05 - .21	----

Table 2: Median event mean concentrations for urban land uses (U.S. Environmental Protection Agency, 1983)

Pollutant	Units	Residential	Mixed	Commercial	Open/Non-Urban
BOD	mg/l	10	7.8	9.3	--
COD	mg/l	73	65	57	40
TSS	mg/l	101	67	69	70
Total Lead	µg/l	144	114	104	30
Total Copper	µg/l	33	27	29	--
Total Zinc	µg/l	135	154	226	195
Total Kjeldahl Nitrogen	µg/l	1900	1288	1179	965
Nitrate + Nitrite	µg/l	736	558	572	543
Total Phosphorus	µg/l	383	263	201	121
Soluble Phosphorus	µg/l	143	56	80	26

Table 3: Percentage of sewershed falling in hotspots and coldspots above 95% confidence

Resolution	Percent in 95-99% Coldspot		Percent in 95-99% Hotspot	
	Nitrate	TP	Nitrate	TP
0.3m	29.4%	4.4%	20.3%	2.2%
1m	14.8%	0.2%	13.2%	1.8%
10m	0.0%	0.0%	3.8%	1.3%

FIGURES
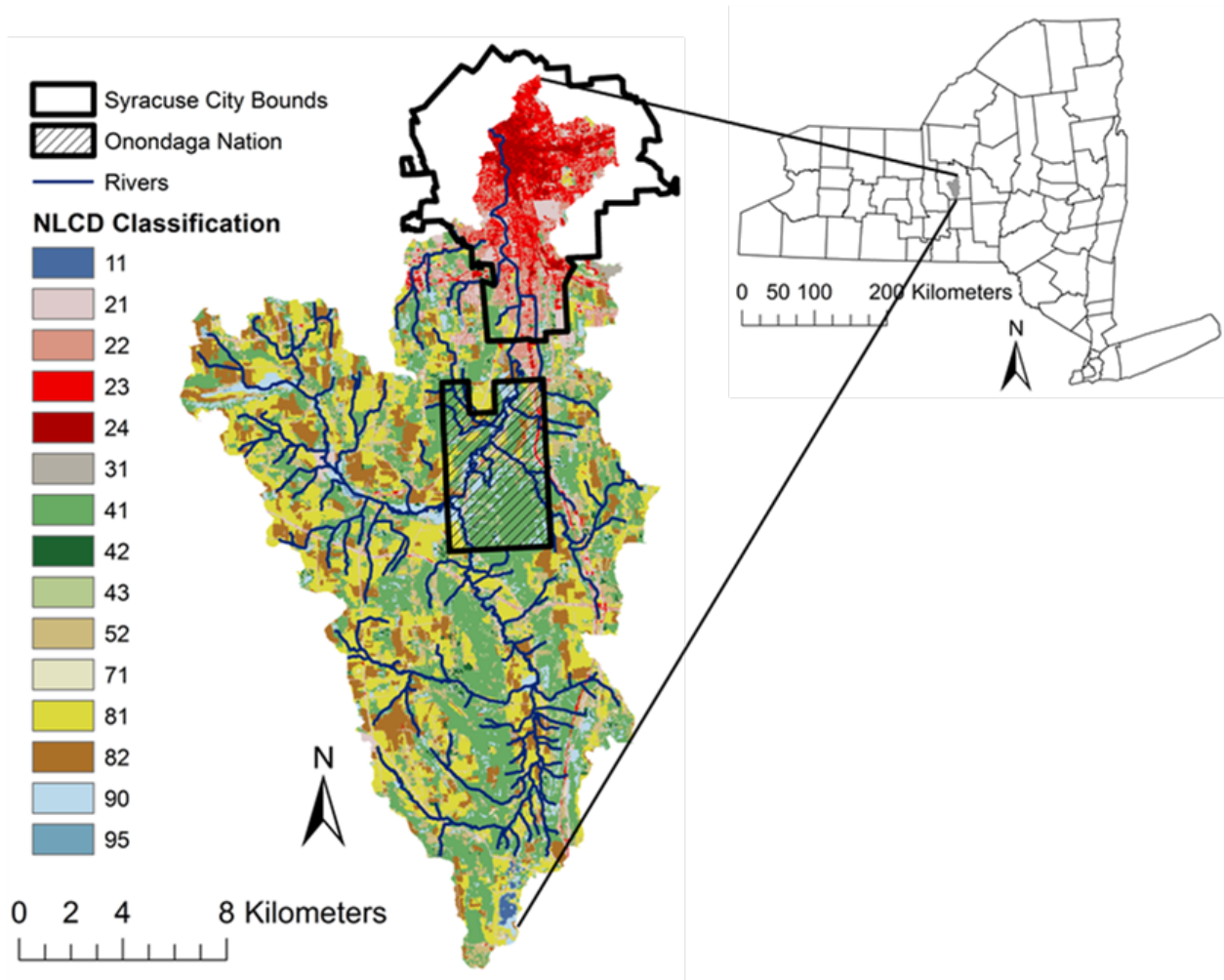
Figure 1: Site map for Onondaga Creek watershed at Spencer St.
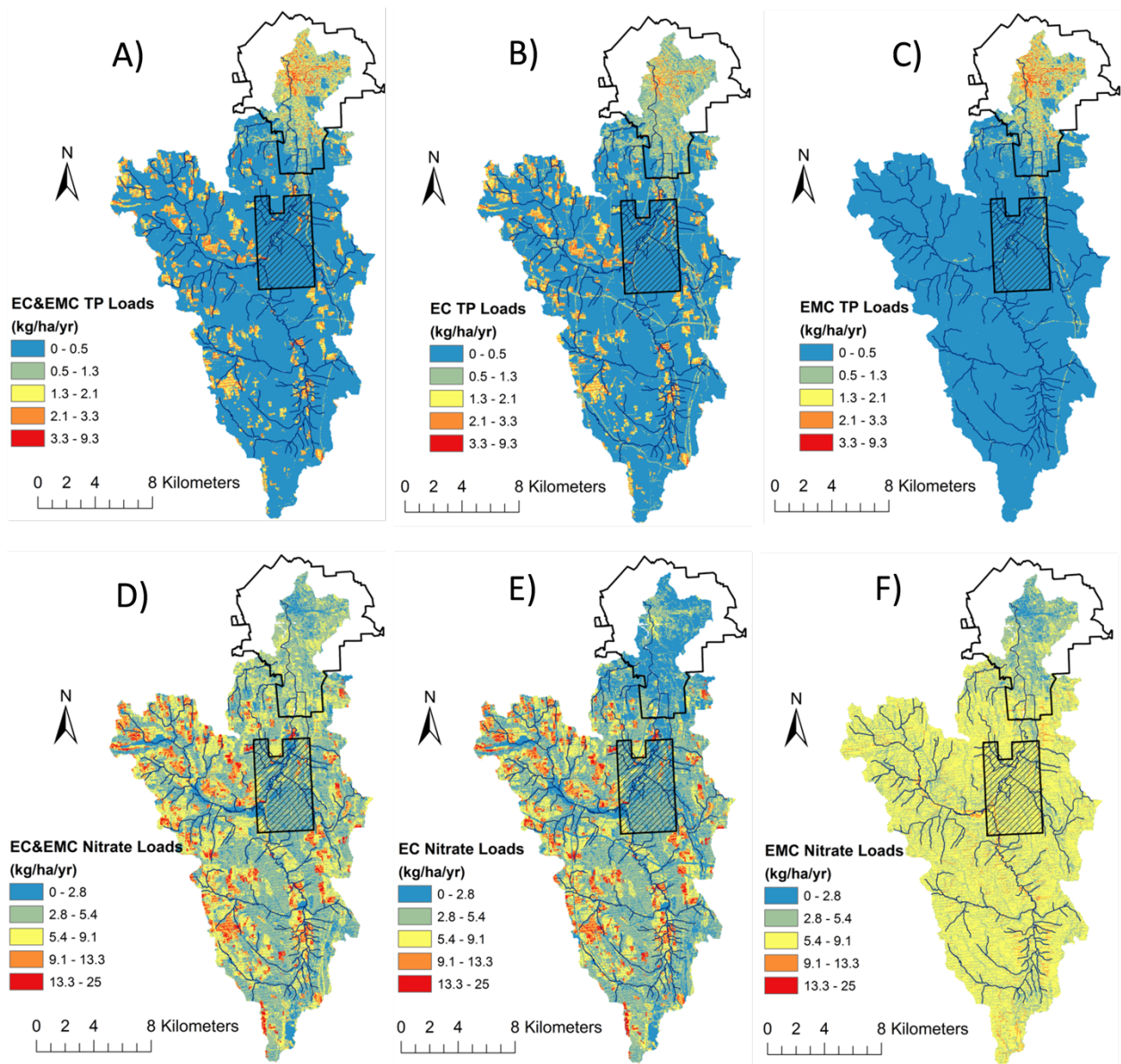
Figure 2: Demonstration of EC&EMC, EC, and EMC for TP (a-c) and nitrate (d-f) loads
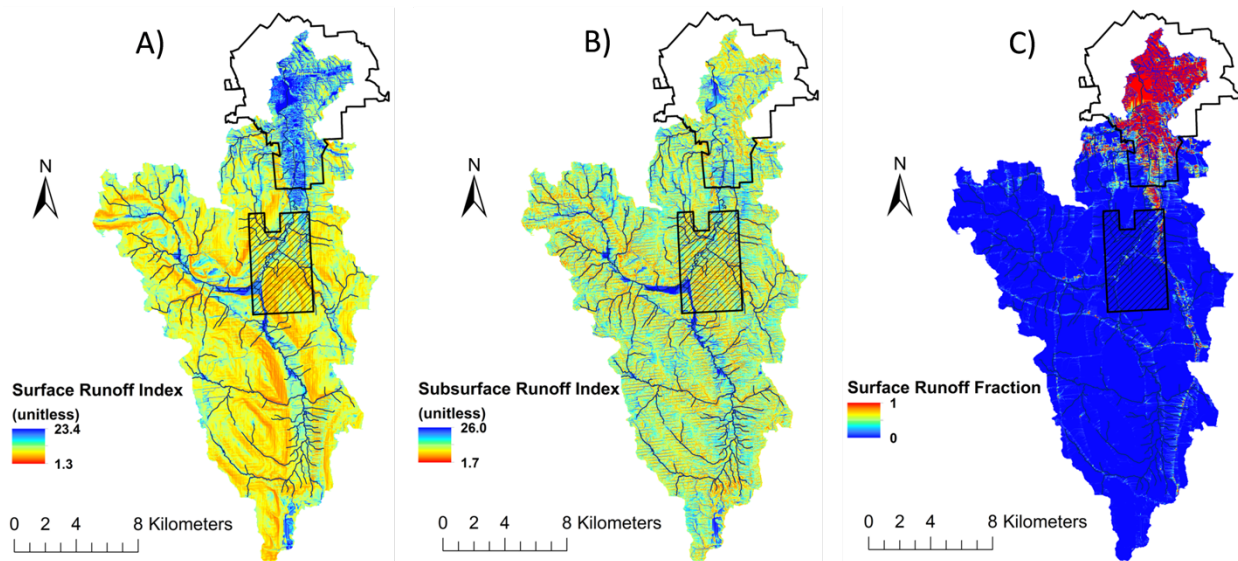
Figure 3: Surface (a) and subsurface (b) runoff indices and percentage of surface runoff (c)
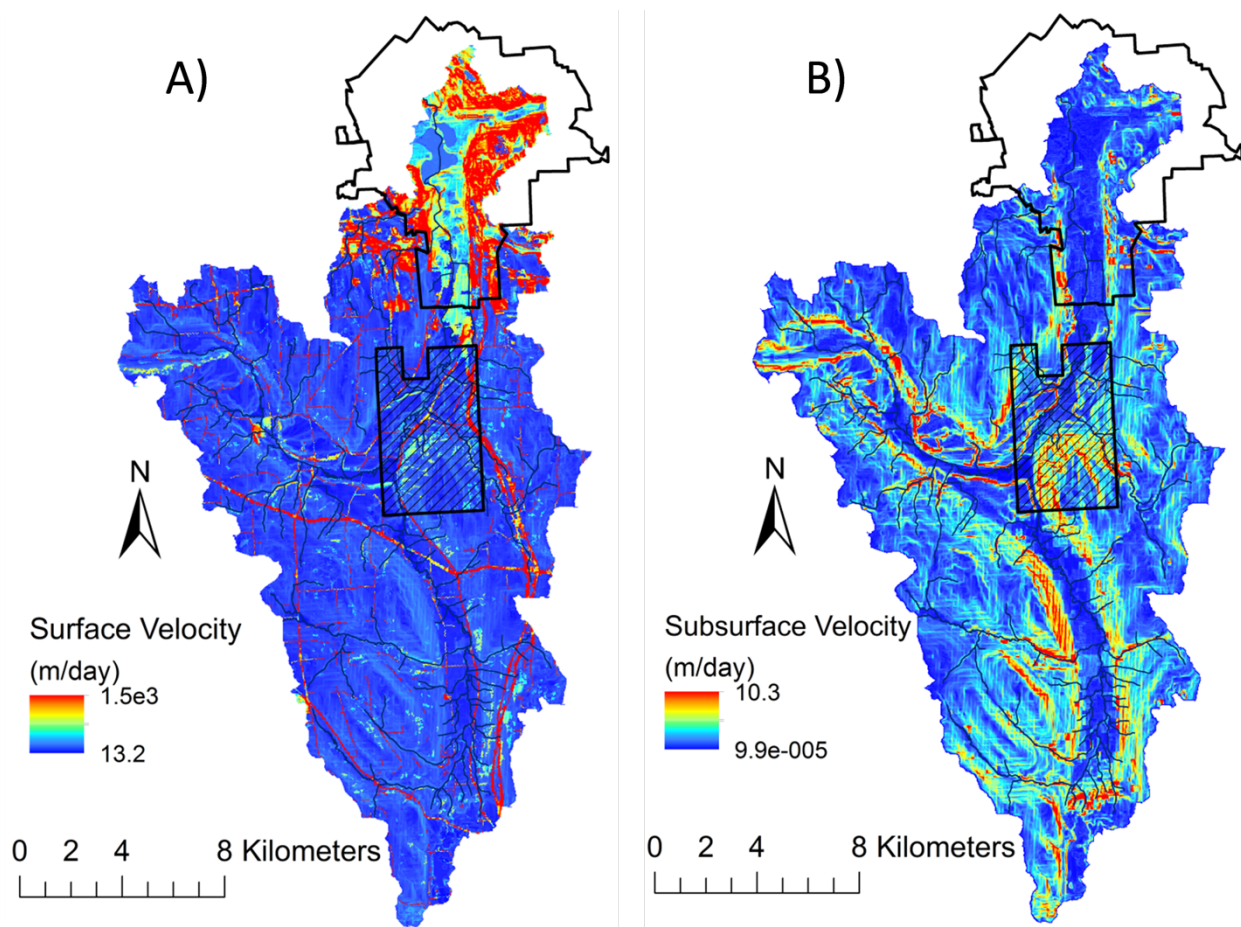
Figure 4: Surface(a) and subsurface velocities (b)
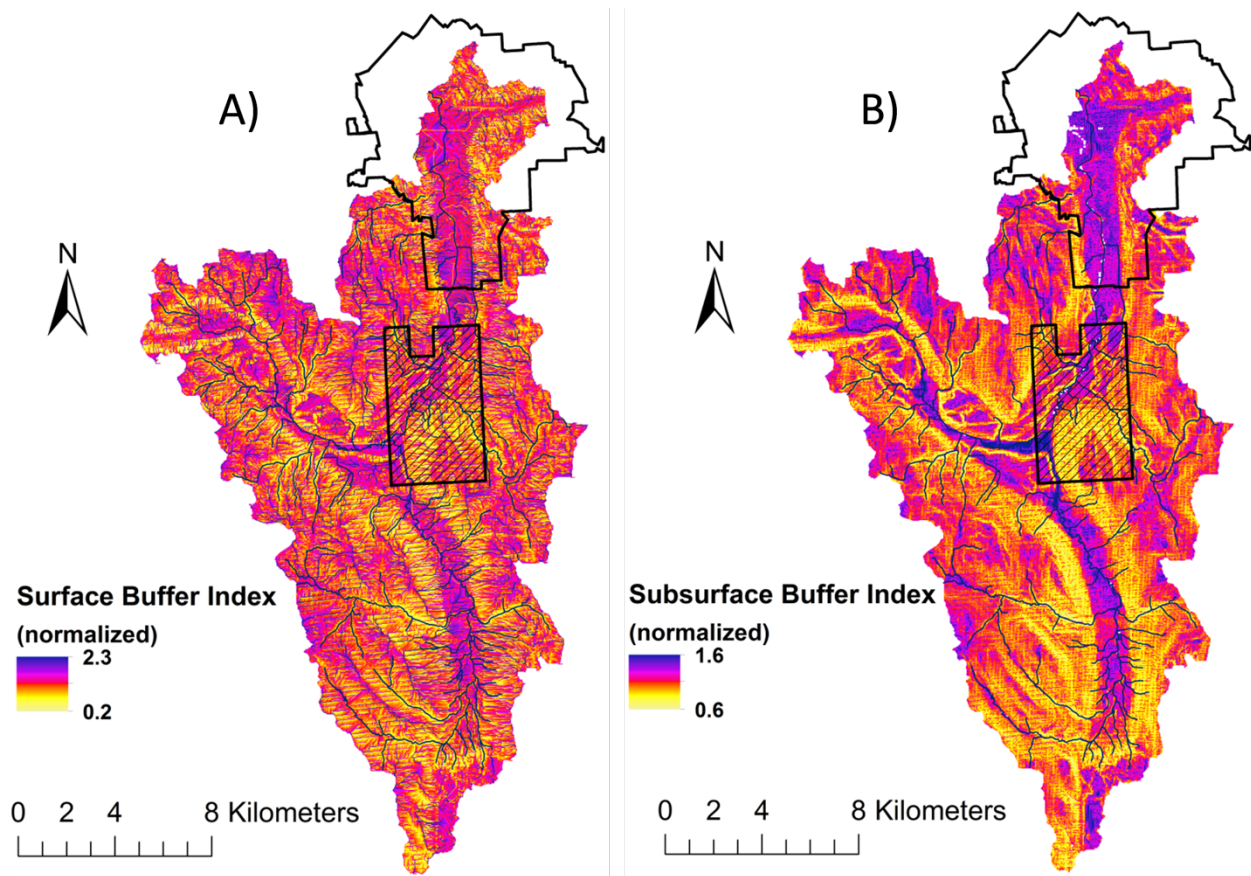
Figure 5: Surface (a) and subsurface (b) buffering indices
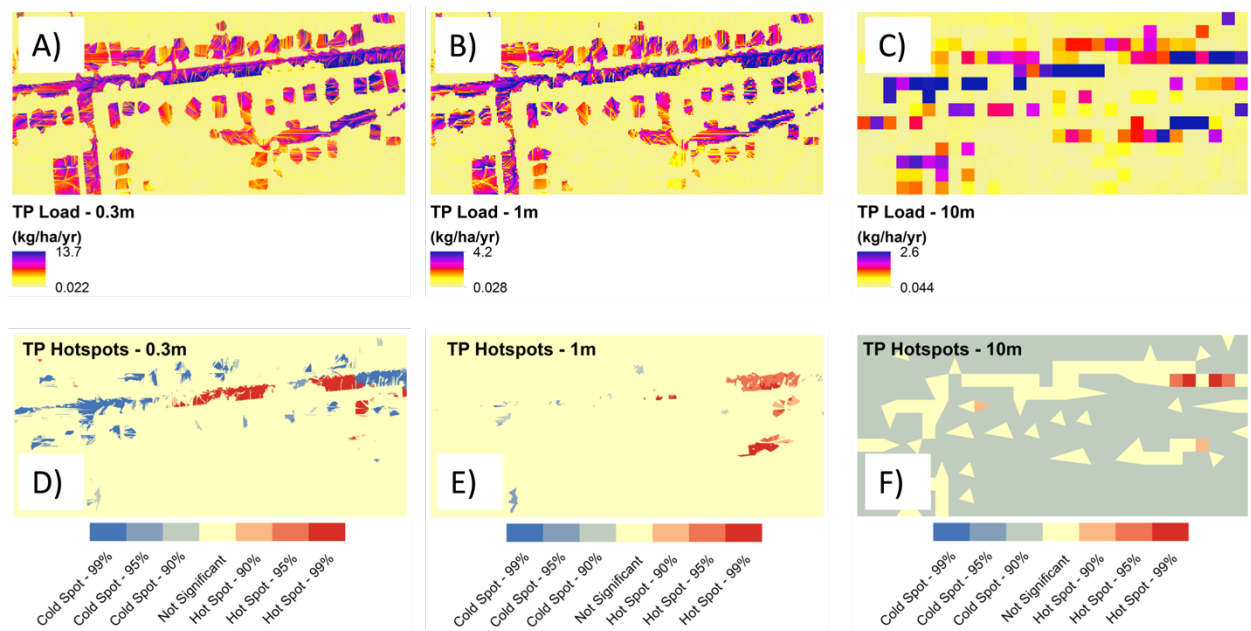
Figure 6: TP Sensitivity and Getis-Ord* Hotspot Analysis

55
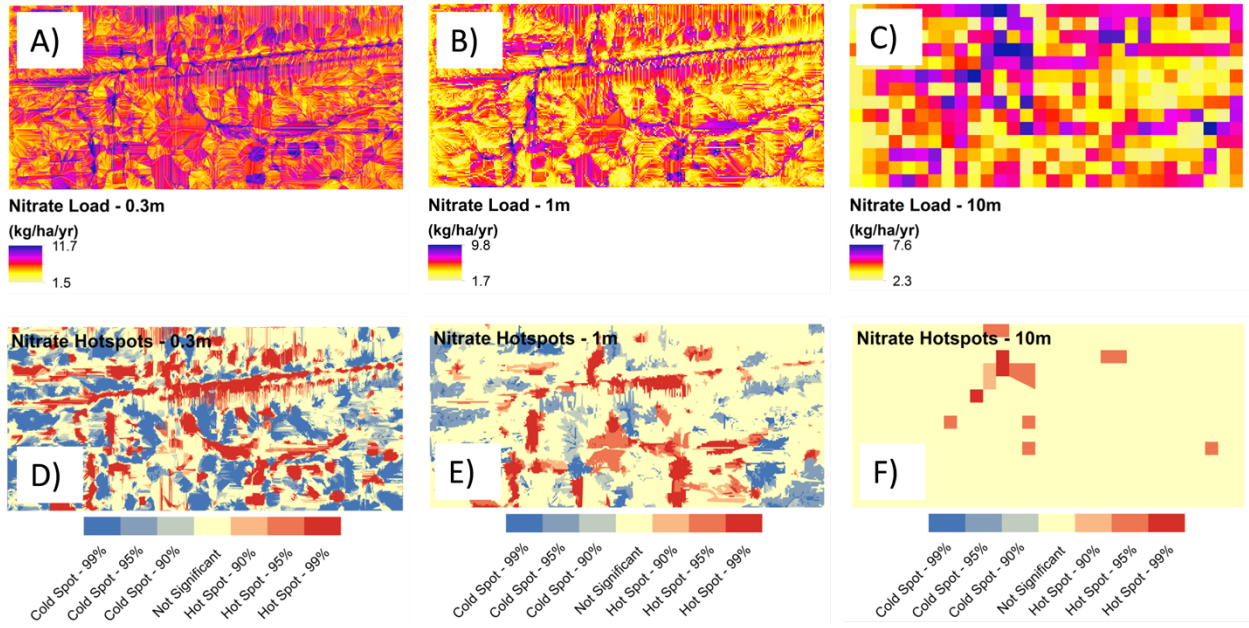
Figure 7: Nitrate Sensitivity and Getis-Ord* Hotspot Analysis

CHAPTER 3: USING WEATHER DATA TO REPRESENT ANNUAL VARIABILITY IN NUTRIENT LOADING USING THE PRECIPITATION-ENHANCED EXPORT COEFFICIENT (EC-PRECIP) MODEL

ABSTRACT: Watershed models often estimate annual nitrogen (N) or phosphorus (P) pollutant loads in rural areas with export coefficients (EC) (kg/ha/yr) values based on land cover, and is independent of changing weather and runoff conditions. Actual N and P nonpoint source (NPS) pollutant loading varies significantly seasonally and annually, yet simple models (e.g., EC model) have not been enhanced to reflect temporal loading variation. This research develops an EC-PRECIP model to simulate how the addition of rainfall intensity to the scoping level EC modeling framework can improve predictive capabilities. The model uses widely available daily precipitation data to reflect trends in rainfall intensity. Ranges of EC values generated for watershed-scale areas in the United States are coupled with rainfall intensities to reflect the higher NPS loading potential associated with more extreme precipitation events. The research illustrates how the EC modeling framework can be modified to be sensitive to the temporal influence of weather, and tests the innovative EC-PRECIP modeling framework against observed P loading into Onondaga Lake in Syracuse, New York. The model provides managers with a tool to rapidly predict how NPS loading values may change with increasingly intense rainfall events resulting from a changing climate.

KEY TERMS: nonpoint source pollution, watershed management, nutrients, runoff, rainfall intensity

INTRODUCTION

Nonpoint source (NPS) pollution is a pervasive problem across the United States, delivering excess nitrogen (N), phosphorus (P), and sediment to rivers, lakes, and estuaries. The U.S. Environmental Protection Agency lists that nutrients and sediment impair 6,908 and 6,165 water bodies, respectively (USEPA, 2012). To address this impairment and improve aquatic ecosystem health, watershed management programs often seek to model nutrient and sediment loading to receiving waters by using models. These models range widely in complexity. Due to the widespread nature and vast magnitude of impaired streams and water bodies, simple analyses of nutrient and sediment loading are justified to evaluate numerous areas of impairment, even where more complex simulation models are available (Lin, 2004). First order model approaches allow for rapid evaluation of potential areas of poor water quality, to identify locations where more complex models are warranted.

The EC model is a widely-used comparative tool to evaluate nutrient loading patterns in landscapes around the world, and is beneficial due to its simplicity. Managers, however, have thus far been limited to export coefficient data that is either far too general (e.g. representative of their region), or is too location-specific and, therefore, requires expensive and time-intensive sampling efforts. Ideally, this model could be used nationally, given the availability of export coefficient data ranges for ecoregions across the United States. EC values are reported as a load per area per time (e.g., kg/ha/yr), and are specific to certain land uses for a site; a map of standard EC values for each site would be homogeneous for each land cover type.

Annual variation in water quality and nutrient loading can be attributed to many factors. Land use and land cover changes contribute to differences in nutrient loading and has been incorporated into many modeling frameworks (Johnes, 1996). Rainfall erosivity has also been used as a driver for nutrient loading to receiving waters (Haith & Shoenaker, 1987). Phosphorus loading in streams is a function of water quality and streamflow; water quality has been shown to correlate strongly with land use, and streamflow is strongly related to precipitation (Robertson, Saad, Christiansen, & Lorenz, 2016). The EC model addresses land use variation by simulating annual loads of N, P, and sediment in a watershed given its proportional land cover classification (Reckhow, Beaulac, & Simpson, 1980; Reckhow & Simpson, 1980). However, the traditional EC model fails to represent changing streamflow conditions.

The availability of site-specific EC data is sparse; available nutrient loading values have been compiled (Lin, 2004), revealing that comprehensive EC selection guidance is lacking. ECs are typically developed from small watershed monitoring data, making field-based approaches impractical for wide-scale availability of export coefficient data. In order to mitigate this problem, a large dataset of EC values for all HUC8 hydrologic units across the United States (White et al., 2015) was developed. HUC8s are the geographic areas classified as representing a distinct hydrologic feature, of which there are 2264 in the U.S.; these are sometimes called "watersheds" although they may actually represent truncated versions of watersheds (Seaber, Kapinos, & Knapp, 1987). Simulations were run using the Soil Water Assessment Tool (SWAT) model (Douglas-Mankin, Srinivasan, & Arnold, 2010). White et al. (2015) used SWAT simulations to develop export coefficients that reflect the climate, topography, soils,

weather, land use, management, and conservation implementation conditions, which are unique to each HUC8, to provide more accurate EC estimates at the national scale. The 45 million simulations run in SWAT as part of the White et al. (2015) study provide ranges in values for locations across the United States, and have been validated by small-scale edge-of-field estimates generated by previous field studies. The EC database of White et al. (2015) contains average annual values simulated for randomly generated five-year periods from 1965 to 2004.

The EC model has been modified to allow for spatial variation in loading across homogeneous land uses. The actual export of load for each area, or pixel, is hypothesized to vary as a function of the relative contributing area and dispersal area (CADA) of the pixel, due to variation in runoff and buffering likelihood (Endreny & Wood, 2003; Stephan & Endreny, 2016). The CADA weighting of EC values is constrained such that variation is distributed about the original unweighted EC values so the sum of EC values for the watershed is not changed. The CADA EC model allows for mapping the areas of concern, identifying hotspots for potential pollutant loading and thereby identifying priorities for best management practices that can reduce pollutant loading. The limit of the EC and CADA-weighted approaches proves to be the lack of annually-varying EC data.

Temporal variation in nutrient loading in catchments of interests has been demonstrated both seasonally and annually through modification of the EC model (e.g., Hanrahan, Gledhill, House, & Worsfold, 2001) However, this prior research relies on catchment-specific monitoring, such as flow data or historic nutrient loading data, to develop temporal nutrient loading models. To evaluate seasonal variation in nutrient

loading in the Frome catchment, Hanrahan et al. [2001] weighted each export coefficient by the total discharge and baseflow discharge of water from the catchment during each month. Although flow data is less costly and more commonly available than water quality data, requiring these inputs limits the accessibility of the EC modeling framework to watershed managers and planners. Due to the proven relationship between streamflow and precipitation (Robertson et al., 2016), precipitation data can be utilized as a stand-in for watershed-specific stream discharge data, as precipitation is more widely available than consistent runoff data. Although antecedent moisture conditions influence whether precipitation is infiltrated or runs off, precipitation is easily obtained and measured at high spatial and temporal resolutions across the world. High rainfall intensity and the associated hydrologic responses have been shown to significantly increase nutrient losses due to larger runoff volumes (Kleinman et al., 2006).

This article presents the EC-PRECIP model, an update to the traditional EC model, which incorporates precipitation data to account for the effects of changing streamflow. We hypothesize that more extreme daily precipitation events will correspond to higher nutrient loading potential, and test our model with observed annual loading data. The EC-PRECIP model simulates annual variability in phosphorus loading to receiving water bodies, and uses Onondaga Creek watershed in Syracuse, New York as a case study. Modeled nutrient loading values are compared to observations in the Onondaga Creek watershed in Syracuse, NY, and common watershed model validation metrics are used to compare the EC model with the updated EC-PRECIP model developed through this research. The model's response to changing a significant input

parameter is also tested. The goal of this research is to 1) develop a method that represents the influence of weather on non-point source pollution watershed models and 2) to assess the performance of the EC-PRECIP model in a watershed in Syracuse, New York. The science question addressed by this research is whether daily precipitation frequency analysis can be used to temporally weight annual EC values and thereby simulate the observed inter-annual variation in loading.

METHODS

Study Site

The study site is a watershed that drains to Onondaga Lake, a central New York lake with long-term water quality records. Onondaga Lake lies within the Seneca HUC8, 04140201. The watershed draining to Onondaga Lake is delineated from Onondaga Creek at Spencer Street (USGS gage 02420010, located at 43°03'27", -76°09'45"). The watershed drains south to north, with headwaters in the Appalachian Plateau reaching an elevation of 587 m, with its outlet in the City of Syracuse at an elevation of 110 m. The watershed has an area of 298 km^2; based on the National Land Cover Database (NLCD), 53 km^2 of which is classified as developed (NLCD 21, 22, 23, or 24), 109 km^2 of which is forested (NLCD 41, 42, or 43), and 100 km^2 of which is agricultural (NLCD 81 and 82). The remaining 33 km^2 of watershed area are classified as open water (NLCD 11), barren land (NLCD 31), shrub/scrub (NLCD 52), and grassland/herbaceous (NLCD 71). The annual average precipitation for Syracuse, NY is 96.5 cm depth, with an average annual liquid equivalent snowfall of 32 cm and an average monthly total precipitation ranging between 8.1 and 10.4 cm. From 1980 to 2014, the minimum annual precipitation was 78.6 cm (1999) and the maximum was 125.9 cm (1990). The

average annual air temperature is 9.1°C with a February average low of -8.3°C and July

average high of 27.8°C. Flow in Onondaga Creek is regulated by an earthen dam near

the northern edge of Onondaga Nation land, designed to allow non-flood flows to pass

at grade with the channel bed through a 2 m diameter concrete culvert. Syracuse

climatic data shows that the highest average monthly rainfall occurs in July, and the

lowest in February ("NRCC US Comparative Climatic Data," n.d.).

In 1998, Onondaga County implemented the Ambient Monitoring Program (AMP)

to evaluate the quality of waterways and track changes brought about by improvements

in a) wastewater collection and treatment infrastructure and b) reductions in watershed

sources of nutrients. Onondaga County has also developed the Save the Rain Program,

which has been in effect since 2010. This program has developed a comprehensive

network of grey and green infrastructure solutions to manage stormwater runoff to help

protect Onondaga Lake and its tributaries. Nutrient data have been collected biweekly

from 1998 to present, and are published annually in an Onondaga Lake Ambient

Monitoring Program report. In this study, we use the data collected at the Onondaga

Creek sampling site closest to Onondaga Lake.

Model Structure

EC-PRECIP is structured to consider higher daily precipitation values as being

more significant, and therefore have a larger impact on total annual nutrient loads. We

assume that the exceedance probability of daily rainfall events corresponds to the set of

EC probability distributions developed by White et al. [2015]. The EC-PRECIP model

uses publicly available weather, pollutant load, and land cover (NLCD) data to 1)

calculate a daily precipitation cumulative distribution function based on a long-term

precipitation record, 2) assign an exceedance probability to each significant precipitation event in the desired year, 3) associate an export coefficient value with each exceedance probability, and 4) produce the mean export coefficient value to represent the annual pollutant load. The model sets a threshold precipitation depth *Th* to represent the daily amount required to catalyze pollutant movement to the outlet. For phosphorus delivery, *Th* is set to 2.54 cm to reflect the 90th percentile storm in accordance with the water quality design criteria for New York State ("New York State Stormwater Management Design Manual," 2015).

A long term daily rainfall record is used to create an exceedance probability distribution for all precipitation values greater than *Th*. In the case of our study, we used daily precipitation records from 1980 to 2014 taken at the Syracuse Hancock International Airport. $P_{Pr}[X]$ represents the probability of exceeding a daily precipitation of X. The data developed by White et al. [2015] is used to create another probability distribution, P_{EC}, where $P_{EC}[y]$ represents the exceedance probability of the EC value y for a given year. In the simulated year, exceedance probabilities of daily precipitation events over *Th* are calculated using the distribution P_{Pr}. For *n* daily precipitation events exceeding *Th* over the year, the associated export coefficient for $P_{Pr}[P_i]$ is calculated using the quantile function, returning the EC_i value such that:

$$F_{EC}[EC_i] := P_{EC}(X \leq EC_i) = P_{Pr}[P_i] \qquad\qquad 1$$

Note that each land use type has an EC value for each of the *n* events within the year. For each of the *n* rainfall events over the study year, a representative "annual EC"

value is calculated by taking the F_{EC} value for each land use j and weighting it by the proportion of the study area within that land use:

$$EC_{ann} = \sum_{j=1}^{k} EC_j \times P_j \qquad\qquad 2$$

where P_j is the proportion of the watershed in land use j, and k represents the total number of land uses within the study area. This representative EC_{ann} value is calculated for each of the n events, so that an average EC value, EC_{avg}, over that year can be calculated:

$$EC_{avg} = \left(\sum_i^n EC_{ann}\right)\big/n \qquad\qquad 3$$

where EC_{avg} is the representative EC for the year, based on the n event-based EC values.

A delivery ratio D is established to distinguish pollutants moving through the system from those culminating at the receiving water body, as the HUC8-specific export coefficient data represents an "edge-of-field" estimate of pollutant delivery to receiving waters. Sediment delivery ratio data (Chinnasamy et al., undated) has been compiled for HUC8 watersheds in major United States basins and was used to identify D as 0.36 for this simulation. Because particulate phosphorus sorbs to sediment, the sediment delivery ratio can be used to approximate phosphorus. Equation 4 converts $EC_{avg,i}$ to annual load to the outlet.

$$EC_{ann} = EC_{avg} \times D \times A + PS \qquad\qquad 4$$

where EC_{ann} is the annual load to the outlet, A is the area of the watershed, and PS is the sum of the point source contribution to pollutant load.

Combined sewer overflows (CSOs) contribute a point source load of phosphorus to Onondaga Lake, and thus must be accounted for in equation 4. The New York State Department of Environmental Conservation (NYSDEC) modeled the Onondaga Lake watershed, and determined that the annual average delivered total phosphorus load to Onondaga Lake was 2.94 metric tons for land within CSO areas (NYSDEC, 2012). Average annual point source loads into Onondaga Creek were estimated to be 73.4% of the total average delivered load into Onondaga Lake, which is the percent of Onondaga Lake CSO areas within the Onondaga Creek watershed. Through this calculation, we can assume an average annual point source phosphorus load of 2.16 metric tons.

Model performance evaluation metrics

Standard methods for watershed model validation are used to assess model outputs (Moriasi et al., 2007). The Nash-Sutcliffe efficiency (NSE) determines the magnitude of residual variance compared to the measured data variance. NSE ranges from negative infinity to 1.0, with NSE=1 reflecting a perfectly accurate model. An NSE equal to or less than 0 indicates that the mean observed value of the data is a better predictor than the modeled value. Percent bias (PBIAS) measures the tendency of modeled data to be larger or smaller than observed counterparts. PBIAS can be positive or negative, reflecting a model underestimation bias and a model overestimation bias, respectively. Lower magnitudes of PBIAS values indicate accurate model simulation. The root mean square error (RMSE) is a commonly used error index; however, the magnitude of the value is not normalized to the standard deviation of the dataset, which

prevents application to various constituents. The RMSE-observation standard deviation ratio (RSR) has been proposed to alleviate the shortcoming of the RMSE, and normalizes the RMSE by the standard deviation of observed values. RSR ranges from the optimal value of 0 to a large positive value. Model sensitivity to changing T was explored by increasing T by 10%, 25%, and 50% (2.79 cm, 3.18 cm, and 3.81 cm) and decreasing T by 10%, 25%, and 50% (2.29 cm, 1.91 cm, and 1.27 cm).

RESULTS

Modeled vs. observed phosphorus loading

The EC-PRECIP model provides accurate first-order estimates of observed total phosphorus loading to Onondaga Lake via the Onondaga Creek watershed. The model predicts observed phosphorus loading to Onondaga Lake accurately; the trend lines indicates that the modeled values are representing the observed values (Figure 8). Figure 9 reflects the EC-PRECIP model prediction of annual phosphorus loading over time, demonstrating that the model accurately phosphorus loading and follows the trend of the observed data, providing guidance as to which years are likely problematic for phosphorus loading likelihood.

Model performance

The EC-PRECIP model successfully predicted phosphorus loading to Onondaga Lake via the Onondaga Creek watershed. The predictive capacity of the model was tested to assess model performance. Using the watershed model performance metrics provided by Moriasi et al. (2007), our EC-PRECIP model surpasses the predictive power of the traditional EC model. The metrics achieved by each model for the Onondaga Creek watershed are found in Table 4.

To compare the EC and EC-PRECIP models, the EC value was calculated using the median EC for each land use in HUC 04140201. Using the updates provided in the EC-PRECIP model, the NSE, PBIAS, and RSR all improved significantly from the EC model.

Model sensitivity

Adjusting the threshold *Th* significantly alters the model performance and reveals information about the complex nonlinear nature of the model. NSE decreases to below an acceptable level when *Th* is adjusted to 3.18 cm. Because the model disregards events below *Th*, setting *Th* higher results in fewer events considered for that year. Similarly, setting *Th* too low would result in too many events being considered, and perhaps resulting in a lack of differentiation between years. Table 5 shows that setting *Th* at 1.91 cm, 2.29 cm, or 2.79 cm all result in satisfactory NSE values, suggesting that the model operates effectively using many *Th* values to represent phosphorus delivery to the Onondaga Creek watershed outlet. However, 2.54 yields the greatest NSE value, and thus we proceed with analysis using *Th* of 2.54 cm.

DISCUSSION

Modeled vs. observed phosphorus loading

The observed phosphorus loading to Onondaga Lake via Onondaga Creek ranges from 6.8 metric tons in 2012 to 25 metric tons in 2010. Sampling occurs biweekly at many locations along tributaries within the Onondaga Lake watershed. Concentrations obtains from water quality sampling are coupled with flow data to produce annual loading estimates, to assess the state of water quality over time in Onondaga Lake and its tributaries.

The number of events each year totaling greater than 2.54 cm of precipitation daily ranged from one to ten over the 35-year simulation period. Taking a subset of this data between 1998 and 2013 (the years for which phosphorus loading data is available at Onondaga Creek), the frequency of phosphorus-triggering events (precipitation values above *Th*) ranges from three to ten events (Figure 10). Of the 172 daily precipitation events from 1980 to 2014 in Syracuse that exceeded 2.54 cm, the majority occurred in October, and the fewest occurred in February (Figure 11). Because February has the lowest average monthly precipitation ("NRCC US Comparative Climatic Data," n.d.), we expect to see the fewest events exceeding 2.54 cm over the study period. Although July has the highest daily average rainfall, October showed a higher frequency of extreme precipitation events over our course of study. This suggests that July storms are flashier and produce higher rainfall amounts, but are also less frequent.

Because the EC-PRECIP model scales rainfall events based on their magnitude, the extremeness of those events is weighted based on the number of events occurring within that month or year. Therefore, years that experience the same number of events will show different modeled phosphorus loads based on differences in event magnitude. Figure 10 shows that the years 2012 and 2013 both experienced three events exceeding the *Th* of 2.54 cm. However, the observed loading value for 2013 (15.5 Mt) is greater than twice that of 2012 (6.8 Mt). The magnitudes of precipitation events in 2013, then, are greater than those of 2012, and therefore are associated with higher export coefficient values. The time-series plot in Figure 9 demonstrates that the EC-PRECIP

model reflects this difference, and predicts the years' phosphorus load values differently to match well with observations.

Our point source estimate of CSO discharges presents a limitation to the model, in that not all CSO outlets within the Onondaga Lake watershed are monitored. Therefore, we used an estimate of total CSO phosphorus delivery and scaled it based on the proportion of CSOs in the Onondaga Creek watershed. Other factors may be more relevant study areas, including population density, volumes and concentrations of wastewater, and the likelihood for CSO discharges based on rainfall intensity. Our PS estimate in equation 4 is a lump sum, with the same estimated value for each year. In the future, the CSO loading could also be dependent on extreme rainfall events, since large precipitation events can trigger CSO overflows. A 2015 EPA rule requires the electronic publication of National Pollutant Discharge Elimination System (NPDES) permits for regulated facilities, and these reports may also be used to understand the magnitudes of allowable pollutant loading into receiving waters from various sources.

Model performance

The EC model performance is significantly worse than that of the EC-PRECIP model, with the addition of weather data as a driver providing greater accuracy to the EC modeling framework. The negative NSE calculated for the EC model indicates that using the mean value of the observed data would provide a more accurate result than using modeled nutrient loads. An NSE value of 0.636, conversely, represents a satisfactory fit for a parsimonious model utilizing national datasets. The PBIAS value is decreased by nearly 38% with the addition of temporal variation provided by the EC-PRECIP model, and the RSR decreases by 1.

A compilation of model evaluation of watershed simulations (Moriasi et al., 2007)

suggests that satisfactory watershed models have NSE values above 0.75, PBIAS

values below 25%, and RSR values below 0.70. Our PBIAS and RSR values meet

these criteria, but our NSE value is slightly less than the satisfactory threshold. The

models compiled for these metrics, however, are complex in nature, with many input

parameters and oftentimes complex calibrate routines (e.g., SWAT). The EC-PRECIP

model is meant to occupy the space between the widely-used traditional EC model and

the calibrated, highly-parameterized watershed simulation models such as SWAT.

Although the Onondaga Creek watershed application of the EC-PRECIP model does

not meet the standards of a satisfactory watershed simulation model as set forth by

Moriasi (2007), the EC-PRECIP model demonstrates a significant improvement in

predictive capacity over the traditional EC model. The incorporation of precipitation as a

new input to drive nutrient delivery progresses the first-order EC model framework,

while allowing for national model utilization with minimal additional inputs.

Model sensitivity to Th *parameter*

Increasing *Th* also reduces the number of events considered significant in each

simulated year, creating a wider range of resulting annual load values. This is reflected

in Table 5; the range of annual load values calculated increases dramatically when *Th* is

set to 3.81 cm. As the number of influential events decreases, their relative importance

increases, and fewer precipitation events are modeled to represent an entire year. In

the case of setting *T* as high as 3.81 cm, in 2003 and 2012, the daily precipitation did

not exceed *Th*, and therefore no annual load value could be calculated. Conversely,

setting *Th* to a low value (1.27 cm) reduces the range of loading values, since the

higher number of influential precipitation events in each year mutes the effects of the extreme precipitation events within that year. The range in observed phosphorus loading values for the Onondaga Creek watershed during the study simulation period is 18.2, suggesting that setting *Th* at 2.54 cm is appropriate.

The PBIAS metric also increases as *Th* increases, due to the increasing importance of single events as the threshold is raised. The lowest *Th* value, 1.27 cm, results in the lowest PBIAS, due to the muted response for each single precipitation event during that year. However, the low PBIAS must be taken in context, and the low NSE fit reflects the poor capacity of the model given a *Th* value of 1.27 cm.

CONCLUSIONS

The EC-PRECIP model has proven effective as a scoping level tool in the Onondaga Creek watershed in Syracuse, New York. Comparing the updated EC-PRECIP model to the traditional EC model, NSE, PBIAS, and RSR all improved significantly. Since the EC model has been endorsed by the USEPA as an accurate watershed modeling framework, the EC-PRECIP model is the next step in providing better water quality estimates without increasing data or sampling requirements.

The EC model is widely accepted as a scoping model when monitoring data is not feasible or is unavailable. The EC-PRECIP update moves closer to a comprehensive method for determining inter-annual nutrient loading variations, and brings widely available precipitation data together with typical nutrient loading values to produce a range of likely annual loads. The use of national data in this model is novel due to the ease of use and high level of accuracy evidenced in its application to

Onondaga Creek watershed. The EC-PRECIP model fills a niche for simple models that take advantage of the large amount of weather, land use, and soils data being collected by governmental organizations such as the United States Geological Survey, the National Oceanic and Atmospheric Administration, and the Natural Resources Conservation Service.

The EC-PRECIP model represents a critical step in modifying the commonly-used EC modeling framework to allow for the influence of weather, specifically rainfall intensity, on nutrient loading in watershed across the United States. Since the EC-PRECIP model uses rainfall events as a proxy for runoff, the model will be most effective in environments with relatively high water tables, where runoff is generated quickly following a precipitation event. Extreme precipitation events create Hortonian flow, or infiltration excess overland flow, where precipitation rate exceeds the infiltration capacity of the soil. The study area in Syracuse, NY, represents an area of high precipitation magnitudes and rainfall events. In order to truly determine the effectiveness of the model in other types of environments, further studies must occur which explore the accuracy of modeling efforts using EC-PRECIP.

Currently, our society has access to more environmental data than ever before. Traditionally, watershed models have been limited in their use to those with the resources to undertake extensive soil and water quality sampling for accurate environmental monitoring data. With the recent availability of new data, researchers are developing methods of combining these data in unique ways to predict environmental impacts of land use conversion and climate change. A prime example of this type of

management tool, i-Tree (itreetools.org), would benefit from incorporation of the EC-PRECIP model into its collection of first-order tools.

LITERATURE CITED

Chinnasamy, S., Wang, X., Arnold, J., Williams, J., White, M., Kannan, N., & Diluzio, M.
(undated). Documentation on Delivery Ratio used for CEAP Cropland Modeling
for Various River Basins in the United States. *NRCS*. Retrieved from
https://www.nrcs.usda.gov/Internet/FSE_DOCUMENTS/stelprdb1045451.pdf

Douglas-Mankin, K. R., Srinivasan, R., & Arnold, J. G. (2010). SOIL AND WATER
ASSESSMENT TOOL (SWAT) MODEL: CURRENT DEVELOPMENTS AND
APPLICATIONS. *Transactions of the ASABE*, *53*(5), 1423–1431.

Endreny, T. A., & Wood, E. F. (2003). Watershed Weighting of Export Coefficients to
Map Critical Phosphorous Loading Areas1. *JAWRA Journal of the American
Water Resources Association*, *39*(1), 165–181. https://doi.org/10.1111/j.1752-
1688.2003.tb01569.x

Haith, D. A., & Shoenaker, L. L. (1987). Generalized Watershed Loading Functions for
Stream Flow Nutrients1. *JAWRA Journal of the American Water Resources
Association*, *23*(3), 471–478. https://doi.org/10.1111/j.1752-1688.1987.tb00825.x

Hanrahan, G., Gledhill, M., House, W. A., & Worsfold, P. J. (2001). Phosphorus Loading
in the Frome Catchment, UK. *Journal of Environment Quality*, *30*(5), 1738.
https://doi.org/10.2134/jeq2001.3051738x

Johnes, P. J. (1996). Evaluation and management of the impact of land use change on
the nitrogen and phosphorus load delivered to surface waters: the export
coefficient modelling approach. *Journal of Hydrology*, *183*(3–4), 323–349.
https://doi.org/10.1016/0022-1694(95)02951-6

Kleinman, P. J. A., Srinivasan, M. S., Dell, C. J., Schmidt, J. P., Sharpley, A. N., & Bryant, R. B. (2006). Role of Rainfall Intensity and Hydrology in Nutrient Transport via Surface Runoff. *Journal of Environmental Quality*, *35*(4), 1248–1259. https://doi.org/10.2134/jeq2006.0015

Lin, J. P. (2004). Review of published export coefficient and event mean concentration (EMC) data. *Vicksburg, Miss. : U.S. Army Engineer Research and Development Center*.

Moriasi, D. N., Arnold, J. G., Van Liew, M. W., Bingner, R. L., Harmel, R. D., & Veith, T. L. (2007). Model evaluation guidelines for systematic quantification of accuracy in watershed simulations. *Transactions of the ASABE*, *50*(3), 885–900.

New York State Stormwater Management Design Manual. (2015, January). NYS Department of Environmental Conservation. Retrieved from http://www.dec.ny.gov/chemical/29072.html

NRCC US Comparative Climatic Data. (n.d.). Retrieved April 16, 2017, from http://www.nrcc.cornell.edu/wxstation/comparative/comparative.html#

Reckhow, K. H., Beaulac, M. N., & Simpson, J. T. (1980). Modeling Phosphorus Loading and Lake Response Under Uncertainty: A Manual and Compilation of Export Coefficients | US EPA.

Reckhow, K. H., & Simpson, J. T. (1980). A Procedure Using Modeling and Error Analysis for the Prediction of Lake Phosphorus Concentration from Land Use Information. *Canadian Journal of Fisheries and Aquatic Sciences*, *37*(9), 1439–1448. https://doi.org/10.1139/f80-184

Robertson, D. M., Saad, D. A., Christiansen, D. E., & Lorenz, D. J. (2016). Simulated

impacts of climate change on phosphorus loading to Lake Michigan. *Journal of*

Great Lakes Research, *42*(3), 536–548. https://doi.org/10.1016/j.jglr.2016.03.009

Seaber, P. R., Kapinos, F. P., & Knapp, G. L. (1987). *Hydrologic unit maps* (USGS

Numbered Series No. 2294). U.S. G.P.O.,. Retrieved from

http://pubs.er.usgs.gov/publication/wsp2294

Stephan, E. A., & Endreny, T. A. (2016). Weighting Nitrogen and Phosphorus Pixel

Pollutant Loads to Represent Runoff and Buffering Likelihoods. *JAWRA Journal*

of the American Water Resources Association, *52*(2), 336–349.

https://doi.org/10.1111/1752-1688.12390

Total Maximum Daily Load (TMDL) for Phosphorus in Onondaga Lake. (2012, May).

NYS Department of Environmental Conservation. Retrieved from

http://www.dec.ny.gov/docs/water_pdf/tmdlonfinal12.pdf

USEPA. (2012). National Summary of Impaired Waters and TMDL Information.

Retrieved from

http://ofmpub.epa.gov/tmdl_waters10/attains_nation_cy.control?p_report_type=T

#status_of_data

White, M., Harmel, D., Yen, H., Arnold, J., Gambone, M., & Haney, R. (2015).

Development of Sediment and Nutrient Export Coefficients for U.S. Ecoregions.

JAWRA Journal of the American Water Resources Association, *51*(3), 758–775.

https://doi.org/10.1111/jawr.12270

TABLES

Table 4: Comparison of model performance evaluation metrics for the export coefficient (EC) and EC-PRECIP models using the Onondaga Lake loading dataset from 1998-2013.

Metric	EC-PRECIP model	EC model
NSE	0.636	-1.739
PBIAS	2.64%	40.6%
RSR	0.60	1.655

Table 5: Response of EC-PRECIP model to variation in T parameter. The default T value of 2.54 cm is adjusted +/-10%, +/-25%, and +/-50%, and resulting model performance metrics are shown below.

T (cm)	1.27	1.91	2.29	**2.54**	2.79	3.18	3.81
NSE	0.035	0.591	0.496	**0.636**	0.400	-0.210	0.441
PBIAS	-1.22	0.37	0.63	**2.64**	5.06	5.80	8.96
RSR	0.98	0.64	0.71	**0.60**	0.77	1.10	0.75
Range	9.13	11.32	13.61	**14.71**	16.18	20.78	24.69
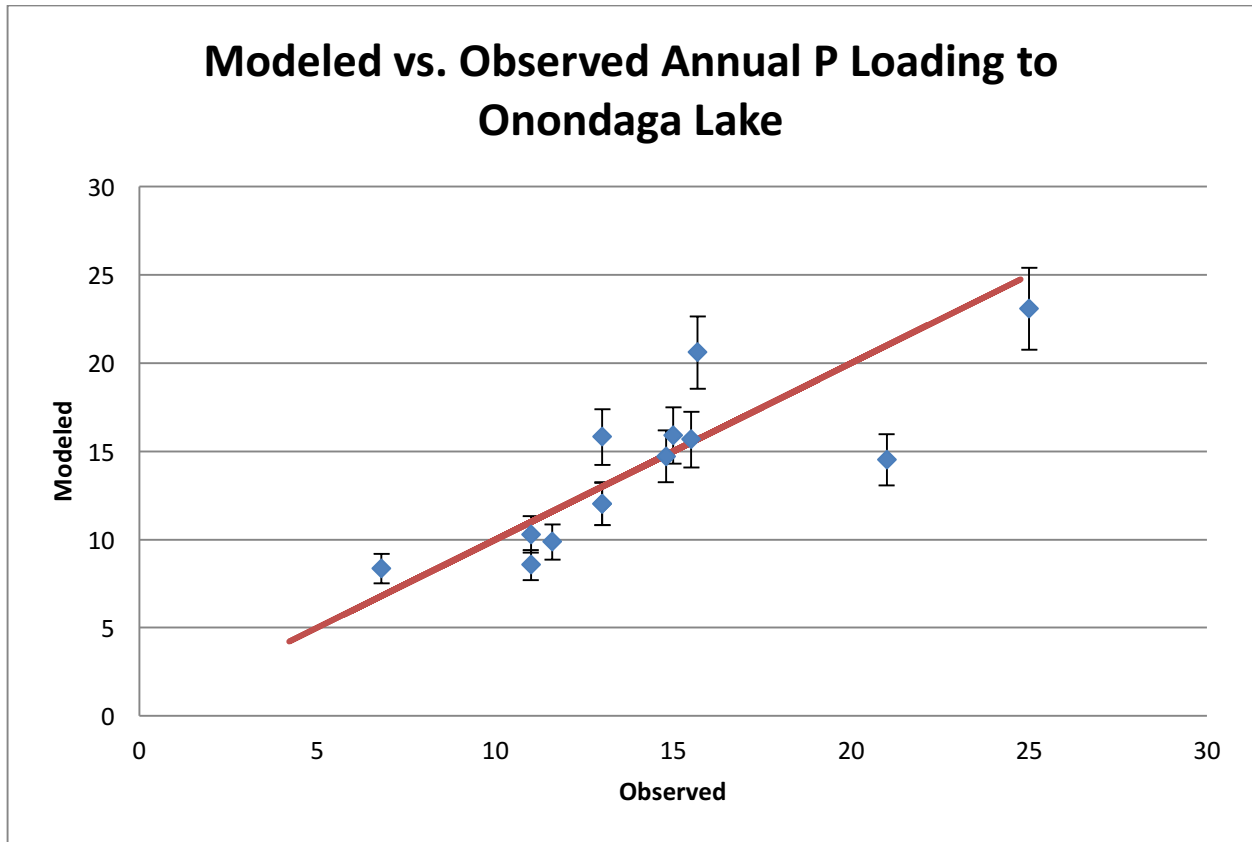
Figure 8: Plot of the observed Onondaga Lake P loading data against the P loading data modeled using the EC-PRECIP model. Error bars represent +/-10% error.
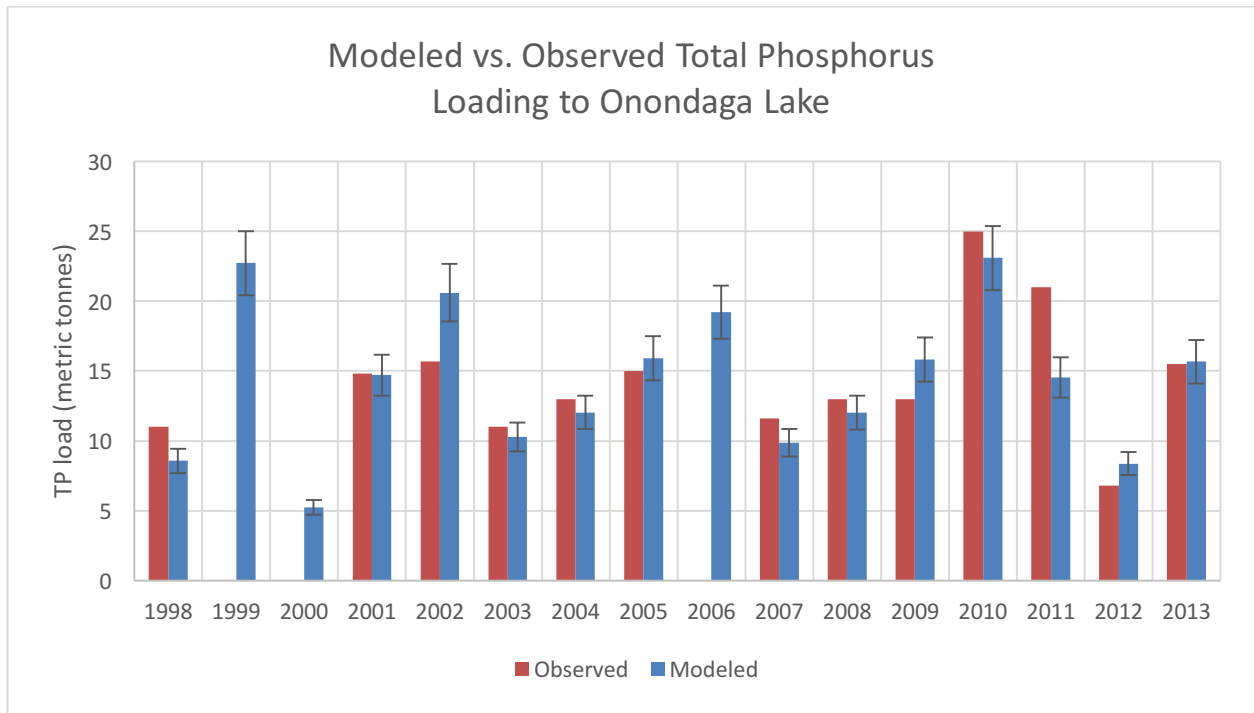
Figure 9: Time-series plot of Onondaga Lake observed P loading versus P loading modeled with EC-PRECIP. Note that observed P loading values were not obtained for 1999, 2000, and 2006.
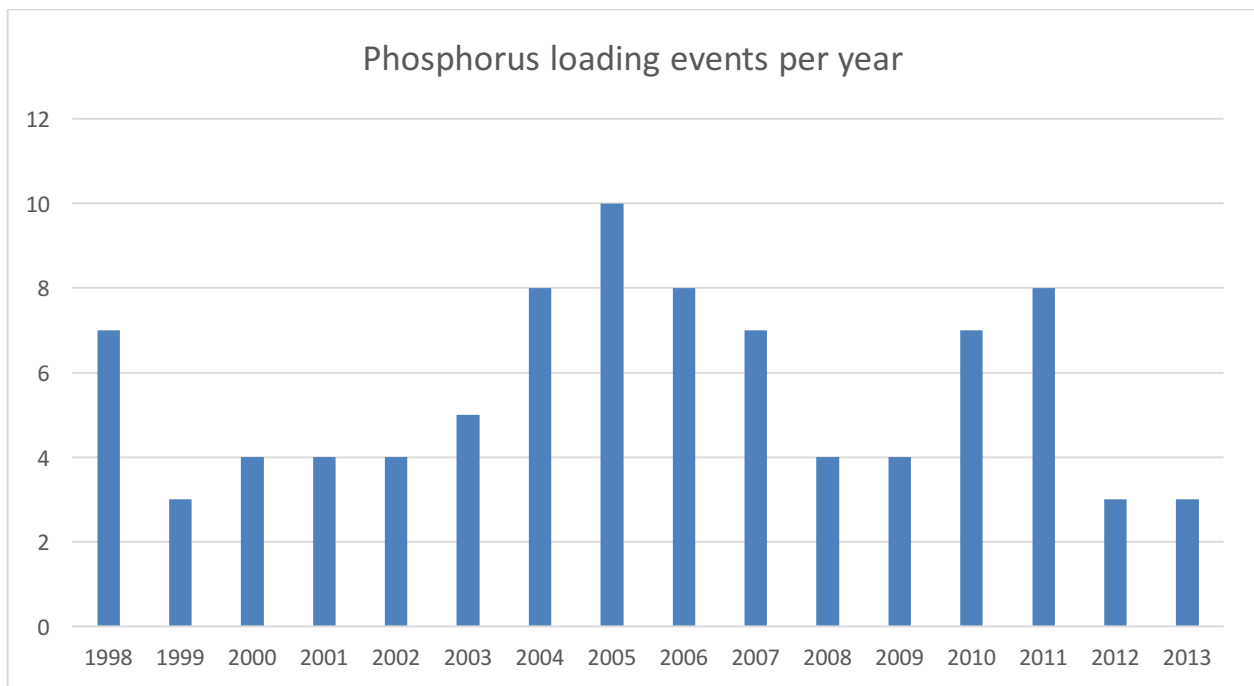
Figure 10: The frequency of phosphorus-triggering events (those daily precipitation values exceeding the threshold T=2.54 cm) between 1998 and 2014.
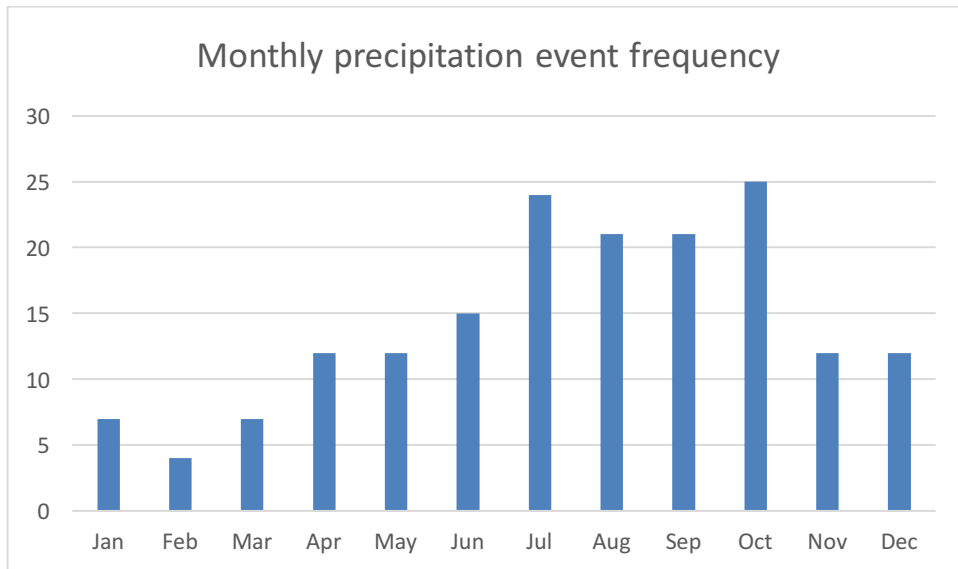
Figure 11: The relative frequency of phosphorus-triggering events (those daily precipitation values exceeding the threshold Th=2.54 cm) for each month between 1980-2014. Over this 35 year span, the daily precipitation exceeded Th 172 times.

CHAPTER 4: DEVELOPMENT OF A PREDICTIVE TOOL TO ASSESS DENITRIFICATION POTENTIAL IN URBAN, SUBURBAN, AND FORESTED SAMPLING SITES

ABSTRACT: We examined relationships between denitrification potential and predictor variables associated with soil and landscape properties to build a predictive tool for denitrification potential at a landscape level. Denitrification potential, ancillary soil variables and physical landscape attributes were measured at a range of urban, suburban, and forested environments in the Gwynns Falls watershed in Baltimore, Maryland in a series of studies between 1998 to 2014. Data from these studies was used to develop a statistical model for denitrification potential using a subset of the samples (N=205) and another subset (N=133) was used to validate the model. Soil moisture and soil respiration were the best predictors of denitrification potential (R^2_{adj} = 0.314), with the validated model obtaining a Nash-Sutcliffe efficiency of 0.472. Our results suggest that soil denitrification potential can be modeled successfully using these two parameters, and that this model performs well in a watershed consisting of mixed land uses.

KEY TERMS: denitrification, topographic indices, hotspots, urbanization

INTRODUCTION

Human activity that has accelerated fixation of atmospheric to plant-available, reactive nitrogen (N) forms (Vitousek et al., 1997) has motivated studies of regional N fate and transport. There is particular interest in denitrification, an anaerobic microbial process that converts reactive N into N gases, but this process is difficult to quantify, especially at large scales (Seitzinger et al., 2002). In an analysis of 16 large watersheds in the northeastern United States, denitrification was estimated as the remaining N loss once known input, output and storage terms were considered (Breemen et al., 2002). Although these landscape denitrification estimates incorporated accumulated uncertainties from other terms, soil denitrification was the dominant sink for N inputs to the watersheds, accounting for 34% of total storage and loss on average. While regional mass balances are helpful in quantifying the importance of landscape denitrification, they provide no predictive power or assessment of spatial variation in the process.

Regional-scale denitrification models vary in complexity and driving factors, as well as in their approach (Boyer et al., 2006). Rather than attempting to model microbial processes and dynamics, these regional models typically focus on environmental conditions in which denitrification is expected to occur. The DAYCENT model (Parton et al., 1996) assumes denitrification is controlled by soil NO_3^- concentration, organic carbon availability, and oxygen availability. The DNDC model (Li, 1996) is a soil biogeochemistry model which utilizes sub-models of soil climate, plant growth, and decomposition to predict soil environmental factors, which drive kinetics of relevant biochemical or geochemical reactions. Agricultural management models often simulate denitrification in soils. For example, the EPIC (Environmental Policy Integrated Climate)

model (J. R. Williams, C. A. Jones, & P. T. Dyke, 1984) simulates all major N cycling processes in agricultural soils (i.e., mineralization, nitrification, immobilization) on a daily time step and requires specific field validation to obtain necessary parameters. As in other models, denitrification in EPIC is governed by NO_3^- and carbon availability and soil temperature and moisture content (Boyer et al., 2006). SWAT (Soil Water Assessment Tool), developed by the United States Department of Agriculture Agricultural Research Service, uses climate, soil, topography, vegetation, and land management data to predict water movement, sediment transport, crop growth, and nutrient cycling. Inputs required for SWAT are extensive and facilitate simulation of processes in watersheds of varying characteristics (Gassman, Reyes, Green, & Arnold, 2007). RHESSys (Regional Hydro-Ecological Simulation System) (Tague & Band, 2004) couples hydrology with C and N cycling, simulating denitrification through computation of a maximum denitrification rate (based on available soil nitrate), which is then scaled by soil moisture, temperature, and carbon availability (Tague & Band, 2004). While these models cover a wide range of perspectives and conceptual frameworks (i.e., agricultural, hydrological, ecological), none are explicitly designed for use in urban landscapes, where hydrology and biogeochemistry depend on human inputs and alterations of the system. The models all require extensive knowledge of the specific landscape system being studied, which limits their use to highly specialized purposes.

Field studies are necessary to validate the above models, as well as to understand controls that are driven by spatial variation in land use and management. Denitrification is difficult to model at a landscape scale because of the presence of small areas (hotspots) and short periods (hot moments) (Groffman et al., 2009; Groffman,

2012; McClain et al., 2003; P. Vidon et al., 2010) of high activity that account for a high

proportion of activity. Denitrification is also difficult to measure, and there is often

concern that results obtained depend on the method used (Groffman et al. 2006).

Denitrification can be measured as an *in situ* rate in the field, or as a potential rate

representing the maximum possible denitrification capacity given adequate anoxic

conditions and carbon source. Measurements of denitrification potential that assay the

maximum biological capacity of soils for denitrification have been useful in landscape

scale studies of undisturbed forested areas, as well as agricultural and urban

landscapes (Bettez & Groffman, 2012; Bruland, Richardson, & Whalen, 2006; P.M.

Groffman & Crawford, 2003).

Studies of denitrification potential in urban riparian zones have demonstrated that

urban conditions do not necessarily lead to low denitrification potentials. These studies

have focused on surficial soils (0-10cm), since overland flow is an important vector of

reactive N transport in these urban landscapes. A study conducted in watersheds with

various levels of disturbance in the Baltimore, MD USA area found no significant

differences in denitrification potential between urban and rural or forested versus

herbaceous sites (P.M. Groffman & Crawford, 2003) . As long as these soils were wet

and had high levels of organic matter, they had high denitrification potential (P.M.

Groffman & Crawford, 2003). These results were useful for identifying potential

denitrification hotspots in the landscape.

In another Baltimore study, denitrification potentials were compared between

natural riparian areas and stormwater control measures (SCMs), structures designed to

mitigate the increased volume and intensity of runoff from urban landscapes (Bettez &

Groffman, 2012). Because SCMs are extremely common in urban areas (Driscoll et al., 2015), there is great interest in determining their effectiveness in mitigating nutrient loading into receiving waters. Bettez and Groffman (2012) found that denitrification potential in SCM was significantly higher than that of the natural riparian areas. Even though the drivers of denitrification potential, soil moisture and organic matter, were similar between the riparian and SCM areas, SCM denitrification potential values were higher, indicating that SCMs may function as hotspots of denitrification (McClain et al., 2003). In the precipitation-heavy northeastern United States, DEA has been shown to be controlled primarily by soil moisture and organic matter (McPhillips & Walter, 2015), and the efficiency of N retention in SCMs relies on seasonality, temperature, and oxygen availability (Rosenzweig, Smith, Baeck, & Jaffé, 2011). The overall effect of these SCMs on water quality at a watershed scale remains uncertain, and variability between different SCMs in N removal effectiveness is large (Collins et al., 2010).

The influence of urbanization and SCMs on N retention and processing has also been studied in the southwestern United States, in more arid urban watersheds. Extensively modified urban streams in these regions experience lower rates of N retention (Grimm et al., 2005), and green retention basins and other examples of SCMs have proven effective in creating conditions to facilitate higher denitrification rates (Larson & Grimm, 2012; Zhu, Dillard, & Grimm, 2005). Stormwater management in these arid regions has been shown to greatly increase the heterogeneity of N, P, and dissolved organic carbon (DOC) fluxes, leading to variable denitrification rates (Hale, Turnbull, Earl, Childers, & Grimm, 2015).

The need for watershed and regional scale assessments of denitrification highlights the need for first-order models which reduce the need for costly site-specific data sampling. Denitrification correlates with soil moisture and organic matter (P.M. Groffman & Crawford, 2003), yet few studies have analyzed the predictive power of these variables (or others) to identify key areas of denitrification potential within a landscape. First-order models of denitrification (Anderson, Groffman, & Walter, 2015; Florinsky, McMahon, & Burton, 2004) have focused primarily on soil moisture as a driving factor, assuming that high levels of soil moisture and organic matter co-occur within particular landscape zones. Recent studies (Anderson et al., 2015; Florinsky et al., 2004) have used topography to represent the spatial distribution of both soil moisture and organic matter. Soil organic matter (SOM) is thought to correlate significantly with terrain variables as studies have shown that soils with high moisture content have high SOM due to the promotion of plant growth and the slowdown of organic matter decomposition in wet soils (Pei et al., 2010). However, urban hydrology disrupts natural connections between soil moisture and organic matter, with increased fragmentation of pervious areas and higher prevalence of channelized or piped flow paths (Walsh et al., 2005). The relationship between soil moisture and organic matter in urban environments is therefore more complex than in more natural environments, necessitating the modeling of these variables separately to obtain better estimates of denitrification potential.

In this study, we compiled data from multiple studies of denitrification potential in the Baltimore metropolitan area to assess the role of soil, hydrologic, and other landscape properties on denitrification potential with an eye towards developing

predictive tools for landscape and watershed-scale modeling of this process. Our objectives were to 1) examine controls on denitrification potential across a wide range of sites in the urban landscape, with a focus on soil moisture and organic matter content and 2) develop a predictive model that could be linked to geographic tools that depict the distribution of these variables across the landscape.

METHODS

Data sources

We utilized published (Bettez & Groffman, 2012; Gift, Groffman, Kaushal, & Mayer, 2010; Groffman et al., 2002; P.M. Groffman & Crawford, 2003; Hale & Groffman, 2006; Harrison, Groffman, Mayer, & Kaushal, 2012; Waters, Morse, Bettez, & Groffman, 2014) and unpublished data (sampled in 2014) from the Baltimore Ecosystem (BES) study, a component of the U.S. National Science Foundation funded long-term ecological research (LTER) network. Most studies were carried out in the Gwynns Falls watershed, a main study site for BES that includes a mix of urban, suburban, and forested land and numerous SCM (Doheny, 1999).

The BES denitrification potential dataset (available at http://beslter.org) contains 465 observations of denitrification potential and a set of ancillary variables including soil nitrate (NO_3^-), ammonium (NH_4^+), microbial respiration, potential net N mineralization, potential net nitrification, soil organic matter, soil moisture, microbial biomass C, microbial biomass N, and root biomass, along with the sampling date, site name, researcher, associated publications, habitat, land use context, latitude, longitude, and depth of sample. Microbial biomass C, microbial biomass N, and root biomass were often missing and were therefor not used as predictor variables for our study. Data

came from 66 urban, 112 suburban, and 83 forested sites. There were 387, 58, and 37

shallow, mid-depth, and deep samples (represented by 0-10 cm, 10-70 cm, and 70+

cm, respectively).

Data analysis and modeling

We split the shallow depth data into two groups for model development and

cross-validation. The 387 points were derived from 35 discrete locations. Since data

were taken at some locations at several points in time, we used 25 of these locations for

model development and 10 for cross-validation.

We compiled soil and environmental variables from the model development

points (N=205) and excluded observations with missing values for any predictor

variables (N=187). We used principal components analysis (PCA) and a correlation

matrix to identify correlations between predictor variables based on this dataset.

We developed linear regression models using R software (R Core Team, 2017)

to minimize the Akaike information criterion (AIC). We selected seven models

representing the most likely influential terms, chosen from the PCA (Figure 14, Table 7).

Interaction terms were also included in the models based on high correlations between

variables (Table 6). After building the model for denitrification potential, we tested model

performance with the cross-validation dataset. Evaluation of model performance was

based on the Nash-Sutcliffe efficiency (NSE).

RESULTS

Denitrification variations with depth and land use

Denitrification potential decreased sharply with depth (Figure 12). Because the

majority of denitrification occurs in the top 10 cm of soil, we focused model development

on this subset of data. There were no significant differences in denitrification potential between urban, suburban or forested sites (Figure 13).

PCA analysis

Prior to building multiple regression models for prediction of denitrification potential, correlations between variables were analyzed (Table 6). Denitrification potential was positively correlated with soil moisture, soil organic matter, total N, and soil respiration. We also explored correlations of variables through PCA (Table 6 and Figure 14, n=312); the analysis yielded nine linear combinations (PC). The first two components, PC1 and PC2, together explain 53% of the variation (36% and 17%, respectively) in environmental variables across the samples. We found that NH_4, total N, soil moisture, DEA, and respiration correlated in axis 1, and the orthogonal axis grouped net nitrification and net N mineralization.

Multiple regression models for available shallow denitrification potential data

For the available shallow (<10 cm) observations designated for model development (N=205), models ranked 1 and 2 had equivalent AICc values, using the criterion that models within ΔAICc < 2 are equivalent (Table 8). Models with interaction terms were tested, and the interactions retained in the best model were those between moisture and respiration, and moisture and total N. The second-ranked model adds the respiration and total N interaction to the best model (rank = 1), but this does not significantly improve the explanation of the data. The rank 1 model achieved an NSE value of 0.511 (Figure 15).

DISCUSSION

Patterns of denitrification potential

We expected denitrification potential to be highest in the shallow samples, due to a higher likelihood of high levels of organic matter near the surface. The observed trend in denitrification potential with depth matches our expectations, and agrees with many previous studies which demonstrate decreasing denitrification capacity with depth (Bettez & Groffman, 2012; Brye, Norman, Bundy, & Gower, 2001; P.M. Groffman & Crawford, 2003; Jefferson et al., 2010; Luo, Tillman, White, & Ball, 1998; Parkin & Meisinger, 1989; Saggar et al., 2013). While our modeling thus focuses on surface soil, it is important to note that activity at depth can be significant (Morse et al., 2014) and is especially important for processing of NO_3^- moving in shallow groundwater (Gold et al., 2001; P. G. F. Vidon & Hill, 2004). Our focus on surface processes is appropriate for urban landscapes, where there is great interest in capturing and processing stormwater surface runoff.

Somewhat surprisingly, there were no differences in denitrification potential between urban, suburban and forested sites. Due to altered urban hydrology (Walsh et al., 2005), changing nutrient export pathways (Kaushal & Belt, 2012), and a "distinct urban biogeochemistry" (Kaye, Groffman, Grimm, Baker, & Pouyat, 2006), we expected urban environments to be poorly suited for nutrient uptake and processing. However, denitrification potential has been shown to occur at high rates in urban environments (Grimm et al., 2005; P.M. Groffman & Crawford, 2003; Inwood, Tank, & Bernot, 2005). Groffman and Crawford [2003] reported higher variability in denitrification potential in urban areas compared to rural areas, which is logical given the characteristics of urban

91

landscapes. However, for our dataset, variability was higher in forested and suburban land uses as compared to urban (Figure 13). Changes in variation with land use would complicate landscape-scale modeling in urban areas.

It should be noted that denitrification potential does not necessarily reflect the actual denitrification rates occurring in the field. Denitrification potential and rate have been shown to correlate well (Groffman & Tiedje, 1989), but a lack of anoxic conditions, carbon source, or available nitrate can explain a location with high denitrification potential but low rate.

Predicting denitrification potential

We identified robust multiple regression models of denitrification potential for sampled shallow (0-10 cm) locations. The best predictors for DEA for the Baltimore dataset are soil moisture, respiration, and total N. Soil moisture is the primary factor used in previous denitrification modeling efforts, and was assumed to be critical in our model. Previous analyses of relationships between soil moisture and denitrification potential using subsets of our dataset had R^2 values of 0.55 (urban and rural riparian areas) (P.M. Groffman & Crawford, 2003), 0.66 (in SCMs) (Bettez & Groffman, 2012), and 0.35 (forested and herbaceous riparian areas) (Bettez & Groffman, 2012). We also included various interaction effects, including those between soil moisture and respiration, soil moisture and total N, and respiration and total N. The interactions between soil moisture and respiration and soil moisture and total N are included in the best model (rank = 1). The interaction between soil moisture and respiration is positive, indicating that increased soil moisture boosts the effect of respiration. However, the interaction between soil moisture and total N is negative, suggesting that higher soil

92

moisture decreases the effect of total N. Since DEA represents the potential

denitrification at a site, the presence of high N at a site may create denitrifying

conditions, which decreases the total N. The relationship between total N and DEA is

complex, since the process of removal affects the presence of total N at the sampling

location. This interaction may require further exploration to determine how to best

account for this behavior.

Soil moisture is frequently identified as the key driver of terrestrial denitrification

as this variable controls soil oxygen levels which are the primary controller of this

anaerobic process at the cellular level (Tiedje, Sexstone, Parkin, & Revsbech, 1984).

Many other variables were also highly correlated with soil moisture (NH_4^+, total inorganic

N, respiration, organic matter), demonstrating the strong role soil moisture plays in C

and N cycling processes. At a larger scale, soil moisture (as represented by the soil

topographic index) was shown to predict sampled denitrification rates in an agricultural

catchment with an R^2 value of 0.86 (Anderson et al., 2015). Many other studies have

explored the connection between soil denitrification and topographic controls with less

explicit goals of modeling denitrification likelihoods (Hayakawa, Nakata, Jiang,

Kuramochi, & Hatano, 2012; Xiong et al., 2015). Our results show that soil moisture

remains a strong driver of denitrification in highly altered and variable urban

watersheds, suggesting that the fundamental controls that operate in more well studied

agricultural and forested ecosystems are still valid and useful for modeling these

watersheds.

We hypothesized that soil organic matter would be a strong predictor of

denitrification potential. Bettez and Groffman [2012] demonstrated strong correlations

between denitrification potential and soil moisture (R^2=0.66), soil organic matter (R^2=0.89), microbial biomass C (R^2=0.79), and respiration (R^2=0.81) in an analysis of a subset of the samples in our data sets. Many other studies have also found soil organic matter to be a strong predictor of denitrification potential (Burford & Bremner, 1975). Organic matter is a logically strong predictor of denitrification potential as it provides an index of the supply of carbon to support heterotrophic denitrifiers and of the potential for oxygen consumption by overall heterotrophic activity. However, our model development concludes that soil respiration was a stronger predictor than organic matter. This is perhaps not a surprising result as respiration is driven by levels of labile carbon and is therefore a more direct controller of heterotrophic activity than total organic matter content. Respiration may be a particularly useful/important predictor of denitrification in urban watersheds, where hydrologic changes have altered relationships between water table depth, stream channel depth, soil moisture and organic matter content (Groffman et al., 2003). Total N also emerged as a key factor in predicting DEA in our study dataset. Denitrifiers require anoxic conditions for denitrification, as well as carbon and nitrogen sources. The best model (rank = 1) represents these three facets through soil moisture, respiration, and total N. In order to successfully apply this modeling framework, proxies must be determined for each of these three variables, to maintain the intended parsimonious nature of the model.

Soil moisture modeling presents a challenge which has been studied for many decades, particularly in urban environments. The addition of grey infrastructure in urban environments, which routes water independently of topographic influence, requires a new understanding of soil moisture processes. The TOPURBAN model was developed

for use in urban environments, using a topographic framework but only including the pervious areas to upslope contributing areas, allowing impervious area flow to become runoff (Valeo & Moin, 2000). This TOPURBAN model does not account for impervious areas which may route water to pervious areas to infiltrate. Watershed models have used road network maps to enhance NLCD maps to improve runoff quantity estimates (Endreny & Thomas, 2009), but have not explicitly explored the resulting soil moisture regimes. There is a need for the coupling of natural and human-influenced water routing processes to allow for better estimates of soil moisture across landscapes.

Soil temperature has been shown to drive month-to-month variation in soil respiration (Raich, Potter, & Bhagawati, 2002). Raich, Potter, & Bhagawati (2002) demonstrated that monthly variation in soil respiration could be predicted using monthly precipitation and temperature values (T&P model). However, these predictors cannot be measured with high spatial resolution; in order to predict inter-site variability, leaf area index (LAI) was successfully incorporated into the model to predict temporally and spatially different soil respiration values (Reichstein et al., 2003). The availability of satellite images of LAI provides greater access to parameters necessary to model soil respiration, in both spatial and temporal dimensions. The development of the "T&P&LAI model" suggests that soil respiration may be feasibly modeled without need for costly, time-intensive sampling efforts, provided the necessary data is available. Total N may also be modeled inexpensively, through modification of simple export coefficient models. In addition to modeling the spatial distribution of nonpoint source N through a modified export coefficient framework (Stephan & Endreny, 2016), point sources of N

can be included to create a more accurate representation of N loading through landscapes.

In order to effectively model DEA in these mixed-use watersheds, our study shows that effective means of predicting soil moisture, soil respiration, and total N are critical. There is a great deal of current research seeking to represent hydrological modeling and routing in urban environments (for a review of the current research, see Elga, Jan, & Okke, 2015). Modeling CO_2 flux from respiration is also a subset of climate change research (e.g., Davidson & Janssens, 2006). Updated export coefficient models are also being developed to represent the nutrient export from particular land uses, which can be used in this DEA model as well. As topographic methods are modified to suit urban environments more appropriately, or other spatially variable soil moisture routines for urban areas are developed, DEA can be more easily understood and mapped across a landscape. In addition, the successful modeling of soil respiration using precipitation, temperature, and LAI factors, as well at total N using land use parameters, will enhance our understanding of DEA locations within a mixed-use watershed and highlight landscape locations prime for nitrate removal.

Nitrate yield in suburban and urban watersheds has also been shown to be more than 10 times higher than that of completely forested watersheds, and yet retention of N in these disturbed watersheds was surprisingly high, approaching that of forested catchments (Groffman, Law, Belt, Band, & Fisher, 2004). The sources of N in disturbed watersheds, as well as the flowpaths and removal mechanisms in these watersheds, must be linked in order to get a full picture of how we can manage N water quality concerns. The mechanism of transport of nitrate between soil water and surface

streamflow in disturbed and undisturbed streams was examined in a review paper (Sudduth, Perakis, & Bernhardt, 2013), and no pattern or relationship was found for the disturbed stream nitrate concentrations. Further work is necessary to quantify nitrate loading mechanisms in urban watersheds.

CONCLUSION

Denitrification is an important means of removing reactive N from soil, converting it to its inert gaseous state and preventing its movement into water bodies. Landscape-scale modeling of this process is needed to identify key areas (hotspots) that provide this important function. Urban environments have only recently become the focus of biogeochemical research, due to their complex hydrologic and nutrient pathways. However, our data suggest that there are coherent controls of denitrification potential in these environments and data are available to produce robust statistical models of this process that can be used in urban watersheds. A major challenge for future research is to develop models and/or geographic data sources that can depict spatial and temporal variation in the key drivers of denitrification in these watersheds. These models will improve our ability to assess and enhance N removal by designing cities to provide areas suitable for denitrification to occur.

LITERATURE CITED

Anderson, T. R., Groffman, P. M., & Walter, M. T. (2015). Using a soil topographic index

to distribute denitrification fluxes across a northeastern headwater catchment.

Journal of Hydrology, *522*, 123–134. https://doi.org/10.1016/j.jhydrol.2014.12.043

Bettez, N. D., & Groffman, P. M. (2012). Denitrification Potential in Stormwater Control

Structures and Natural Riparian Zones in an Urban Landscape. *Environmental*

Science & Technology, *46*(20), 10909–10917. https://doi.org/10.1021/es301409z

Boyer, E. W., Alexander, R. B., PARTON, W. J., Li, C., Butterbach-Bahl, K., Donner, S.

D., … Grosso, S. J. D. (2006). MODELING DENITRIFICATION IN

TERRESTRIAL AND AQUATIC ECOSYSTEMS AT REGIONAL SCALES.

Ecological Applications, *16*(6), 2123–2142. https://doi.org/10.1890/1051-

0761(2006)016[2123:MDITAA]2.0.CO;2

Breemen, N. van, Boyer, E. W., Goodale, C. L., Jaworski, N. A., Paustian, K.,

Seitzinger, S. P., … Billen, G. (2002). Where did all the nitrogen go? Fate of

nitrogen inputs to large watersheds in the northeastern U.S.A. *Biogeochemistry*,

57–58(1), 267–293. https://doi.org/10.1023/A:1015775225913

Bruland, G. L., Richardson, C. J., & Whalen, S. C. (2006). Spatial variability of

denitrification potential and related soil properties in created, restored, and paired

natural. *Wetlands*, *26*(4), 1042–1056. https://doi.org/10.1672/0277-

5212(2006)26[1042:SVODPA]2.0.CO;2

Brye, K. R., Norman, J. M., Bundy, L. G., & Gower, S. T. (2001). Nitrogen and Carbon

Leaching in Agroecosystems and Their Role in Denitrification Potential. *Journal*

of Environmental Quality, *30*(1), 58–70. https://doi.org/10.2134/jeq2001.30158x

Burford, J. R., & Bremner, J. M. (1975). Relationships between the denitrification

    capacities of soils and total, water-soluble and readily decomposable soil organic

    matter. *Soil Biology and Biochemistry*, *7*(6), 389–394.

    https://doi.org/10.1016/0038-0717(75)90055-3

Collins, K. A., Lawrence, T. J., Stander, E. K., Jontos, R. J., Kaushal, S. S., Newcomer,

    T. A., … Cole Ekberg, M. L. (2010). Opportunities and challenges for managing

    nitrogen in urban stormwater: A review and synthesis. *Ecological Engineering*,

    36(11), 1507–1519. https://doi.org/10.1016/j.ecoleng.2010.03.015

Davidson, E. A., & Janssens, I. A. (2006). Temperature sensitivity of soil carbon

    decomposition and feedbacks to climate change. *Nature*. Retrieved from

    http://agris.fao.org/agris-search/search.do?recordID=US201301106728

Doheny, E. J. (1999). Index of hydrologic characteristics and data resources for the

    Gwynns Falls watershed, Baltimore County and Baltimore City, Maryland. USGS

    Report OFR 99-213.U.S. Geological Survey, Denver, CO. 24 pp.

Driscoll, C. T., Eger, C. G., Chandler, D. G., Davidson, C. I., Roodsari, B. K., Flynn, C.

    D., … Groffman, P. M. (2015). Green Infrastructure: Lessons from Science and

    Practice. A publication of the Science Policy Exchange. 32 pages.

Elga, S., Jan, B., & Okke, B. (2015). Hydrological modelling of urbanized catchments: A

    review and future directions. *Journal of Hydrology*, *529*(Part 1), 62–81.

    https://doi.org/10.1016/j.jhydrol.2015.06.028

Endreny, T., & Thomas, K. (2009). Improving Estimates of Simulated Runoff Quality and

    Quantity Using Road-Enhanced Land Cover Data. *Journal of Hydrologic*

Engineering, *14*(4), 346–351. https://doi.org/10.1061/(ASCE)1084-0699(2009)14:4(346)

Florinsky, I. V., McMahon, S., & Burton, D. L. (2004). Topographic control of soil microbial activity: a case study of denitrifiers. *Geoderma*, *119*(1–2), 33–53. https://doi.org/10.1016/S0016-7061(03)00224-6

Gassman, P. W., Reyes, M. R., Green, C. H., & Arnold, J. G. (2007). *Soil and Water Assessment Tool: Historical Development, Applications, and Future Research Directions, The* (Center for Agricultural and Rural Development (CARD) Publications No. 07–wp443). Center for Agricultural and Rural Development (CARD) at Iowa State University. Retrieved from https://ideas.repec.org/p/ias/cpaper/07-wp443.html

Gift, D. M., Groffman, P. M., Kaushal, S. S., & Mayer, P. M. (2010). Denitrification Potential, Root Biomass, and Organic Matter in Degraded and Restored Urban Riparian Zones. *Restoration Ecology*, *18*(1), 113–120. https://doi.org/10.1111/j.1526-100X.2008.00438.x

Gold, A. J., Groffman, P. M., Addy, K., Kellogg, D. Q., Stolt, M., & Rosenblatt, A. E. (2001). Landscape Attributes as Controls on Ground Water Nitrate Removal Capacity of Riparian Zones. *JAWRA Journal of the American Water Resources Association*, *37*(6), 1457–1464. https://doi.org/10.1111/j.1752-1688.2001.tb03652.x

Grimm, N. B., Sheibley, R. W., Crenshaw, C. L., Dahm, C. N., Roach, W. J., & Zeglin, L. H. (2005). N retention and transformation in urban streams. *Journal of the North*

American Benthological Society, *24*(3), 626–642. https://doi.org/10.1899/04-027.1

Groffman, P. M. (2012). Terrestrial denitrification: challenges and opportunities. *Ecological Processes*, *1*(1), 11. https://doi.org/10.1186/2192-1709-1-11

Groffman, P. M., Bain, D. J., Band, L. E., Belt, K. T., Brush, G. S., Grove, J. M., … Zipperer, W. C. (2003). Down by the riverside: urban riparian ecology. *Frontiers in Ecology and the Environment*, *1*(6), 315–321. https://doi.org/10.1890/1540-9295(2003)001[0315:DBTRUR]2.0.CO;2

Groffman, P. M., Boulware, N. J., Zipperer, W. C., Pouyat, R. V., Band, L. E., & Colosimo, M. F. (2002). Soil Nitrogen Cycle Processes in Urban Riparian Zones. *Environmental Science & Technology*, *36*(21), 4547–4552. https://doi.org/10.1021/es020649z

Groffman, P. M., Butterbach-Bahl, K., Fulweiler, R. W., Gold, A. J., Morse, J. L., Stander, E. K., … Vidon, P. (2009). Challenges to incorporating spatially and temporally explicit phenomena (hotspots and hot moments) in denitrification models. *Biogeochemistry*, *93*(1–2), 49–77. https://doi.org/10.1007/s10533-008-9277-5

Groffman, P. M., & Crawford, M. K. (2003). Denitrification potential in urban riparian zones. *Journal of Environmental Quality*, *32*(3), 1144–1149.

Groffman, P. M., Law, N. L., Belt, K. T., Band, L. E., & Fisher, G. T. (2004). Nitrogen Fluxes and Retention in Urban Watershed. *Ecosystems*, *7*(4), 393–403. https://doi.org/10.1007/s10021-003-0039-x

Groffman, P. M., & Tiedje, J. M. (1989). Denitrification in north temperate forest soils:

    Relationships between denitrification and environmental factors at the landscape

    scale. *Soil Biology and Biochemistry*, *21*(5), 621–626.

    https://doi.org/10.1016/0038-0717(89)90054-0

Hale, R. L., & Groffman, P. M. (2006). Chloride Effects on Nitrogen Dynamics in

    Forested and Suburban Stream Debris Dams. *Journal of Environmental Quality*,

    35(6), 2425–2432. https://doi.org/10.2134/jeq2006.0164

Hale, R. L., Turnbull, L., Earl, S. R., Childers, D. L., & Grimm, N. B. (2015). Stormwater

    Infrastructure Controls Runoff and Dissolved Material Export from Arid Urban

    Watersheds. *Ecosystems*, *18*(1), 62–75. https://doi.org/10.1007/s10021-014-

    9812-2

Harrison, M. D., Groffman, P. M., Mayer, P. M., & Kaushal, S. S. (2012). Microbial

    biomass and activity in geomorphic features in forested and urban restored and

    degraded streams. *Ecological Engineering*, *38*(1), 1–10.

    https://doi.org/10.1016/j.ecoleng.2011.09.001

Hayakawa, A., Nakata, M., Jiang, R., Kuramochi, K., & Hatano, R. (2012). Spatial

    variation of denitrification potential of grassland, windbreak forest, and riparian

    forest soils in an agricultural catchment in eastern Hokkaido, Japan. *Ecological*

    Engineering, *47*, 92–100. https://doi.org/10.1016/j.ecoleng.2012.06.034

Inwood, S. E., Tank, J. L., & Bernot, M. J. (2005). Patterns of denitrification associated

    with land use in 9 midwestern headwater streams. *Journal of the North American*

    Benthological Society, *24*(2), 227–245. https://doi.org/10.1899/04-032.1

J. R. Williams, C. A. Jones, & P. T. Dyke. (1984). A Modeling Approach to Determining

    the Relationship Between Erosion and Soil Productivity. *Transactions of the*

    ASAE, *27*(1), 0129–0144. https://doi.org/10.13031/2013.32748

Jefferson, A., O'Driscoll, M., Manda, A., Clinton, S., Jefferson, A., & McMillan, S. (2010).

    Urbanization Effects on Watershed Hydrology and In-Stream Processes in the

    Southern United States. *WATER*, *2*(3), 605–648.

Kaushal, S. S., & Belt, K. T. (2012). The urban watershed continuum: evolving spatial

    and temporal dimensions. *Urban Ecosystems*, *15*(2), 409–435.

    https://doi.org/10.1007/s11252-012-0226-7

Kaye, J. P., Groffman, P. M., Grimm, N. B., Baker, L. A., & Pouyat, R. V. (2006). A

    distinct urban biogeochemistry? *Trends in Ecology & Evolution*, *21*(4), 192–199.

    https://doi.org/10.1016/j.tree.2005.12.006

Larson, E. K., & Grimm, N. B. (2012). Small-scale and extensive hydrogeomorphic

    modification and water redistribution in a desert city and implications for regional

    nitrogen removal. *Urban Ecosystems*, *15*(1), 71–85.

    https://doi.org/10.1007/s11252-011-0208-1

Li, C. (1996). The DNDC Model. In D. S. Powlson, P. Smith, & J. U. Smith (Eds.),

    Evaluation of Soil Organic Matter Models (pp. 263–267). Springer Berlin

    Heidelberg. Retrieved from http://link.springer.com/chapter/10.1007/978-3-642-

    61094-3_20

Luo, J., Tillman, R. W., White, R. E., & Ball, P. R. (1998). Variation in denitrification

    activity with soil depth under pasture. *Soil Biology and Biochemistry*, *30*(7), 897–

    903. https://doi.org/10.1016/S0038-0717(97)00206-X

McClain, M. E., Boyer, E. W., Dent, C. L., Gergel, S. E., Grimm, N. B., Groffman, P. M.,

  … Pinay, G. (2003). Biogeochemical Hot Spots and Hot Moments at the Interface

  of Terrestrial and Aquatic Ecosystems. *Ecosystems*, *6*(4), 301–312.

  https://doi.org/10.1007/s10021-003-0161-9

McPhillips, L., & Walter, M. T. (2015). Hydrologic conditions drive denitrification and

  greenhouse gas emissions in stormwater detention basins. *Ecological*

  Engineering, *85*, 67–75. https://doi.org/10.1016/j.ecoleng.2015.10.018

Morse, J. L., Werner, S. F., Gillin, C. P., Goodale, C. L., Bailey, S. W., McGuire, K. J., &

  Groffman, P. M. (2014). Searching for biogeochemical hot spots in three

  dimensions: Soil C and N cycling in hydropedologic settings in a northern

  hardwood forest. *Journal of Geophysical Research: Biogeosciences*, *119*(8),

  2013JG002589. https://doi.org/10.1002/2013JG002589

Parkin, T. B., & Meisinger, J. J. (1989). Denitrification below the Crop Rooting Zone as

  Influenced by Surface Tillage. *Journal of Environmental Quality*, *18*(1), 12–16.

  https://doi.org/10.2134/jeq1989.00472425001800010002x

Parton, W. J., Mosier, A. R., Ojima, D. S., Valentine, D. W., Schimel, D. S., Weier, K., &

  Kulmala, A. E. (1996). Generalized model for N2 and N2O production from

  nitrification and denitrification. *Global Biogeochemical Cycles*, *10*(3), 401–412.

  https://doi.org/10.1029/96GB01455

Pei, T., Qin, C.-Z., Zhu, A.-X., Yang, L., Luo, M., Li, B., & Zhou, C. (2010). Mapping soil

  organic matter using the topographic wetness index: A comparative study based

  on different flow-direction algorithms and kriging methods. *Ecological Indicators*,

  10(3), 610–619. https://doi.org/10.1016/j.ecolind.2009.10.005

R Core Team. (2017). *R: A language and environment for statistical computing*. R

        Foundation for Statistical Computing, Vienna, Austria. Retrieved from

        https://www.R-project.org

Raich, J. W., Potter, C. S., & Bhagawati, D. (2002). Interannual variability in global soil

        respiration, 1980–94. *Global Change Biology*, *8*(8), 800–812.

        https://doi.org/10.1046/j.1365-2486.2002.00511.x

Reichstein, M., Rey, A., Freibauer, A., Tenhunen, J., Valentini, R., Banza, J., … Yakir,

        D. (2003). Modeling temporal and large-scale spatial variability of soil respiration

        from soil water availability, temperature and vegetation productivity indices.

        Global Biogeochemical Cycles, *17*(4), 1104.

        https://doi.org/10.1029/2003GB002035

Rosenzweig, B. R., Smith, J. A., Baeck, M. L., & Jaffé, P. R. (2011). Monitoring Nitrogen

        Loading and Retention in an Urban Stormwater Detention Pond. *Journal of*

        Environmental Quality, *40*(2), 598–609. https://doi.org/10.2134/jeq2010.0300

Saggar, S., Jha, N., Deslippe, J., Bolan, N. S., Luo, J., Giltrap, D. L., … Tillman, R. W.

        (2013). Denitrification and N2O:N2 production in temperate grasslands:

        Processes, measurements, modelling and mitigating negative impacts. *Science*

        of The Total Environment, *465*, 173–195.

        https://doi.org/10.1016/j.scitotenv.2012.11.050

Seitzinger, S. P., Styles, R. V., Boyer, E. W., Alexander, R. B., Billen, G., Howarth, R.

        W., … Breemen, N. van. (2002). Nitrogen retention in rivers: model development

        and application to watersheds in the northeastern U.S.A. *Biogeochemistry*, *57–*

        58(1), 199–237. https://doi.org/10.1023/A:1015745629794

Stephan, E. A., & Endreny, T. A. (2016). Weighting Nitrogen and Phosphorus Pixel

    Pollutant Loads to Represent Runoff and Buffering Likelihoods. *JAWRA Journal*

    of the American Water Resources Association, *52*(2), 336–349.

    https://doi.org/10.1111/1752-1688.12390

Sudduth, E. B., Perakis, S. S., & Bernhardt, E. S. (2013). Nitrate in watersheds: Straight

    from soils to streams? *Journal of Geophysical Research: Biogeosciences*,

    118(1), 291–302. https://doi.org/10.1002/jgrg.20030

Tague, C. L., & Band, L. E. (2004). RHESSys: Regional Hydro-Ecologic Simulation

    System--An Object-Oriented Approach to Spatially Distributed Modeling of

    Carbon, Water, and Nutrient Cycling. *Earth Interactions*, *8*(1), 1–42.

Tiedje, J. M., Sexstone, A. J., Parkin, T. B., & Revsbech, N. P. (1984). Anaerobic

    processes in soil. *Plant and Soil*, *76*(1–3), 197–212.

    https://doi.org/10.1007/BF02205580

Valeo, C., & Moin, S. M. A. (2000). Variable source area modelling in urbanizing

    watersheds. *Journal of Hydrology*, *228*(1–2), 68–81.

    https://doi.org/10.1016/S0022-1694(00)00153-0

Vidon, P., Allan, C., Burns, D., Duval, T. P., Gurwick, N., Inamdar, S., … Sebestyen, S.

    (2010). Hot Spots and Hot Moments in Riparian Zones: Potential for Improved

    Water Quality Management1. *JAWRA Journal of the American Water Resources*

    Association, *46*(2), 278–298. https://doi.org/10.1111/j.1752-1688.2010.00420.x

Vidon, P. G. F., & Hill, A. R. (2004). Landscape controls on nitrate removal in stream

    riparian zones. *Water Resources Research*, *40*(3), W03201.

    https://doi.org/10.1029/2003WR002473

Vitousek, P. M., Aber, J. D., Howarth, R. W., Likens, G. E., Matson, P. A., Schindler, D.

    W., … Tilman, D. G. (1997). HUMAN ALTERATION OF THE GLOBAL

    NITROGEN CYCLE: SOURCES AND CONSEQUENCES. *Ecological*

    Applications, *7*(3), 737–750. https://doi.org/10.1890/1051-

    0761(1997)007[0737:HAOTGN]2.0.CO;2

Walsh, C. J., Roy, A. H., Feminella, J. W., Cottingham, P. D., Groffman, P. M., &

    Morgan, R. P. (2005). The urban stream syndrome: current knowledge and the

    search for a cure. *Journal of the North American Benthological Society*, *24*(3),

    706–723. https://doi.org/10.1899/04-028.1

Waters, E., Morse, J., Bettez, N., & Groffman, P. (2014). Differential Carbon and

    Nitrogen Controls of Denitrification in Riparian Zones and Streams along an

    Urban to Exurban Gradient. *Journal of Environmental Quality*, *43*(3).

    https://doi.org/10.2134/jeq2013.12.0504

Xiong, Z., Li, S., Yao, L., Liu, G., Zhang, Q., & Liu, W. (2015). Topography and land use

    effects on spatial variability of soil denitrification and related soil properties in

    riparian wetlands. *Ecological Engineering*, *83*, 437–443.

    https://doi.org/10.1016/j.ecoleng.2015.04.094

Zhu, W.-X., Dillard, N. D., & Grimm, N. B. (2005). Urban nitrogen biogeochemistry:

    status and processes in green retention basins. *Biogeochemistry*, *71*(2), 177–

    196. https://doi.org/10.1007/s10533-005-0683-7

TABLES

Table 6: Correlation matrix (r values) among denitrification potential and select groundwater and soil physiochemical characteristics.

	Groundwater				Soil				
	DEA (ng/g/hr)	NO$_2$/NO$_3$ (ug N/g dry soil)	NH$_4$ (ug N/g dry soil)	Initial Total N (ug N/g dry soil)	Soil Respiration (ug C/g/d)	Potential Net N Mineralization (ug N/g/d)	Potential Net N Nitrification (ug N/g/d)	Soil organic matter (g/g)	Soil moisture (g/g)
Denitrification potential	1								
NO$_2$/NO$_3$	0.339	1							
NH$_4$	**0.352**	-0.072	1						
Total N	**0.515**	**0.648**	**0.556**	1					
Respiration	**0.469**	0.217	**0.459**	**0.445**	1				
Mineralization	**-0.134**	0.190	**-0.347**	**-0.154**	**-0.111**	1			
Nitrification	-0.017	0.137	0.008	0.090	-0.102	**0.693**	1		
Soil organic matter	**0.189**	0.078	0.195	0.205	0.248	-0.049	-0.132	1	
Soil moisture	**0.460**	0.062	**0.434**	**0.318**	**0.419**	**-0.238**	-0.206	**0.467**	1

Table 7: Loadings and correlation coefficients for the first two principal components (PC1 and PC2) for all shallow samples (n = 312)

	PC1		PC2	
Variable	Loading	Correlation coefficient	Loading	Correlation coefficient
DEA	0.41	0.73	-0.21	-0.26
NO_2 / NO_3	0.08	0.15	0.16	0.20
NH_4	0.48	0.86	-0.08	-0.10
Total N	0.48	0.85	0.02	0.02
Respiration	0.32	0.58	-0.06	-0.08
N mineralization	-0.27	-0.48	-0.60	-0.74
N nitrification	-0.11	-0.19	-0.68	-0.85
Organic Matter	0.12	0.21	-0.25	-0.31
Moisture	0.41	0.73	-0.20	-0.25
Eigenvalue	3.20		1.55	
% Variance explained	35.59%		17.26%	

Table 8: Model selection criterial used in ranking linear regression models predicting the denitrification potential (DEA) of sampled sites (N=205). The best model (rank = 1) had the lowest AICc value and the highest Akaike weight. There were eight candidate models, including a null model with intercept only (model rank = 8).

DEA model rankings								Coefficient estimates (with standard error)					
Rank	df	AICc	ΔAICc	Akaike weight	Cum. weight	Log-likelihood	Deviance	Moisture	Resp.	Total N	Moisture: Resp.	Moisture: Total N	Resp.: Total N
1	5	3167.1	0	0.59	0.59	-1576.23	3152.46	6628.15± 1330.98	-15.30± 3.37	166.17± 33.9	62.06± 9.94	-514.66± 96.85	
2	6	3167.8	0.7	0.41	1	-1575.49	3150.98	6522.50± 1332.4	-13.17± 3.81	171.22± 34.12	60.60± 10	-506.36± 96.98	-0.16± 0.14
3	4	3192.0	24.9	<0.001	1	-1589.78	3179.56	208.22± 314.36	-15.79± 3.61	2.65± 15.24	65.55± 10.63		
4	4	3201.4	34.3	<0.001	1	-1594.47	3188.94	11063.25± 1237.66	4.82± 1.10	164.31± 37.27		-554.71± 106.24	
5	3	3208.0	40.9	<0.001	1	-1598.83	3197.66	1653.32± 979.38	-15.53± 3.54		64.96± 10.49		
6	3	3225.4	58.3	<0.001	1	-1607.52	3215.04	5943.27± 807.47	5.51± 1.17	-12.82± 16.49			
7	2	3241.5	74.4	<0.001	1	-1616.64	3233.28	5764.12± 789.88	5.40± 1.15				
8	0	3597.0	429.9	<0.001	1	-1796.48	3592.96						

FIGURES
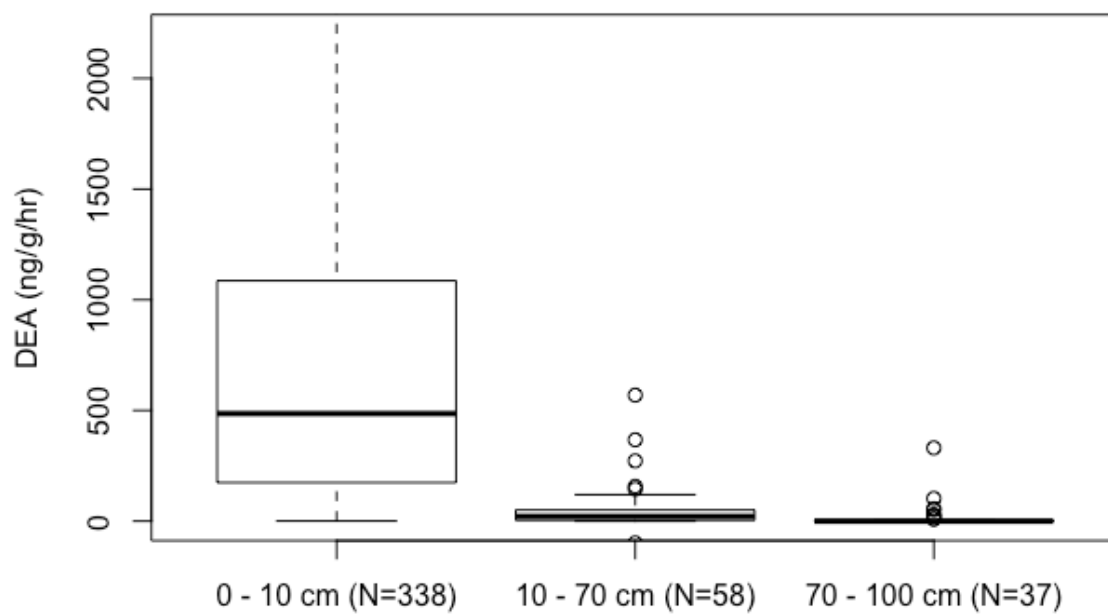
Figure 12: Variation in denitrification potential with depth
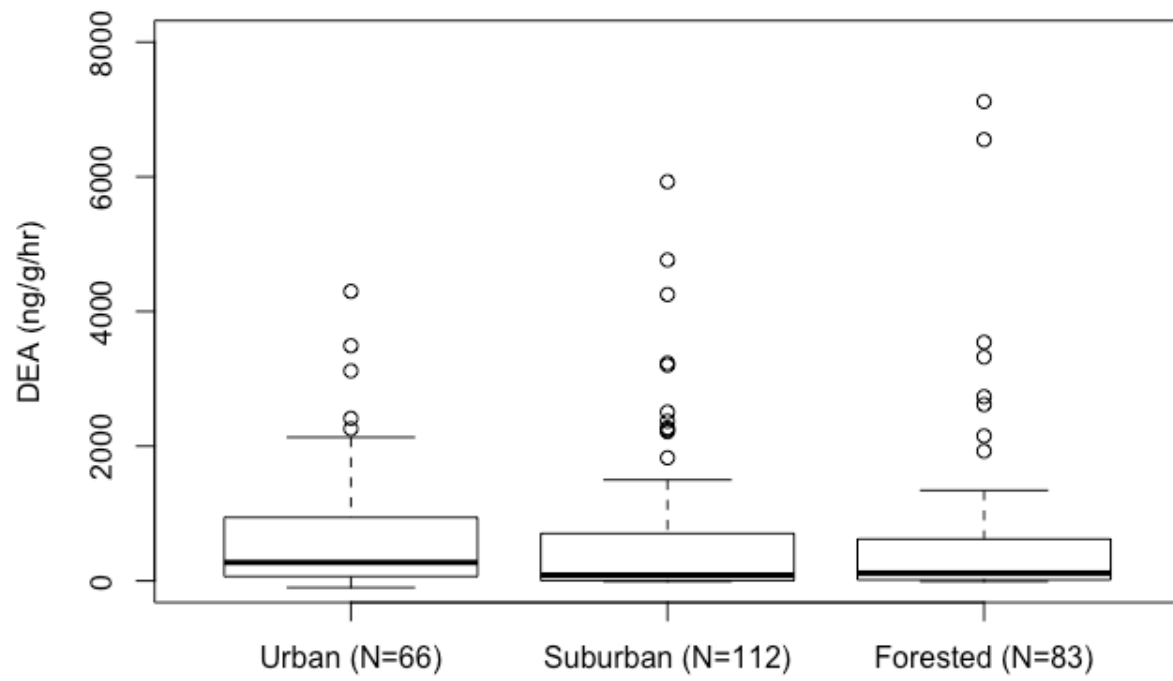
Figure 13: Variation in denitrification potential with land use
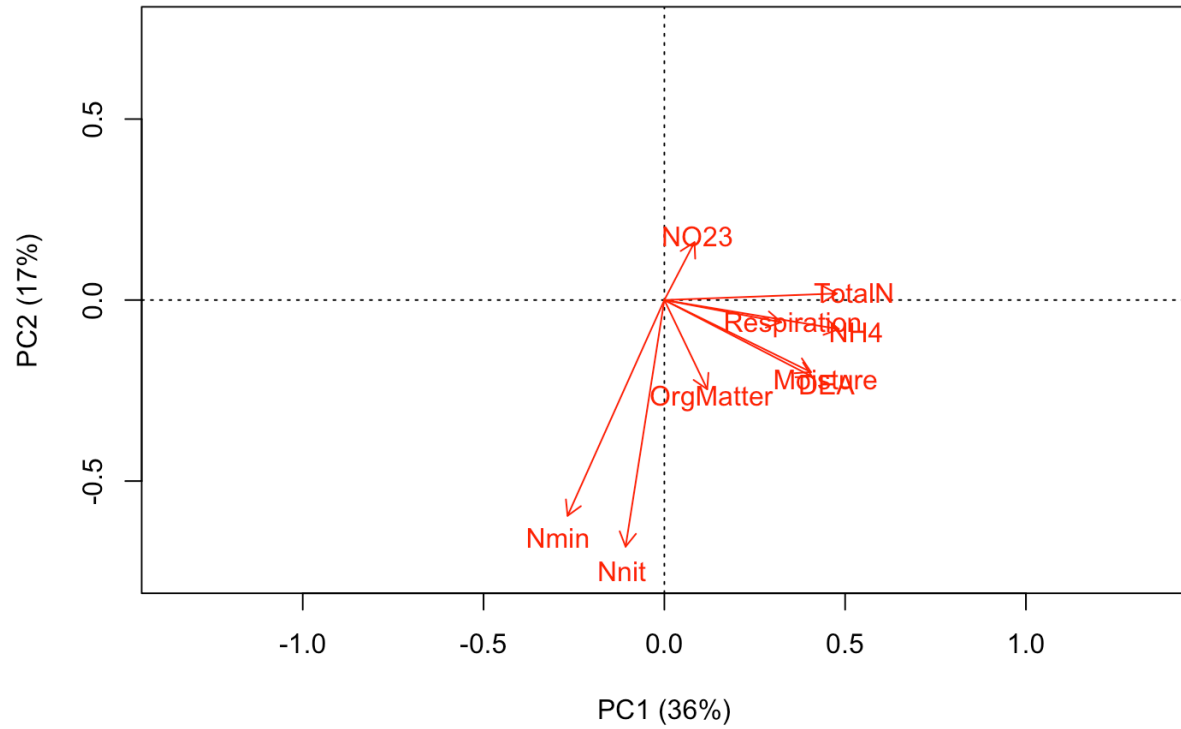
Figure 14: PCA analysis for all denitrification potential samples
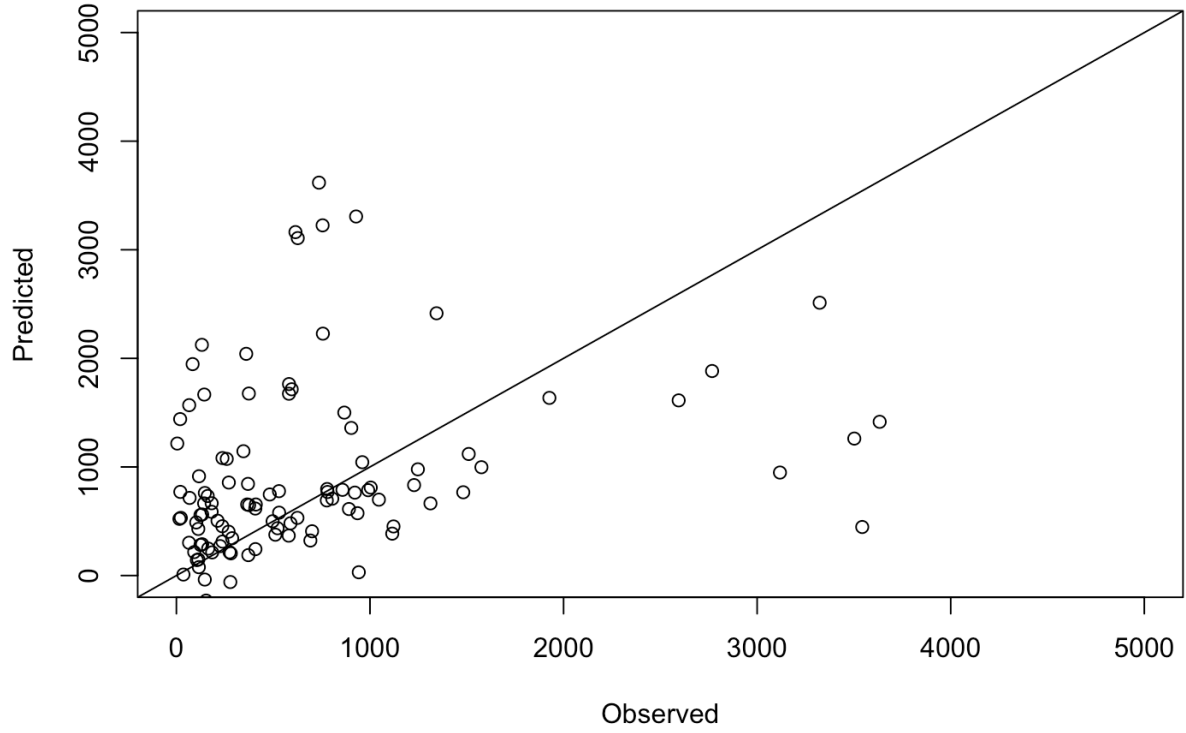
Figure 15: Predicted vs. observed DEA for model validation (NSE = 0.511)

CHAPTER 5: SYNTHESIS

In this dissertation, methods of enhancing first-order models to incorporate newly available datasets are highlighted. Water quality models were improved through the addition of spatial and temporal weighting techniques to the otherwise static export coefficient (EC) model framework, to provide better estimates of nutrient loading and, ultimately, guide management decisions and strategies. The research answers the following questions:

1)   Can algorithms for runoff and buffering likelihood be used to weight land cover specific EC and EMC values to represent the likely spatial variation in nitrogen loading to waterbodies across the landscape?

2)   Can national datasets which represent temporal variation in potential discharge rates be incorporated into a modified EC model to represent changing weather and discharge conditions to better predict annual nutrient loading variation?

3)   Which key soil variables have the largest influence on denitrification potential in urban and mixed-use landscapes, and how can these variables be combined to develop a predictive denitrification model?

Chapter 2 highlights the enhancement of the EC model via the runoff and buffering likelihood indices. The research enhanced the CADA NPS model to achieve three goals in watershed simulation of nutrient hotspot mapping: a) flexibility to use EC, EMC or other NPS loading data for N or P loads; b) representation impervious and pervious runoff paths in the contributing area; and c) representation of surface and subsurface buffer paths in the dispersal area. These updates are critical for the co-management of P and N, which often occur in the surface and subsurface runoff

flowpaths at different proportions. The urban biogeochemistry of complex social-infrastructure-environmental interactions result in elevated nutrient concentrations along accelerated flow paths with a high level of apparently random individual decisions affecting receiving water quality (Kaye et al., 2006). The enhanced CADA NPS model allows for simulation of urban and rural pollutant sources from mixed land use watersheds, and the surface and subsurface runoff pathways connecting this pollution with contributing area and dispersal area processes, providing an important management tool for inland and coastal communities.

The enhanced CADA NPS model provides spatial maps of the weighted EC and EMC hotspots and coldspots contributing to watershed nutrient loads, and allows managers to differentiate between interventions that reduce surface transported pollutants, such as particulate phosphorus, from interventions targeting subsurface transported pollutants, such as dissolved nitrate. While the spatial maps and provide a first order estimate of loading hotspots, they do not represent the uncertainty in the predictions and users should run CADA NPS with low and high values of EC and EMC inputs to simulate a range of possible NPS loads, which are more likely to capture the observed loading value for the pixel and the watershed (Theodore A. Endreny & Wood, 2003).

Chapter 3 focuses on the development of the EC-PRECIP model to provide temporal variation in nutrient loading estimates. The EC-PRECIP model has proven effective as a scoping level tool in the Onondaga Creek watershed in Syracuse, New York. Comparing the updated EC-PRECIP model to the traditional EC model, NSE, PBIAS, and RSR all improved significantly. Since the EC model has been endorsed by

the USEPA as an accurate watershed modeling framework, the EC-PRECIP model is the next step in providing better water quality estimates without increasing data or sampling requirements.

The EC model is widely accepted as a scoping model when monitoring data is not feasible or is unavailable. The EC-PRECIP update moves closer to a comprehensive method for determining inter-annual nutrient loading variations, and brings widely available precipitation data together with typical nutrient loading values to produce a range of likely annual loads. The use of national data in this model is novel due to the ease of use and high level of accuracy evidenced in its application to Onondaga Creek watershed. The EC-PRECIP model fills a niche for simple models that take advantage of the large amount of weather, land use, and soils data being collected by governmental organizations such as the United States Geological Survey, the National Oceanic and Atmospheric Administration, and the Natural Resources Conservation Service.

The EC-PRECIP model represents a critical step in modifying the commonly-used EC modeling framework to allow for the influence of weather, specifically rainfall intensity, on nutrient loading in watershed across the United States. Since the EC-PRECIP model uses rainfall events as a proxy for runoff, the model will be most effective in environments with relatively high water tables, where runoff is generated quickly following a precipitation event. Extreme precipitation events create Hortonian flow, or infiltration excess overland flow, where precipitation rate exceeds the infiltration capacity of the soil. The study area in Syracuse, NY, represents an area of high precipitation magnitudes and rainfall events. In order to truly determine the

effectiveness of the model in other types of environments, further studies must occur which explore the accuracy of modeling efforts using EC-PRECIP.

Chapter 4 focuses on the primary predictors of denitrification potential in mixed-use watershed landscapes. Landscape-scale modeling of this process is needed to identify key areas (hotspots) that provide this important function. Urban environments have only recently become the focus of biogeochemical research, due to their complex hydrologic and nutrient pathways. However, our data suggest that there are coherent controls of denitrification potential in these environments and data are available to produce robust statistical models of this process that can be used in urban watersheds. A major challenge for future research is to develop models and/or geographic data sources that can depict spatial and temporal variation in the key drivers of denitrification in these watersheds. These models will improve our ability to assess and enhance N removal by designing cities to provide areas suitable for denitrification to occur.

Overall, this dissertation is comprised of studies which seek to improve the capacity for scoping level models to represent variation in nutrient loading both spatially and temporally. The improvements presented in the prior chapters serve to enhance nutrient loading predictions without requiring more extensive data collection. The implications of this research extend to community organizations, planners, and managers seeking a better understanding of the effects of different decisions on water quality. The creation of spatially and temporally variable scoping model for N and P nutrient loading through the landscape will assist managers in identifying areas of high loading potential, which generate high concentrations of nutrients and have little opportunity for downslope filtration. Similarly, areas of high denitrification potential can

be identified and utilized as areas for nitrate uptake. The low level data needs and

process-based features of the scoping model allow for its implementation into freely

available tools such as the i-Tree Hydro toolkit, a peer-reviewed software suite that is

used to assess the effects of management and land use change on water quality and

quantity.

APPENDIX A: CADA-NPS PYTHON CODE

The Python code requires DEM, watertable, saturated hydraulic conductivity, land cover, impervious cover, and canopy cover inputs. These inputs should be in a .tif format and read into the program. The modules are as follows:

1) Preliminary calculations – ArcMap functions are used to fill the DEM and identify the pixels likely to be rivers.
2) Soil Topographic Index (STI) calculations – topographic index calculations obtain a runoff index (RI) for both surface and subsurface pollutant species.
3) Buffer Index (BI) calculations – surface and subsurface buffering indices (RI) are obtained through the calculation of the time spent on each cell.
4) Determine Dynamic Export Coefficient Values – initial export coefficient (EC) values are weighted by the RI and BI for the surface and subsurface, respectively, to obtain weighted EC values for each pixel.

The outputs from this model are gridded weighted EC values for surface and subsurface nutrient species.


```
# Title: Contributing Area Dispersal Area Export Coefficient Model (CADA-ECM)
#        for ArcGIS
# Description: Performs a series of calculations to determine the accumulation
#             of N and P within a study site
# Requirements: ArcGIS 10, Spatial Analyst Extension
# Author: Emily Stephan, Ted Endreny
# Last Edited: 8/30/2016


# Import system modules
import arcpy
from arcpy import env
from arcpy.sa import *
arcpy.env.overwriteOutput = True #Allow Python to overwrite files


#Check out the ArcGIS Spatial Analyst extension license
arcpy.CheckOutExtension("Spatial")


#Set environment settings (Adjust this for different computers)
env.workspace = "C:/Users/Emily/Documents/ESF/Fall2016/SodusBay_CADA/"
```

```
# Set local variables
#This DEM is NED 1/3-arcsecond (~9mx9m pixel size) DEM, clipped around
# delineated watershed
inDEM = "demtest.tif"
inWT = "wt_clip.tif"
inKsat = "ksat_clip.tif"
inLC = "lc_clip.tif"
inImp = "imp_clip.tif"
inCan = "can_clip.tif"


#File Definitions
#This file needs to be created outside of a function below so that
# it can be written to
tmprise = "C:/Users/Emily/Documents/ESF/Fall2016/SodusBay_CADA/tmprise"




#================================================================
=============
#Preliminary Calculations
#================================================================
=============
#Create Grid Weight File
#Rivers are cells receiving > 3300 pixels
#River pixels set to 0 while other pixels are set to DEM res of 10m
#Process will then: Fill DEM, calculate flow direction, and calculate
# flow accumulation

filledDEM = Fill(inDEM)
filledDEM.save("C:/Users/Emily/Documents/ESF/Fall2016/SodusBay_CADA/filledDEM"
)


flowDirec = FlowDirection(filledDEM)
flowDirec.save("C:/Users/Emily/Documents/ESF/Fall2016/SodusBay_CADA/FlowDirec"
)
```

```python
print("Direc Complete")

flowacc = FlowAccumulation(flowDirec)
flowacc.save("C:/Users/Emily/Documents/ESF/Fall2016/SodusBay_CADA/flowacc")

print("Accum Complete")

#Execute Conditional to assign cell size weight to non river cells
river0 = Con(flowacc, 0, 9, "VALUE > 3300")

river0.save("C:/Users/Emily/Documents/ESF/Fall2016/SodusBay_CADA/river0")

print("Con Complete")


#===============================================================
=============
#Soil Topographic Index (STI) Calculation
#===============================================================
=============

#Determine the local pixel slope as a percent rise
#For pixels with a zero slope, assign the minimum slope of 0.00001497%
#Divide by 100 to convert to a decimal slope

slp =
Con(Slope(filledDEM,"PERCENT_RISE"),(0.00001497/100),Divide(Slope(filledDEM,"P
ERCENT_RISE"),100),"VALUE = 0")
slp.save("C:/Users/Emily/Documents/ESF/Fall2016/SodusBay_CADA/slp")

#Determine the Topographic Index for each cell
#TI = ln(A/Sl) where A is the weighted accumulation area and Sl is
# the local pixel slope as determined above
```

```
Impervious = Lookup(inImp, "impfloat")
Impervious.save("C:/Users/Emily/Documents/ESF/Fall2016/SodusBay_CADA/Impervio
us")
Pervious = 100-Impervious
Pervious.save("C:/Users/Emily/Documents/ESF/Fall2016/SodusBay_CADA/Pervious")

TIp = Ln(Divide((FlowAccumulation(FlowDirection(inDEM),Pervious)+river0),slp))
TIimp = Ln(Divide((FlowAccumulation(FlowDirection(inDEM),Impervious)+river0),slp))

TIp.save("C:/Users/Emily/Documents/ESF/Fall2016/SodusBay_CADA/TIp")
TIimp.save("C:/Users/Emily/Documents/ESF/Fall2016/SodusBay_CADA/TIimp")

print("TI Complete")

trans = Times(0.000864,(Times(inWT,inKsat)))
trans.save("C:/Users/Emily/Documents/ESF/Fall2016/SodusBay_CADA/trans")

transMean = float(str(arcpy.GetRasterProperties_management(trans, "MEAN")))

STIp = TIp-Ln(Divide(trans,transMean))
STIimp = TIimp-Ln(Divide(trans,transMean))

STIp.save("C:/Users/Emily/Documents/ESF/Fall2016/SodusBay_CADA/STIp")
STIimp.save("C:/Users/Emily/Documents/ESF/Fall2016/SodusBay_CADA/STIimp")
print("STI Complete")

#================================================================
==============
#Buffer Index (BI) Calculation
#================================================================
==============

#Negate the DEM
negDEM = filledDEM * -1
```

```
#-----------------------------------------------------------------------
#Determining the average slope for each of the pixel's dispersal area
#Based on the basic slope = rise/run principle


#*****************************************************************************
#RISE

#Determine the change in elevation between the pixel and the river pixel
#Uses the ArcGIS slope command and the length of each cell
tmprise = Times(Slope(negDEM, "PERCENT_RISE"),0.09)
tmp2rise = Con(river0, tmprise, 0, "VALUE <> 0")


#Create a raster that is the sum of elevation change between the pixel and
# the nearest river cell
tmp3rise = FlowAccumulation(FlowDirection(negDEM), tmp2rise)+tmp2rise

#Assign riparian cells (zero slope) to a minimum elevation change and set this
# as the final RISE using the Con command:
#Check where the previous grid is zero
#If true - use the slope command to assign a percent rise value from the negDEM
#If false - use the value from the previously created raster

rise = Con(tmp3rise, 0.000149*9/100, tmp3rise, "VALUE = 0")
rise.save("C:/Users/Emily/Documents/ESF/Fall2016/SodusBay_CADA/rise")

print("Rise Complete")

#*****************************************************************************
#RUN

#Determine the sum of the distance from each ridge cell (valleys in the negDem)
# to river cells (ridges in negDem)
```

```python
tmprun = FlowAccumulation(FlowDirection(negDEM),river0)+river0

#Convert river cells to a value of 1 and tmprun elsewhere
run = Con(tmprun, 1, tmprun, "VALUE = 0")
run.save("C:/Users/Emily/Documents/ESF/Fall2016/SodusBay_CADA/run")

print("Run Complete")

#Determine the final slope for each pixel area, 0.1 in rivers
hillslp = Con(river0, 0.000149,Divide(rise,run),"VALUE = 0")
hillslp.save("C:/Users/Emily/Documents/ESF/Fall2016/SodusBay_CADA/hillslp")


print("Hillslope Complete")

#================================================================
==============
# Determine Time Spent on Each Cell
#================================================================
==============

# Surface Routing (Manning equation, phosphorus)
n = Lookup(inLC,"n")
n.save("C:/Users/Emily/Documents/ESF/Fall2016/SodusBay_CADA/n")
R = Lookup(inLC, "R")
R.save("C:/Users/Emily/Documents/ESF/Fall2016/SodusBay_CADA/R")
surf_vel = Times(Divide(1.49,n),Times(R^(2/3),slp^(1/2)))
surf_vel.save("C:/Users/Emily/Documents/ESF/Fall2016/SodusBay_CADA/surf_vel")
surf_time = Divide(98.4252,surf_vel)
surf_time.save("C:/Users/Emily/Documents/ESF/Fall2016/SodusBay_CADA/surf_time")
#surf_time is in seconds

arcpy.CalculateStatistics_management(STIp)
STIpMean = float(str(arcpy.GetRasterProperties_management(STIp, "MEAN")))
```

```
print(STIpMean)
arcpy.CalculateStatistics_management(STIimp)
STIimpMean = float(str(arcpy.GetRasterProperties_management(STIimp, "MEAN")))
print(STIimpMean)


# Subsurface Routing (Darcy, nitrogen)
arcpy.CalculateStatistics_management(inWT)
avgWT = float(str(arcpy.GetRasterProperties_management(inWT, "MEAN")))
print(avgWT)
# 50 was chosen based on a f parameter of 0.02.
# WTdepth is depth to water table in m
WTdepth = Divide((avgWT - Times(50,(STIp - STIpMean))),100)
#
WTdepth.save("C:/Users/Emily/Documents/ESF/Fall2016/SodusBay_CADA/WTdepth")
WTslope = Divide(Slope(WTdepth,"PERCENT_RISE","1"),100)
#
WTslope.save("C:/Users/Emily/Documents/ESF/Fall2016/SodusBay_CADA/WTslope")
sub_vel = Times(0.000001,Times(inKsat,WTslope))
sub_vel.save("C:/Users/Emily/Documents/ESF/Fall2016/SodusBay_CADA/sub_vel")
sub_time = Divide(30, sub_vel)
sub_time.save("C:/Users/Emily/Documents/ESF/Fall2016/SodusBay_CADA/sub_time")
# This gives us the subsurface velocity in m/s
# sub_time is in seconds


#*****************************************************************************
#Export Coefficient - Surface BI

###Set P retention values to 0 in all cells that are classified as rivers
tmp2filter = Con(river0, 0, surf_time, "VALUE = 0")
tmp2filter.save("C:/Users/Emily/Documents/ESF/Fall2016/SodusBay_CADA/tmp2filter")
##
###Use the flow accumulation routine to determine the nutrient trapping
### efficiency for the downslope area
tmp3filter = FlowAccumulation(FlowDirection(negDEM),surf_time)+surf_time
```

```
tmp3filter.save("C:/Users/Emily/Documents/ESF/Fall2016/SodusBay_CADA/tmp3filter")
##
###Use the con command to set a minimum trapping value of greater than or equal
### to 1 for all non river cells (add 1)
tmp4filter = Con(tmp3filter,Con(river0,(tmp3filter+1),tmp3filter,"VALUE <>
0"),tmp3filter,"VALUE <= 1")
tmp4filter.save("C:/Users/Emily/Documents/ESF/Fall2016/SodusBay_CADA/tmp4filter")
##
##
###Use the con command to set a trapping value of 1 for all river cells
###This is done to avoid division by zero
filter1 = Con(river0, 1, tmp4filter,"VALUE = 0")
filter1.save("C:/Users/Emily/Documents/ESF/Fall2016/SodusBay_CADA/filter1")
##
###Calculate the final BI, where BI = ln(filtered/hillslope)
surfBI = Ln(Divide(filter1,hillslp))
surfBI = Con(surfBI, 0, surfBI, "VALUE < 0")
surfBI.save("C:/Users/Emily/Documents/ESF/Fall2016/SodusBay_CADA/surfBI")
##
print("Surf BI Complete")


#*******************************************************************************


#Export Coefficient - Subsurface BI


###Set P retention values to 0 in all cells that are classified as rivers
tmp5filter = Con(river0, 0, sub_time, "VALUE = 0")
tmp5filter.save("C:/Users/Emily/Documents/ESF/Fall2016/SodusBay_CADA/tmp5filter")
##
###Use the flow accumulation routine to determine the nutrient trapping
### efficiency for the downslope area
tmp6filter = FlowAccumulation(FlowDirection(negDEM),sub_time)+ sub_time
tmp6filter.save("C:/Users/Emily/Documents/ESF/Fall2016/SodusBay_CADA/tmp6filter")
##
```

```
###Use the con command to set a minimum trapping value of greater than or equal
### to 1 for all non river cells (add 1)
tmp7filter = Con(tmp6filter,Con(river0,(tmp6filter+1),tmp6filter,"VALUE <>
0"),tmp6filter,"VALUE <= 1")
tmp7filter.save("C:/Users/Emily/Documents/ESF/Fall2016/SodusBay_CADA/tmp7filter")
##
##
###Use the con command to set a trapping value of 1 for all river cells
###This is done to avoid division by zero
filter2 = Con(river0, 1, tmp7filter,"VALUE = 0")
##
###Calculate the final BI, where BI = ln(filtered/hillslope)
subBI = Ln(Divide(filter2,hillslp))
subBI.save("C:/Users/Emily/Documents/ESF/Fall2016/SodusBay_CADA/subBI")
##
print("Sub BI Complete")


#==============================================================
=============
# Determine Dynamic Export Coefficient Values
#==============================================================
=============

#Calculate average BI and TI to use for normalized indices
#Calculate statistics for the rasters
# (This function will exclude NODATA cells within the watershed)
#Extract the mean from the statistics and convert to a floating point number

arcpy.CalculateStatistics_management(surfBI)
surfBIMean = float(str(arcpy.GetRasterProperties_management(surfBI, "MEAN")))
print(surfBIMean)
arcpy.CalculateStatistics_management(subBI)
subBIMean = float(str(arcpy.GetRasterProperties_management(subBI, "MEAN")))
print(subBIMean)
```

```
###Generate image of normalized BI for display
BImsurf = Divide(surfBIMean,surfBI)
BImsurf.save("C:/Users/Emily/Documents/ESF/Fall2016/SodusBay_CADA/BImsurf")
BImsub = Divide(subBIMean,subBI)
BImsub.save("C:/Users/Emily/Documents/ESF/Fall2016/SodusBay_CADA/BImsub")

print("Averages Complete")


#================================================================
=============
# Determine Hydrologically Sensitive Areas (HSAs)
#================================================================
=============
STIpsd = float(str(arcpy.GetRasterProperties_management(STIp, "STD")))
print(STIpsd)
drysd = STIpsd + STIpMean
print(drysd)
wetsd = STIpMean - STIpsd
print(wetsd)

STIwet = Divide(STIp,wetsd)
STIwet.save("C:/Users/Emily/Documents/ESF/Fall2016/SodusBay_CADA/STIwet")
STIdry = Divide(STIp,drysd)
STIdry.save("C:/Users/Emily/Documents/ESF/Fall2016/SodusBay_CADA/STIdry")
STIm = Divide(STIimp,STIimpMean)
STIm.save("C:/Users/Emily/Documents/ESF/Fall2016/SodusBay_CADA/STIm")

##
##print("Averages Complete")
##
####Determine the Dynamic Export Coefficient (ECd), where:
####ECd = EC*(TI/TIavg)*(BIavg/BI) for each cell
####
###Nutrient Release
```

```
###Use the table of nutrient release values for N & P from the land use classification
### to specify the amount contributed from that specific cell

ECTN = Lookup(inLC,"TN")
ECTN.save("C:/Users/Emily/Documents/ESF/Fall2016/SodusBay_CADA/ECTN")
ECTP = Lookup(inLC,"TP")
ECTP.save("C:/Users/Emily/Documents/ESF/Fall2016/SodusBay_CADA/ECTP")

##
ECdTNann = Times(Times(BImsub,STIwet),ECTN)
ECdTNann.save("C:/Users/Emily/Documents/ESF/Fall2016/SodusBay_CADA/ECdTNa
nn")

ECdTPann = Times(Times(BImsurf,STIm),ECTP)
ECdTPann.save("C:/Users/Emily/Documents/ESF/Fall2016/SodusBay_CADA/ECdTPa
nn")

##

print("ECd Complete")
##

#Clean Up Files:
arcpy.Delete_management(tmprise)
arcpy.Delete_management(filledDEM)
arcpy.Delete_management(flowDirec)
arcpy.Delete_management(flowacc)
arcpy.Delete_management(river0)
arcpy.Delete_management(slp)
# arcpy.Delete_management(TI)
arcpy.Delete_management(trans)
# arcpy.Delete_management(STI)
arcpy.Delete_management(rise)
arcpy.Delete_management(run)
```

```
arcpy.Delete_management(hillslp)
arcpy.Delete_management(n)
arcpy.Delete_management(R)
# arcpy.Delete_management(surf_vel)
# arcpy.Delete_management(surf_time)
# arcpy.Delete_management(sub_vel)
# arcpy.Delete_management(sub_time)
arcpy.Delete_management(tmp2filter)
arcpy.Delete_management(tmp3filter)
arcpy.Delete_management(tmp4filter)
arcpy.Delete_management(tmp5filter)
arcpy.Delete_management(tmp6filter)
arcpy.Delete_management(tmp7filter)
#arcpy.Delete_management(surfBI)
#arcpy.Delete_management(subBI)
arcpy.Delete_management(BImsurf)
arcpy.Delete_management(BImsub)
```

APPENDIX B: EC-PRECIP R CODE

The R code develops a continuous exceedance probability curve a daily precipitation record in the area of interest. It will serve to assign a precise value for exceedance probability for each rainfall event based on the distribution. The exceedance probabilities are mapped to the distribution of EC values, assigning a higher export likelihood to days with more extreme precipitation events.

Required inputs to this program include a daily precipitation record (with columns for precipitation [PRCP] and year, month, and day of event) and export coefficient information for each land use within the watershed of interest (with columns for all pollutants of interest [Total_P]). These inputs should be in a .csv format and read into the program. The model:

1) Creates a daily precipitation exceedance probability curve using only daily events above a user-defined threshold,
2) Assigns an exceedance probability value to each daily rainfall event in the years of interest,
3) Creates an exceedance probability for EC values for each land use,
4) Matches the exceedance probability of daily rainfall events found in step 2 to the EC exceedance probability, and
5) Weights the EC values from step 4 to obtain a representative annual EC value.

The outputs from this model are 1) the average EC value for each year of interest [EC_TP.csv] and 2) the percentile values for each land cover type [ECtable.csv].

```
# Emily Stephan
# last modified: 10/10/2016


setwd("/Users/emilystephan/Documents/StephanPapers/Paper2-JAWRAtemporal")
weather <- read.csv("DailySyracusePrecip1.csv")
weather$PRCP <- weather$PRCP/254 # Converts to inches (from 1/10th mm)


weather1 <- weather[,c(3,4,5,6)]
weather1 <- na.omit(weather1)
weather1 <- weather1[weather1$PRCP > 1,]


# Number of events annually for each simulated year
weather2 <- weather1
```

```
uniqueyr <- unique(weather2$Year)
annevents <- vector()
for (i in 1:length(uniqueyr)){
  annevents[i] <- nrow(weather2[weather2$Year==uniqueyr[i],])
}


# Number of precipitation events occuring each month
monthevents <- vector()
for (j in 1:12){
  monthevents[j] <- nrow(weather2[weather2$Month==j,])
}


install.packages("lubridate")
library(lubridate)


years <- unique(weather$Year)


matrix <- matrix(data=NA, nrow = 366, ncol = length(years))
colnames(matrix) <- years


# In tempyr[j] >= XX, set XX to the threshold above which events are significant.
for (i in 1:length(years)){
  tempyr <- weather[weather$Year == years[i],6]
  tempyr <- tempyr[!is.na(tempyr)]
  for (j in 1:length(tempyr)){
    if (tempyr[j] >= 1){
      matrix[j,i] <- ecdf(weather1$PRCP)(tempyr[j])
    } else {
      matrix[j,i] <- NA
    }
  }
}


events <- apply(matrix, 2, sort)
```

```r
ECmatrix <- matrix(data=NA, nrow = 366, ncol = length(years))
colnames(ECmatrix) <- years

setwd("/Users/emilystephan/Documents/StephanPapers/Paper2-
JAWRAtemporal/HUC04140201_LULC")

# NLCD11 <- EC_huc[EC_huc$LULC == "Water",]
NLCD21 <- read.csv("NLCD21-4140201.csv")
NLCD22 <- read.csv("NLCD22-4140201.csv")
NLCD23 <- read.csv("NLCD23-4140201.csv")
NLCD24 <- read.csv("NLCD24-4140201.csv")
NLCD31 <- read.csv("NLCD31-4140201.csv")
NLCD41 <- read.csv("NLCD41-4140201.csv")
NLCD42 <- read.csv("NLCD42-4140201.csv")
NLCD43 <- read.csv("NLCD43-4140201.csv")
NLCD52 <- read.csv("NLCD52-4140201.csv")
NLCD71 <- read.csv("NLCD71-4140201.csv")
NLCD81 <- read.csv("NLCD81-4140201.csv")
NLCD82 <- read.csv("NLCD82-4140201.csv")
# NLCD90 <- EC_huc[EC_huc$LULC == "Woody Wetlands",]
# NLCD95 <- EC_huc[EC_huc$LULC == "Herbaceous Wetlands",]

LULC <- c(956, 20844, 18062, 13895, 5698, 731, 101471, 3468, 8085, 31085, 2029,
68480, 35390, 20393, 921)
LULC_cells <- sum(LULC[2:13])

avg_EC <- array(data = NA, dim = length(years))

for (k in 1:length(events)){
  prcp_events <- events[k]
  tempstore <- array(data=NA, dim=length(prcp_events[[1]]))
  for (m in 1:length(prcp_events[[1]])){
    EC21 <- quantile(NLCD21$Total_P, as.numeric(prcp_events[[1]][m]))*LULC[2]
```

```r
    EC22 <- quantile(NLCD22$Total_P, as.numeric(prcp_events[[1]][m]))*LULC[3]

    EC23 <- quantile(NLCD23$Total_P, as.numeric(prcp_events[[1]][m]))*LULC[4]

    EC24 <- quantile(NLCD24$Total_P, as.numeric(prcp_events[[1]][m]))*LULC[5]

    EC31 <- quantile(NLCD31$Total_P, as.numeric(prcp_events[[1]][m]))*LULC[6]

    EC41 <- quantile(NLCD41$Total_P, as.numeric(prcp_events[[1]][m]))*LULC[7]

    EC42 <- quantile(NLCD42$Total_P, as.numeric(prcp_events[[1]][m]))*LULC[8]

    EC43 <- quantile(NLCD43$Total_P, as.numeric(prcp_events[[1]][m]))*LULC[9]

    EC52 <- quantile(NLCD52$Total_P, as.numeric(prcp_events[[1]][m]))*LULC[10]

    EC71 <- quantile(NLCD71$Total_P, as.numeric(prcp_events[[1]][m]))*LULC[11]

    EC81 <- quantile(NLCD81$Total_P, as.numeric(prcp_events[[1]][m]))*LULC[12]

    EC82 <- quantile(NLCD82$Total_P, as.numeric(prcp_events[[1]][m]))*LULC[13]

    tempstore[m] <-
(EC21+EC22+EC23+EC24+EC31+EC52+EC71+EC81+EC82)/LULC_cells

 }

 avg_EC[k] <- mean(tempstore)*29.8*.36

 # kg/ha to metric tonnes -> kg/ha*29800ha*1/1000, conversion is 29.8 to get to metric
tonnes, 0.36 is SDR

}


write.table(avg_EC, file="/Users/emilystephan/Documents/StephanPapers/Paper2-
JAWRAtemporal/EC_TP.csv")


Trendmatrix <- matrix(data=NA, nrow = length(avg_EC), ncol = 3)

colnames(Trendmatrix) <- c("Year","Observed","Modeled")

Observed <- c(NA, NA, NA, NA, NA, NA, NA, NA, NA, NA, NA, NA, NA, NA, NA, NA,
NA, NA, 11, NA, NA, 14.79482, 15.682, 11, 13, 15, NA, 11.6, 13, 13, 25, 21, 6.8, 15.5,
NA)

Trendmatrix[,1] <- years

Trendmatrix[,2] <- Observed

Trendmatrix[,3] <- avg_EC


# Trend tests

cor.test(Trendmatrix[,2], Trendmatrix[,3], method="pearson")

cor.test(Trendmatrix[,2], Trendmatrix[,3], method="spearman", exact=FALSE)

cor.test(Trendmatrix[,2], Trendmatrix[,3], method="kendall", exact=FALSE)
```

```
Model_res <- Trendmatrix[,2]-Trendmatrix[,3]
plot(Observed, Model_res)
abline(0,0, lty=2)


res_noNA <- Model_res[!is.na(Model_res)]
Bias <- sum(abs(res_noNA))/length(res_noNA)


install.packages("hydroGOF")
library(hydroGOF)
NSE(Trendmatrix[,3], Trendmatrix[,2])


# Plotting the cdfs for precip
plot(ecdf(weather1$PRCP))


# Table of precipitation quantiles for each land cover type
prcntles <- c(0.05, 0.1, 0.25, 0.5, 0.75, 0.9, 0.95)
ECtable <- matrix(data=NA, nrow = 12, ncol = length(prcntles))
for (m in 1:length(prcntles)){
  ECtable[1,m] <- quantile(NLCD21$Total_P, prcntles[m])
  ECtable[2,m] <- quantile(NLCD22$Total_P, prcntles[m])
  ECtable[3,m] <- quantile(NLCD23$Total_P, prcntles[m])
  ECtable[4,m] <- quantile(NLCD24$Total_P, prcntles[m])
  ECtable[5,m] <- quantile(NLCD31$Total_P, prcntles[m])
  ECtable[6,m] <- quantile(NLCD41$Total_P, prcntles[m])
  ECtable[7,m] <- quantile(NLCD42$Total_P, prcntles[m])
  ECtable[8,m] <- quantile(NLCD43$Total_P, prcntles[m])
  ECtable[9,m] <- quantile(NLCD52$Total_P, prcntles[m])
  ECtable[10,m] <- quantile(NLCD71$Total_P, prcntles[m])
  ECtable[11,m] <- quantile(NLCD81$Total_P, prcntles[m])
  ECtable[12,m] <- quantile(NLCD82$Total_P, prcntles[m])
}
```

```
write.table(ECtable, file="/Users/emilystephan/Documents/StephanPapers/Paper2-
JAWRAtemporal/ECtable.csv")
```

APPENDIX C: DEA MODEL R CODE

The R code evaluates modeling frameworks to predict denitrification potential (DEA) using a collection of sampled ancillary variables.

The program requires a csv file input with columns for land use, sampling depth, DEA, NO23, NH4, total N, respiration, N mineralization, N nitrification, organic matter, and soil moisture. The model:

1) Develops a correlation matrix for all sampled variables,
2) Creates a PCA plot to visualize variable relationships,
3) Splits data 70/30 for model development and validation,
4) Evaluates AICc for selected models for AICc minimization, and
5) Plots the observed vs. modeled DEA values for the chosen model and returns the NSE statistic.

The outputs from this model are 1) correlation matrix (exported as "correlationx.csv"), 2) PCA plot, and 3) observed vs. modeled DEA plot.

```
# Emily Stephan
# Code to process and visualize Baltimore DEA data

setwd("/Users/emilystephan/Documents/MRGP/DenitrificationMapping")
data <- read.csv("BES DEA compilation.csv", stringsAsFactors = FALSE)
data$DEA <- as.numeric(as.character(data$DEA))
data$NO23 <- as.numeric(as.character(data$NO23))
data$NH4 <- as.numeric(as.character(data$NH4))
data$TotalN <- as.numeric(as.character(data$TotalN))
data$Respiration <- as.numeric(as.character(data$Respiration))
data$Nmin <- as.numeric(as.character(data$Nmin))
data$Nnit <- as.numeric(as.character(data$Nnit))
data$MicrobialC <- as.numeric(as.character(data$MicrobialC))
data$MicrobialN <- as.numeric(as.character(data$MicrobialN))
data$RootBiomass <- as.numeric(as.character(data$RootBiomass))
data <- data[!is.na(data$DEA),]
data <- data[data$Publication!="Groffman et al. (2005)",]
data <- data[data$Publication!="Hale and Groffman (2006)",]
# data$DEA <- log(data$DEA)
attach(data)
```

```
library(MASS)
library(sme)
library(hydroGOF)

# Looking at depths for all Baltimore data

shallow <- data[data$Depth=="0 - 10",]
shallow2 <- data[data$Depth=="0-5",]
mid <- data[data$Depth=="30-Oct",]
mid2 <- data[data$Depth=="30-May",]
mid3 <- data[data$Depth=="30-50",]
mid4 <- data[data$Depth=="50-70",]
deep <- data[data$Depth=="70 - 100",]
deep2 <- data[data$Depth=="70-100",]

shallow <- rbind(shallow, shallow2)
mid <- rbind(mid, mid2, mid3, mid4)
deep <- rbind(deep, deep2)

mean(shallow$DEA, na.rm = TRUE)
mean(mid$DEA, na.rm = TRUE)
mean(deep$DEA, na.rm = TRUE)

# Looking at depths for only urban data

urban <- data[data$Land.use.context=="Urban",]
suburban <- data[data$Land.use.context=="Suburban",]
forested <- data[data$Land.use.context=="Forested",]

boxplot(urban$DEA,suburban$DEA,forested$DEA, names=c("Urban
(N=66)","Suburban (N=112)","Forested (N=83)"), ylab = "DEA (ng/g/hr)", ylim =
c(0,8000))
boxplot(shallow$DEA,mid$DEA,deep$DEA, names=c("0 - 10 cm (N=338)","10 - 70 cm
(N=58)","70 - 100 cm (N=37)"), ylab = "DEA (ng/g/hr)", ylim = c(0,2200))
```

CORRELATION MATRIX

```
DEAcor <- shallow[,12:20]
DEAcor[,1] <- as.numeric(DEAcor[,1])
DEAcor[,2] <- as.numeric(DEAcor[,2])
DEAcor[,3] <- as.numeric(DEAcor[,3])
DEAcor[,4] <- as.numeric(DEAcor[,4])
DEAcor[,5] <- as.numeric(DEAcor[,5])
DEAcor[,6] <- as.numeric(DEAcor[,6])
DEAcor[,7] <- as.numeric(DEAcor[,7])
CorrTable <- cor(DEAcor, use="complete.obs", method="spearman")
#
write.table(CorrTable, file="correlationx.csv", append=TRUE)
#
corrtest <- matrix(NA, 9, 9)
for (n in 1:9){
  for (p in 1:9){
    corresult<-cor.test(DEAcor[,n],DEAcor[,p])
    if (corresult$p.value > 0.05) {
      corrtest[n,p]<-NA
    } else {
      corrtest[n,p]<-corresult$p.value
    }
  }
}
```

####### CREATING PCA PLOT FOR SHALLOW DATA #########

```
shallowPCA <- shallow[,12:20]
shallowPCA <- shallowPCA[complete.cases(shallowPCA), ]
stddata2 <- scale(shallowPCA)
PCA.biplot2 <- princomp(na.omit(stddata2), cor=TRUE)
```

```r
mydata.pca <- prcomp(shallowPCA, retx=TRUE, center=TRUE, scale.=TRUE)
sd <- mydata.pca$sdev
loadings <- mydata.pca$rotation
rownames(loadings) <- colnames(shallowPCA)
scores <- mydata.pca$x

R <- cor(shallowPCA)
myEig <- eigen(R)
sdLONG <- sqrt(myEig$values)
loadingsLONG <- myEig$vectors

# Plot the frame
plot(loadings, asp=1, type="n", ylim=c(-0.75,0.75), xlim=c(-0.75,0.75), xlab="PC1
(36%)", ylab="PC2 (17%)")
abline(v=0, lty=3)
abline(h=0, lty=3)
# Plot arrows: see ?arrows for the syntax
arrows(0, 0, loadings[,1], loadings[,2], len=0.1, col="red")
# Label the arrows
text(1.1*loadings, rownames(loadings), col="red", xpd=T)


## MODEL SELECTION AND VALIDATION

AICcs <- matrix(data=NA, ncol = 8, nrow = 1)
colnames(AICcs) <- c("lm.1", "lm.2", "lm.3", "lm.4", "lm.5", "lm.6", "lm.7", "lm.null")

adjRmatrix <- matrix(data=NA, ncol = 8, nrow = 1)
colnames(adjRmatrix) <- c("lm.1", "lm.2", "lm.3", "lm.4", "lm.5", "lm.6", "lm.7", "lm.null")

# Splitting data into model selection and validation

longitudes <- unique(shallow$Longitude)
samp_longs <- vector()
```

```
for (j in 1:length(longitudes)){
  samp_longs[j] <- nrow(shallow[shallow$Longitude==longitudes[j],])
}
sort(samp_longs)


# Using a 60/40 or 70/30 split, choose your model validation and sample data
# Use a random number generator to choose either 21 or 25 samples to use to validate

select_pts <- matrix(data=NA, nrow = 0, ncol = ncol(shallow))
valid_pts <- matrix(data=NA, nrow = 0, ncol = ncol(shallow))
n <- 25
index <- sample(1:35, 35, replace=F)
for (j in 1:n){
  select_pts <- rbind(select_pts, shallow[shallow$Longitude==longitudes[index[j]],])
}
nonindex <- index[(n+1):35]
for (k in 1:length(nonindex)){
  valid_pts <- rbind(valid_pts, shallow[shallow$Longitude==longitudes[nonindex[k]],])
}

## MODEL SELECTION

lm.1 = lm(select_pts$DEA ~ select_pts$Moisture + select_pts$Respiration, data = select_pts)
lm.2 = lm(select_pts$DEA ~ select_pts$Moisture + select_pts$Respiration + select_pts$Moisture:select_pts$Respiration, data = select_pts)
lm.3 = lm(select_pts$DEA ~ select_pts$Moisture + select_pts$Respiration + select_pts$TotalN, data = select_pts)
lm.4 = lm(select_pts$DEA ~ select_pts$Moisture + select_pts$Respiration + select_pts$TotalN + select_pts$Moisture:select_pts$Respiration, data = select_pts)
lm.5 = lm(select_pts$DEA ~ select_pts$Moisture + select_pts$Respiration + select_pts$TotalN + select_pts$Moisture:select_pts$TotalN, data = select_pts)
lm.6 = lm(select_pts$DEA ~ select_pts$Moisture + select_pts$Respiration + select_pts$TotalN + select_pts$Moisture:select_pts$Respiration + select_pts$Moisture:select_pts$TotalN, data = select_pts)
```

```
lm.7 = lm(select_pts$DEA ~ select_pts$Moisture + select_pts$Respiration +
select_pts$TotalN + select_pts$Moisture:select_pts$Respiration +
select_pts$Moisture:select_pts$TotalN + select_pts$Respiration:select_pts$TotalN,
data = select_pts)
lm.8 = lm(select_pts$DEA ~ 1, data = select_pts)


AICcs[1, 1] <- AICc(lm.1)
AICcs[1, 2] <- AICc(lm.2)
AICcs[1, 3] <- AICc(lm.3)
AICcs[1, 4] <- AICc(lm.4)
AICcs[1, 5] <- AICc(lm.5)
AICcs[1, 6] <- AICc(lm.6)
AICcs[1, 7] <- AICc(lm.7)
AICcs[1, 8] <- AICc(lm.8)


adjRmatrix[1, 1] <- summary(lm.1)$adj.r.squared
adjRmatrix[1, 2] <- summary(lm.2)$adj.r.squared
adjRmatrix[1, 3] <- summary(lm.3)$adj.r.squared
adjRmatrix[1, 4] <- summary(lm.4)$adj.r.squared
adjRmatrix[1, 5] <- summary(lm.5)$adj.r.squared
adjRmatrix[1, 6] <- summary(lm.6)$adj.r.squared
adjRmatrix[1, 7] <- summary(lm.7)$adj.r.squared
adjRmatrix[1, 8] <- summary(lm.8)$adj.r.squared

# MODEL VALIDATION


summary(lm.6)
test.pred6 <- summary(lm.6)$coefficient[1,1] +
summary(lm.6)$coefficient[2,1]*valid_pts$Moisture +
summary(lm.6)$coefficient[3,1]*valid_pts$Respiration +
summary(lm.6)$coefficient[4,1]*valid_pts$TotalN +
summary(lm.6)$coefficient[5,1]*valid_pts$Moisture*valid_pts$Respiration +
summary(lm.6)$coefficient[6,1]*valid_pts$Moisture*valid_pts$TotalN


NSE(valid_pts$DEA, test.pred6)
```

plot(valid_pts$DEA, test.pred6, xlim=c(0,5000), ylim=c(0,5000), xlab=c("Observed"), ylab=c("Predicted"))

abline(0,1)

Emily Anna Stephan, EIT

1127 Lancaster Ave.   <u>eastepha@syr.edu</u>
Syracuse, NY 13210   201/572-8320

EDUCATION

State University of New York College of Environmental Science and Forestry (SUNY-ESF)
Department of Environmental Resources Engineering, Syracuse, NY
Ph.D. Ecological Engineering, December 2017
GPA: 3.868/4.0

Cornell University, College of Engineering, Ithaca, NY
BS Environmental Engineering, May 2012
GPA: 3.72/4.0 (cum laude)
Passed Fundamentals of Engineering Exam (EIT)   April 2012

Relevant Courses
Hydrologic Modeling • River Form and Process • Watershed Ecology and Management
Microbial Ecology • Microbial Biodegradation and Biocatalysis • Watershed Engineering
Environmental Systems Analysis • Spatial Analysis • Water Measurement and Analysis

EMPLOYMENT EXPERIENCE

Civil Staff Engineer   Nov 2016-present
Environmental Design and Research, Landscape Architecture, Engineering, & Environmental Services, D.P.C.
SUNY-ESF, Syracuse, NY

Designing stormwater management strategies for New York projects, writing Stormwater Pollution Prevention Plans (SWPPPs) for stormwater permits, working with landscape architects to incorporate effective drainage systems into development designs.

RESEARCH EXPERIENCE

Development of a Parsimonious Urban Landscape   Fall 2012-present
Nutrient Model using Representations of Terrestrial
Denitrification Controls
Environmental Resources Engineering Department
SUNY-ESF, Syracuse, NY

Assessing current urban nutrient models in order to develop appropriate nutrient routines to fit into i-Tree Hydro, a distributed runoff model which simulates water quality and quantity in an urban watershed based on tree and impervious cover characteristics.

Sustainable Mianus River Watershed Management　　　　　　2013 – 2016
Plans Developed with Community-based i-Tree
Hydro Modeling
Research Assistantship Program Grant
Mianus River Gorge Preserve, Bedford, NY

Performing analyses of water quality characteristics at various points throughout the watershed, focusing on nitrogen and phosphorus species. Initiating feedback loops through community-based data collection of watershed land cover data, where knowledge of land cover effects on water quality influences the establishment of new urban forest and green infrastructure cover. Using nutrient data collected to inform appropriate nutrient routines for i-Tree Hydro.

TEACHING EXPERIENCE

Visiting Instructor　　　　　　　　　　　　　　　　　　　　Spring 2016
SUNY-ESF, Syracuse, NY

Instructor for Engineering Hydrology and Hydraulics, a junior-level engineering course of ~40 students.

Graduate Assistant Colloquium Teaching Fellow　　　　2013 - 2016
SUNY-ESF, Syracuse, NY

Led planning and implementation of required two-day graduate assistant training course held prior to the start of the fall semester.

Teaching Assistant, Hydrology and Hydraulics　　　　　Spring 2013
 SUNY-ESF, Syracuse, NY

Held office hours, demonstrated laboratory experiments, graded assignments.

TECHNICAL SKILLS

Coding:　　　R, MATLAB, Python
Software:　　ArcGIS, i-Tree Tools

HONORS AND AWARDS

SUNY Graduate Research Symposium Presenter (poster)　　Spring 2015

O'Brien & Gere ERE Graduate Scholarship　　　　　　　　Fall 2013
Amount: $1,000

Mianus River Gorge Preserve Research Assistantship Grant　　Spring 2013-2016
Amount: $15,000 ($5,000/year)

Engineering Learning Initiatives Research Grant　　　　　Fall 2010
Amount: $400

Joan and Irwin Jacobs Scholar, Cornell University   2008-2012

PRESENTATIONS

ORAL

WEFTEC 2016 Water Quality Conference   September 2016
New Orleans, LA
Technical Session: "i-Tree Hydro: An Accessible Tool for Modeling Hydrological
Benefits of Trees & Green Infrastructure"

WEFTEC 2015 Water Quality Conference   September 2015
Chicago, IL
Technical Session: "Tools to Quantify Environmental Benefits of Trees
for Stormwater/Green Infrastructure Projects"

Virginia i-Tree Hydro Training Workshop   October 2014
Two-day conference providing hands-on training to apply the i-Tree Hydro model using
local project-based scenarios.

Atlanta i-Tree Hydro Training Workshop   March 2014
Two-day conference providing hands-on training to apply the i-Tree Hydro model using
local project-based scenarios.

Vermont DEC Green Infrastructure Education and Training   June 2013
Webinar: "Using i-Tree Hydro to Model Green Infrastructure"

POSTER

SUNY-ESF Spotlight on Student Research   April 2015
"Mapping Areas of Potential Denitrification in Mixed-Use Watersheds by Estimating Soil
Moisture and Organic Matter Controls"

American Geophysical Union Fall Meeting   December 2014
"Weighting Nitrogen and Phosphorus Export Coefficients to Represent Runoff and
Trapping Likelihoods"

SUNY-ESF Spotlight on Student Research   April 2014
"Developing Nitrate Hotspot Maps using Landscape Denitrification Potential Predictions"

American Geophysical Union Fall Meeting   December 2013
"Development of Nutrient Model for i-Tree Hydro Using Sampling Results from the Mianus
River Watershed"

PUBLICATIONS

Stephan, Emily A. and Theodore A. Endreny, 2016. Weighting Nitrogen and Phosphorus Pixel Pollutant Loads to Represent Runoff and Buffering Likelihoods. Journal of the American Water Resources Association (JAWRA) 1–14. DOI: 10.1111/1752-1688.12390.